

**STRUCTURE BASED DESIGN OF PEPTIDOMIMETIC INHIBITORS OF THE  
MLL1-WDR5 INTERACTION**

by

**Hacer Karatas**

**A dissertation submitted in partial fulfillment  
of the requirements for the degree of  
Doctor of Philosophy  
(Medicinal Chemistry)  
in The University of Michigan  
2012**

**Doctoral Committee:**

Professor Shaomeng Wang, Chair  
Professor David H. Sherman  
Associate Professor Anna K. Mapp  
Assistant Professor Yali Dou  
Assistant Professor Sylvie Garneau-Tsodikova

© **Hacer Karatas**  
**2012**

---

To my parents Sultan and Ebubekir Karatas.

## **Acknowledgements**

First and foremost, I would like to thank to my advisor Dr. Shaomeng Wang for his guidance and support throughout my doctoral study.

I am deeply grateful to Dr. Yali Dou and Dou lab members for their extensive and constructive collaboration. I would like to thank Elizabeth C. Townsend for her work in Biacore assay, immunoprecipitation studies, HMTase assay and preparing WDR5 for the binding assay. I also like to thank Dr. Fang Cao who performed qRT-PCR and cell growth inhibition assay.

I am very grateful to Dr. Yong Chen for the crystal structure studies of MM-101 and MM-102. I would like to thank Dr. Denzil Bernard for modeling and MD simulation studies. I also like to thank Dr. Liu Liu for the PAMPA permeability assay. I'm grateful to Dr. Zaneta Nikolovska-Coleska for her training regarding the development of FP-based binding assay.

I would like to acknowledge my committee members Dr. David Sherman, Dr. Anna K. Mapp, Dr. Yali Dou and Dr. Sylvie Garneau-Tsodikova for their helpful discussion and feedback throughout my studies.

I have had the opportunity of working with a number of outstanding researchers in the Wang Lab. I would like to thank all the past and current members, especially Dr. Jianyong Chen, Dr. Angelo Aguilar, Yujun Zhao, Haibin Zhou and Shanghai Yu for the constructive discussions and their invaluable feedback.

I would like to give my special thanks to Dr. George W. A. Milne for his critical reading of this dissertation.

I'm deeply grateful to my former advisor Dr. Hakan Goker, former mentors Dr. Sureyya Olgen and Ilhan Oz for their guidance and training.

My heartfelt thanks go to my little family here in Ann Arbor, especially Arzucan Ozgur, Hande Kocak, Thuy Vu, Ayse and Guniz Buyuktur, Bilgen Ekim and Artagun Yesildere.

Lastly but mostly, my gratitude is to my family whose support made this work possible. I'm grateful to my parents Ebubekir and Sultan Karatas, my brother Mehmet Karatas, my sister Esma K. Karatas and my dear niece Zeynep Tabak who never stopped dreaming with me. New members of the family, Meral and Duru Karatas, will make our dreams even bigger.

## Table of Contents

Dedication.....	ii
Acknowledgements.....	iii
List of Figures.....	viii
List of Tables.....	x
List of Schemes.....	xii
List of Appendices.....	xiii
List of Abbreviations.....	xiv
Abstract.....	xvi
CHAPTER 1.....	1
Introduction.....	1
1.1 Histone Modifications.....	2
1.2 Histone Lysine Methylation.....	3
1.3 H3K4 Methylation.....	4
1.4 Organization and Function of the MLL1 Complex.....	5
1.5 Leukemic Transformation with MLL1 Fusion Proteins.....	7
1.6 Targeting the MLL1-WDR5 Interaction.....	9
CHAPTER 2.....	12
Development of FP-Based Binding Assay.....	12
2.1 Design and Optimization of Fluorescently Tagged Peptides for Assay Development.....	13
2.2 Development and Optimization of Competitive Binding Assay Conditions.....	14
CHAPTER 3.....	16
Analysis of the MLL1 and Histone 3 (H3) Peptides Binding to WDR5.....	16
3.1 Determination of the Minimal Motif in MLL1 for High-Affinity Binding to WDR5.....	16

3.2	Role of Two Intramolecular Hydrogen Bonds in MLL1 Peptides for High-Affinity Binding to WDR5 .....	18
3.3	Binding of H3 Peptides to WDR5 .....	22
3.4	Conclusion .....	24
CHAPTER 4	.....	26
SAR Studies of Ligand-WDR5 Interaction .....		26
4.1	Determination of Favorable Residues for Binding to WDR5 at Ala1, Arg2 and Ala3 Positions in Ac-ARA-NH <sub>2</sub> .....	26
4.2	Further Modifications Using Constrained Hydrophobic Side Chains to Target S1 and S4 Pockets.....	32
4.3	Evaluation of Permeability of Peptides and Peptidomimetics.....	36
4.4	Further Modifications at the <i>N</i> - and <i>C</i> - terminus to Improve Cell Permeability .....	36
4.5	Design of Potent and Cell Permeable Peptidomimetics (MM-101 and MM-102).....	39
4.6	Determination of Crystal Structures of MM-101 and MM-102 in Complex with WDR5 .....	40
4.7	Conclusion .....	43
CHAPTER 5	.....	45
Biochemical and Biological Evaluation MLL1-WDR5 Interaction Inhibitors.....		45
5.1	Solubility Analysis of MM-101.....	46
5.2	Stability Analysis of MM-101 against Trypsin Degradation .....	46
5.3	Stability Analysis of MM-101 in Cell Culture Media .....	48
5.4	Inhibition of MLL1-WDR5 Interaction.....	49
5.5	Inhibition of H3K4 Methyltransferase Activity of the MLL1 Core Complex .....	50
5.6	Inhibition of MLL1 Target Gene Expression .....	53
5.7	Inhibition of Cell Growth .....	54
5.8	Conclusion .....	55
CHAPTER 6	.....	58
Summary and Future Directions .....		58
6.1	Rationale and Design of the Study .....	58
6.2	Significance of the Study.....	60
6.3	Future Directions .....	61
Appendices.....		65

Appendix A.....	66
Experimental.....	66
Appendix B.....	79
Spectral Data.....	79
Bibliography .....	88
Bibliography .....	89



## List of Figures

Figure 1: Crystal structure of nucleosome (PDB:1KX5).....	2
Figure 2: Lysine residue; from left to right, unsubstituted, mono-, di-, trimethylated lysine.....	3
Figure 3: Schematic representation of domain structure of MLL1 before and after the proteolytic cleavage.....	5
Figure 4: Structural organization and role of MLL1 complex.....	6
Figure 5: Schematic representation of leukemic transformation with MLL1 fusion proteins and wild-type MLL1 complex.....	8
Figure 6: Top and bottom binding pockets of WDR5 (PDB:3EG6).....	10
Figure 7: Schematic representation of principle of FP-based competitive binding assay.....	12
Figure 8: Structure of 5-Carboxy Fluorescein.....	13
Figure 9: Saturation binding experiments with 0.6 nM of the tracers.....	14
Figure 10: Competitive binding curves for Ac-10mer, Ac-3mer, WIN and H <sub>2</sub> N-10mer as determined using a fluorescence polarization based assay.....	15
Figure 11: Intramolecular hydrogen bonds.....	19
Figure 12: MD simulations of (a) Ac-ARA-NH <sub>2</sub> and, (b) H <sub>2</sub> N-ARA-NH <sub>2</sub> peptides in Amber comparing probability of intramolecular hydrogen bond formation and the length of the bonds.....	21
Figure 13: (a) Interaction of WDR5 with Ac-ARA-NH <sub>2</sub> peptide in the predicted binding model. (b) Binding pockets (S1-S5) in WDR5 and their interaction with Ac-ARA-NH <sub>2</sub> .....	27

Figure 14: Crystal structure of WDR5-MM-101 complex. ....	41
Figure 15: Crystal structure of WDR5-MM-102 complex. ....	42
Figure 16: Trypsin stability of MM-101 and ARV peptide. ....	47
Figure 17: Stability of MM-101 in RPMI-1640 Media measured by analytical RP-HPLC at the indicated time points. ....	48
Figure 18: Inhibition curve of MLL1 <sup>C</sup> and WDR5 interaction with MM-101 using SPR experiment.....	49
Figure 19: Inhibition of MLL1 <sup>C</sup> -WDR5 interaction in HEK-293T nuclear fractions. ....	50
Figure 20: Comparison of activities of selected compounds in HMTase and competitive binding assays. ....	51
Figure 21: qRT-PCR analysis of <i>MLL1-AF9</i> transduced cells upon MM-102 treatment. ....	53
Figure 22: Growth inhibition of selected leukemia cell lines with MM-102 normalized to DMSO control.....	54
Figure 23: The strategy and rationale to inhibit the function of the MLL1 fusion protein in leukemogenesis. ....	59

## List of Tables

Table 1: The 5-FAM labeled tracers designed in this study. ....	13
Table 2: Sequence of WIN peptide and <i>N</i> -terminal of H3 peptide. Residues 1-10 in H3 and 3762-3773 in MLL1 are shown. ....	16
Table 3: Binding affinities of truncated MLL1 peptides to WDR5. ....	17
Table 4: Removal of intramolecular hydrogen bonds in Ac-ARA-NH <sub>2</sub> . ....	20
Table 5: H3 binding to WDR5. ....	23
Table 6: Binding affinities of Ac-ARA-NH <sub>2</sub> analogs designed to investigate WDR5-ligand interaction through the S1 pocket. ....	28
Table 7: Binding affinities of Ac-ARA-NH <sub>2</sub> analogs designed to investigate WDR5-ligand interaction through the S2 channel. ....	29
Table 8: Binding affinities of Ac-ARA-NH <sub>2</sub> analogs designed to investigate WDR5-ligand interaction through S4 pocket. ....	31
Table 9: Binding affinities of Ac-XRV-NH <sub>2</sub> analogs designed to further investigate S1 pocket. ....	33
Table 10: Binding affinities of Ac-VRX-NH <sub>2</sub> analogs designed to further investigate S4 pocket. ....	34
Table 11: Binding affinities and effective permeability of the trimeric peptidomimetics combining favorable groups at Ala1 and Ala3 positions. ....	35
Table 12: Binding affinities of the ARA peptides with <i>N</i> -terminal modifications. ....	37
Table 13: Binding affinities of the ARA peptides with <i>C</i> -terminal amide modifications. ....	38

Table 14: Structures and binding affinities of MM-101 and analogs. ....	39
Table 15: Data collection and refinement statistics for WDR5-MM-101 and WDR5-MM-102 complexes by molecular replacement. ....	74
Table 16: ESI-Mass characterization and HPLC analysis of the compounds in Chapters 2 and 3. ....	79
Table 17: ESI-Mass characterization and <sup>1</sup> H-NMR spectra of the compounds in Chapter 4. ....	81

## List of Schemes

Scheme 1: Synthesis of <i>C</i> -terminally modified peptides.....	67
Scheme 2: Synthesis of $\Delta 2c$ .....	68
Scheme 3: Synthesis of the tracers.....	69

## **List of Appendices**

Appendix A (Experimental) .....	66
Appendix B (Spectral Data) .....	79

## List of Abbreviations

Ala (A)	alanine
2-Abu	2-amino butyric acid
ALL	acute lymphoid leukemia
AML	acute myeloid leukemia
Arg (R)	arginine
ASH2L	absent, small or homeotic-2-like protein
Asp (D)	aspartate
AUC	area under curve
Cyc (C)	cysteine
DIEA	N,N-diisopropylethylamine
DIC	N,N'-diisopropylcarbodiimide
DTT	dithiothreitol
ESI-MS	electrospray ionization mass spectrometry
5-FAM	5-carboxyfluorescein
FP	fluorescent polarization
Glu (E)	glutamate
Gly (G)	glycine
H3	histone 3
HATU	O-(7-azabenzotriazol-1-yl)-N,N,N',N'-tetramethyluronium hexafluorophosphate
HBTU	O-(benzotriazol-1-yl)-N,N,N',N'-tetramethyluronium hexafluorophosphate
His (H)	histidine
H3K4	histone 3 lysine 4
HMTase	histone methyltransferase
HOAt	1-hydroxy-7-azabenzotriazole
HOBt	1-hydroxybenzotriazole
Leu (L)	leucine
Lys (K)	lysine
MD	molecular dynamics
MLL	myeloid/lymphoid or mixed-lineage leukemia
MLL1 <sup>C</sup>	MLL1 C-terminal
MLL1 <sup>N</sup>	MLL1 N-terminal
MM	MLL1 mimetic
mP	millipolarization
PAMPA	parallel artificial membrane permeability assay
PBS	phosphate buffered saline
RbBP5	retinoblastoma binding protein 5
Phe (F)	phenyl alanine

SAM	<i>S</i> -adenosyl methionine
Ser (S)	serine
SET	su(var)3-9, enhancer-of-zeste, trithorax
TIS	triisopropylsilane
TFA	trifluoroacetic acid
Thr (T)	threonine
Val (V)	valine
WDR5	WD repeat domain 5 protein
WIN	WDR5 interacting motif



## Abstract

MLL1 is a histone-3 lysine-4 (H3K4) methyltransferase, which is misregulated in patients with leukemia and linked with tumorigenicity through upregulation of the target genes *HoxA9* and *Meis-1*. Suppressing expression of these genes by targeting the catalytic activity of MLL1 may be a novel approach in cancer therapy. Methylation of H3K4 by MLL1 requires formation of a core complex consisting of MLL1, WDR5, RbBP5 and ASH2L. The interaction between MLL1 and WDR5 in this complex is essential for its catalytic activity and disruption of the MLL1-WDR5 interaction may provide significant therapeutic benefit to suppress target gene expression and thus tumorigenesis.

In this study, the design of peptidomimetic inhibitors that can disrupt the interaction between MLL1 and WDR5 is presented. Starting from a 12mer peptide, the tripeptide -CO-ARA-NH- in MLL1 was identified as the minimal motif for binding to WDR5. Systematic modifications to the Ac-ARA-NH<sub>2</sub> tripeptide were performed to elucidate the interaction of WDR5 with its ligands, and a number of peptidomimetic compounds with  $K_i < 1$  nM for WDR5 were developed. These compounds were also demonstrated to effectively inhibit the catalytic activity of the reconstituted MLL1 core complex *in vitro*. Further modifications to improve cellular permeability of the peptidomimetic inhibitors led to design of MM-101 and MM-102, which have sub-nanomolar binding affinities for WDR5. Crystal structures of MM-101 and MM-102 provide insight for further development of inhibitors. MM-102 inhibits the interaction

between MLL1 and WDR5 *in vitro*, and reduces expression of *HoxA9* and *Meis-1* genes in *MLL1-AF9* transduced bone marrow cells. These findings, together with the selective growth inhibition of leukemia cell lines with MLL1 fusion proteins upon treatment with MM-102, suggest that inhibitors targeting the MLL1-WDR5 interaction have a therapeutic potential in cancer therapy.

## CHAPTER 1

### Introduction

Mixed Lineage Leukemia 1 (MLL1) is a histone 3 lysine 4 (H3K4) methyltransferase, which plays pivotal role in hematopoiesis.<sup>1-3</sup> H3K4 trimethylation by MLL1 upregulates transcription of certain target genes such as *Hox* genes, whose expression level is high in hematopoietic stem and progenitor cells and repressed with the differentiation to mature blood cells.<sup>4,5</sup> Failure to repress *Hox* expression on the other hand, induces self-renewal and prevents differentiation that leads to leukemia.<sup>6</sup>

Chromosomal rearrangements of the *MLL1* gene are frequent in both acute myeloid leukemia (AML) and acute lymphoid leukemia (ALL).<sup>7,8</sup> Although the exact mechanism for leukemic transformation with MLL1 fusion proteins is poorly understood, two MLL1 target genes, *HoxA9* and *Meis-1* are consistently upregulated with MLL1 abnormalities.<sup>9</sup> These genes have been shown to cooperate with each other to induce AML linking MLL1 with its tumorigenic properties.<sup>10</sup> Therefore inhibiting MLL1 function that would repress *Hox* genes expression might be a promising approach in leukemia therapy.

In order to understand H3K4 methyltransferase activity of MLL1, a brief information to explain covalent histone modifications is necessary.

## 1.1 Histone Modifications

Chromatin, the nuclear material that contains the genetic information, is composed of DNA and proteins, most of which are histones (H). The basic structural unit of chromatin is called nucleosome, where 146-147 base pair (bp) of DNA winds around an octameric histone core which consists of histone proteins (H2A, H2B, H3 and H4).

In the structural organization of the core (Figure 1) H3 and H4 form two distinct heterodimers, which then dimerize together. The resulting tetramer interacts with two corresponding heterodimers of H2A and H2B to form the nucleosome core.<sup>11,12</sup> Linker DNA, which connects two nucleosome cores, completes the nucleosome structure. One



**Figure 1: Crystal structure of nucleosome (PDB:1KX5).**

H2A (cyan), H2B (yellow), H3 (Green), H4 (red), double stranded DNA (orange)

copy of H1 protein usually binds the dyad region of the nucleosome, adding additional DNA linker to the nucleosome core.<sup>13,14</sup>

Histone proteins contain flexible, unstructured, highly basic and conserved *N*-terminal tails, which are accessible for post-translational modifications. There are more than 100 different such sites in the histone proteins and at least nine types of modifications have been described to date. These include lysine acetylation, lysine & arginine methylation, serine & threonine phosphorylation, lysine ubiquitination, lysine sumoylation, arginine deamination, proline isomerization.<sup>15</sup> Such covalent histone modifications play key roles in diverse functions such as transcription, repair and replication of DNA. Some of the modifications, for example acetylation, are believed to cause changes in steric and charge interactions between the DNA and histones, which result in dynamic changes in the chromatin architecture modifying accessibility to DNA.<sup>16</sup> Methylation of histone lysine residues, which do not alter the overall charge, could repress or activate the transcription depending upon the modification site.<sup>17</sup> Phosphorylation, on the other hand, affects DNA repair and cell division.<sup>15,18</sup> In general, post-translational histone modifications have diverse functions which depend on the type and site of the modification.

## 1.2 Histone Lysine Methylation

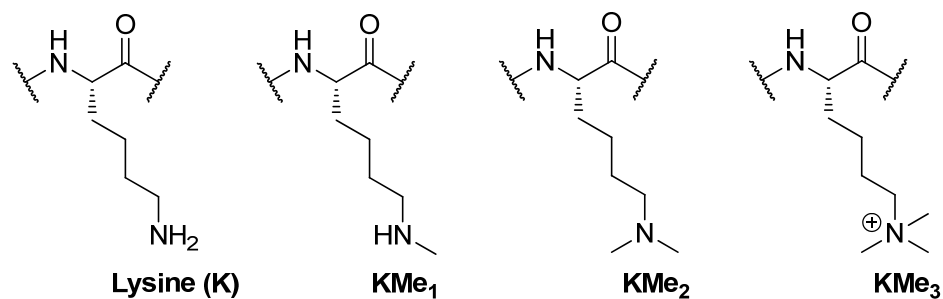


Figure 2: Lysine residue; from left to right, unsubstituted, mono-, di-, trimethylated lysine.

The  $\epsilon$ -nitrogen of lysine residues can be mono- ( $\text{Me}_1$ ), di- ( $\text{Me}_2$ ) or tri- ( $\text{Me}_3$ ) methylated (Figure 2). There are 6 sites in the histone core proteins that have been well-characterized as targets for lysine methylation. Among these, H3K9, H3K27 and H4K20 methylations are enriched in heterochromatin, the condensed form of chromatin, associated with transcriptional repression.<sup>19</sup> H3K4, H3K36 and H3K79 methylations are enriched in euchromatin (the light stained and unfolded state of chromatin) and related to transcriptional activation.<sup>17,20</sup>

### 1.3 H3K4 Methylation

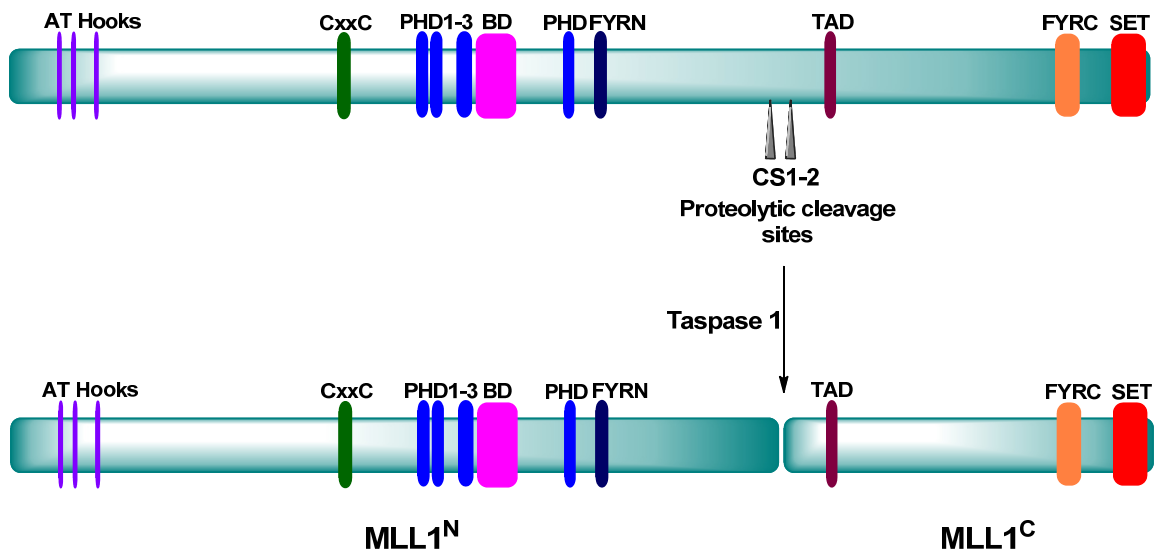
H3K4 trimethylation is an evolutionally conserved epigenetic mark for transcriptionally active chromatin in eukaryotes.<sup>17,21</sup> Genes that are transcriptionally active are enriched with trimethylated H3K4 ( $\text{H3K4Me}_3$ ) near their transcription start sites.<sup>20,21</sup> It is believed that  $\text{H3K4Me}_3$  is used as a recognition mark to recruit downstream modules. These effectors specifically recognize trimethylated H3K4 *via* chromodomains, tudor domain or PHD (Plant Homeo Domain) fingers.<sup>22</sup> BPTF, the largest component of the remodeling complex NURF which is involved in *Hox* gene expression, has been shown to specifically recognize  $\text{H3K4Me}_3$ . Another example is YNG1 (ING1 homolog 1), a component of the NuA3 Histone Acetyl Transferase (HAT) complex, which acetylates H3K14.  $\text{H3K4Me}_3$  recognition by the NuA3 HAT complex has been proposed to induce H3K14 acetylation implying a direct relation between H3K4 methylation and H3K14 acetylation both of which are associated with transcriptionally active genes.<sup>23-25</sup>

H3K4 methylation is a dynamic process; there are writers (histone methyltransferases) that add methyl groups on the lysine residue, and erasers (demethylases) that have been shown to remove the methyl groups on H3K4.<sup>26,27</sup> The

first identified eraser was LSD1, which demethylates di- and mono-methylated lysine.<sup>28</sup> The subsequently described JMJC family proteins, including hSMCX, which is involved in transcriptional repression of target genes in the neurons, has been demonstrated to possess H3K4 demethylase activity for tri- or di-methylated lysine.<sup>29</sup>

#### 1.4 Organization and Function of the MLL1 Complex

MLL1, with a conserved SET (Su(var)3-9, Enhancer-of-zeste, Trithorax) domain as the catalytic subunit, functions within a protein complex.<sup>30</sup> In human, there are six HMTase (Histone Methyltransferase) enzymes identified specific for H3K4. These are hSet1a (human Set 1a), hSet1b (human Set 1a) and MLL isoforms 1-4.<sup>31</sup> MLL1, the most studied analog in this class, is a relatively large protein with 3969 amino acid residues. It is cleaved by an aspartate protease, Taspase 1 in the cytosol, yielding a 320 kDa *N*-terminal (MLL1<sup>N</sup>) and a 180 kDa *C*-terminal (MLL1<sup>C</sup>) as shown in Figure 3.<sup>32</sup> It has



**Figure 3: Schematic representation of domain structure of MLL1 before and after the proteolytic cleavage.** AT-Hooks play role in binding to minor groove of DNA. CxxC domain binds to CpG rich DNA. Plant homodomain (PHD) is involved in protein-protein interaction. Bromodomain (BD) is an acetylated histone lysine recognition motif. FYRN and FYRC domains in MLL1 mediate heterodimerization of MLL1<sup>N</sup> and MLL1<sup>C</sup>. Transactivation domain (TAD) binds CBP, which might acetylate H3 and H4 on *Hox* genes. SET domain is the catalytic domain where *N*-terminal of H3 binds and gets methylated.

been shown that MLL1<sup>N</sup> and MLL1<sup>C</sup> associate non-covalently with each other to form a heterodimer through their FYRN and FYRC domains, respectively, and translocate to the nucleus where they maintain the association and form the MLL1 complex.<sup>32</sup>

MLL1<sup>N</sup> associates with regulatory elements such as Menin and HCFs, while MLL1<sup>C</sup> forms a catalytically active “core complex” with WDR5 (WD repeat domain 5 protein), ASH2L (Absent, Small, or Homeotic-2-Like) and RbBP5 (Retinoblastoma Binding Protein 5), as shown in Figure 4.<sup>30,33</sup> MLL1<sup>C</sup> has minimal catalytic activity and requires all the core complex members for a fully functional activity.<sup>33</sup> Stable interaction of RbBP5 and ASH2L with MLL1<sup>C</sup> is required for the catalytic activity, and WDR5 maintains the stability of the core complex by forming a bridge between MLL1 and RbBP5.<sup>34</sup> In addition to the core components, Menin is believed to direct the complex to the target genes, but the role of HCFs and DPY30 in MLL1 complex is obscure.<sup>35</sup>

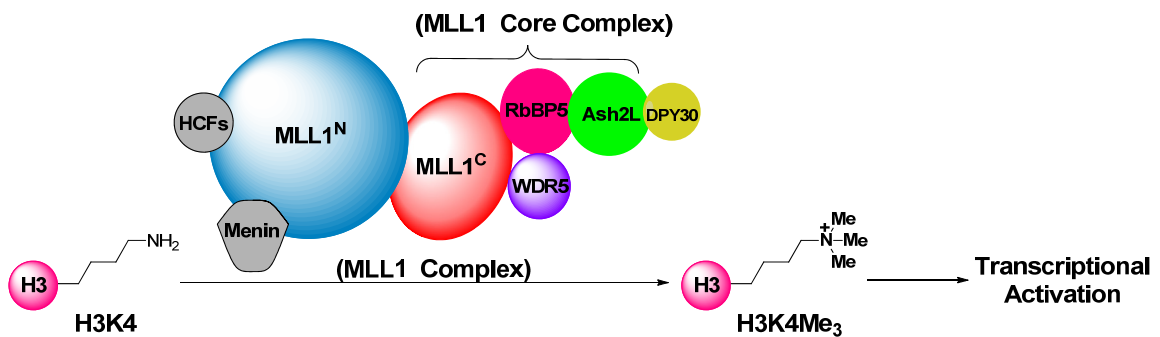


Figure 4: Structural organization and role of MLL1 complex.

The best well known targets for MLL1 are the *Hox* genes. Organized in 4 clusters (A-D) located on chromosomes 7, 17, 12 and 2, *Hox* genes encode for a class of homeodomain transcriptional factors that regulate cell proliferation and differentiation during embryonic development as well as proper hematopoiesis in adults.<sup>1,36-38</sup> *Hox* proteins use their homeodomain (helix-turn-helix motif) to interact with major groove in



their target genes and require a co-factor, PBX1 or Meis-1, to increase their binding affinity to DNA.<sup>38</sup> The direct downstream targets for Hox proteins in hematopoiesis are not clear but HoxA9 is preferentially expressed in hematopoietic stem cells (HSC) and plays an essential role in self-renewal while blocking differentiation of HSC to mature blood cells.<sup>5,39</sup>

### **1.5 Leukemic Transformation with MLL1 Fusion Proteins**

MLL1 was initially identified as the common target for 11q23 chromosomal translocations in acute myeloid leukemia (AML) and acute lymphoid leukemia (ALL).<sup>40</sup> MLL1 translocation is a hallmark of infant ALL and observed in 80% of cases with relatively poor prognosis and survival rate.<sup>41,42</sup> It is also common in childhood AML and chemotherapy-induced leukemia. Patients previously treated with topoisomerase II inhibitors frequently develop secondary AML and are found to have chimeric MLL1 proteins.<sup>43,44</sup> In these proteins, the C-terminal region of MLL1, including PHD domains, is replaced with C-terminal of variety of cytosolic and nuclear proteins.<sup>45,46</sup> There are more than seventy fusion partners identified for MLL1, only a subset of which is associated with aggressive leukemia. The MLL1-AF4, MLL1-AF9, MLL1-AF10, MLL1-ENL and MLL1-ELL fusion proteins account for the majority of cases with poor prognosis.<sup>8</sup> Although the exact mechanism for leukemic transformation with chimeric MLL1 proteins is poorly understood, certain MLL1 target genes, including *HoxA9* and *Meis-1* are consistently upregulated with MLL1 abnormalities and required for leukemic transformation linking MLL1 fusion proteins with their tumorigenic properties.<sup>10,47-49</sup> *HoxA9* depletion in MLL1-rearranged leukemia significantly reduces the cell viability and induces apoptosis. MLL1-ENL transduced bone marrow (BM) transplantation

induces AML *in vivo* in the presence of *HoxA9* expression.<sup>50</sup> Enforced overexpression of *HoxA9* can induce AML with a long latency, but co-expression with *Meis-1* leads to rapid onset of the leukemia suggesting that both *HoxA9* and *Meis-1* play a central role for the leukemic transformation with MLL1 fusion proteins.<sup>51</sup>

It is unclear how the chimeric MLL1 proteins can upregulate expression of wild-type MLL1 target genes (e.g. *HoxA9* and *Meis-1*) while they lack H3K4 methylating activity. Recent studies suggest that the wild-type MLL1 is also involved in the mechanism of leukemic transformation of MLL1 fusion proteins.<sup>52,53</sup> It has been shown that both wild-type MLL1 complex and MLL1-AF9 fusion proteins are recruited to the *HoxA9* locus and required for leukemogenesis, as represented in Figure 5. In the absence of wild-type *MLL1* allele, the MLL1-AF9 fusion protein is unable to develop leukemia in mice.<sup>53</sup> Therefore, targeting the activity of wild-type MLL1 represents a novel approach to develop new therapies for acute leukemia.

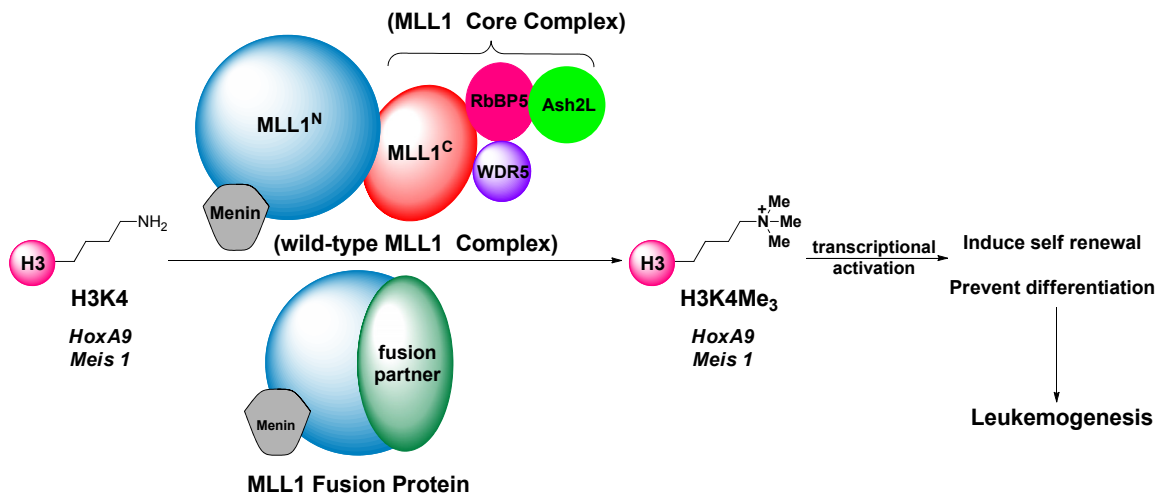


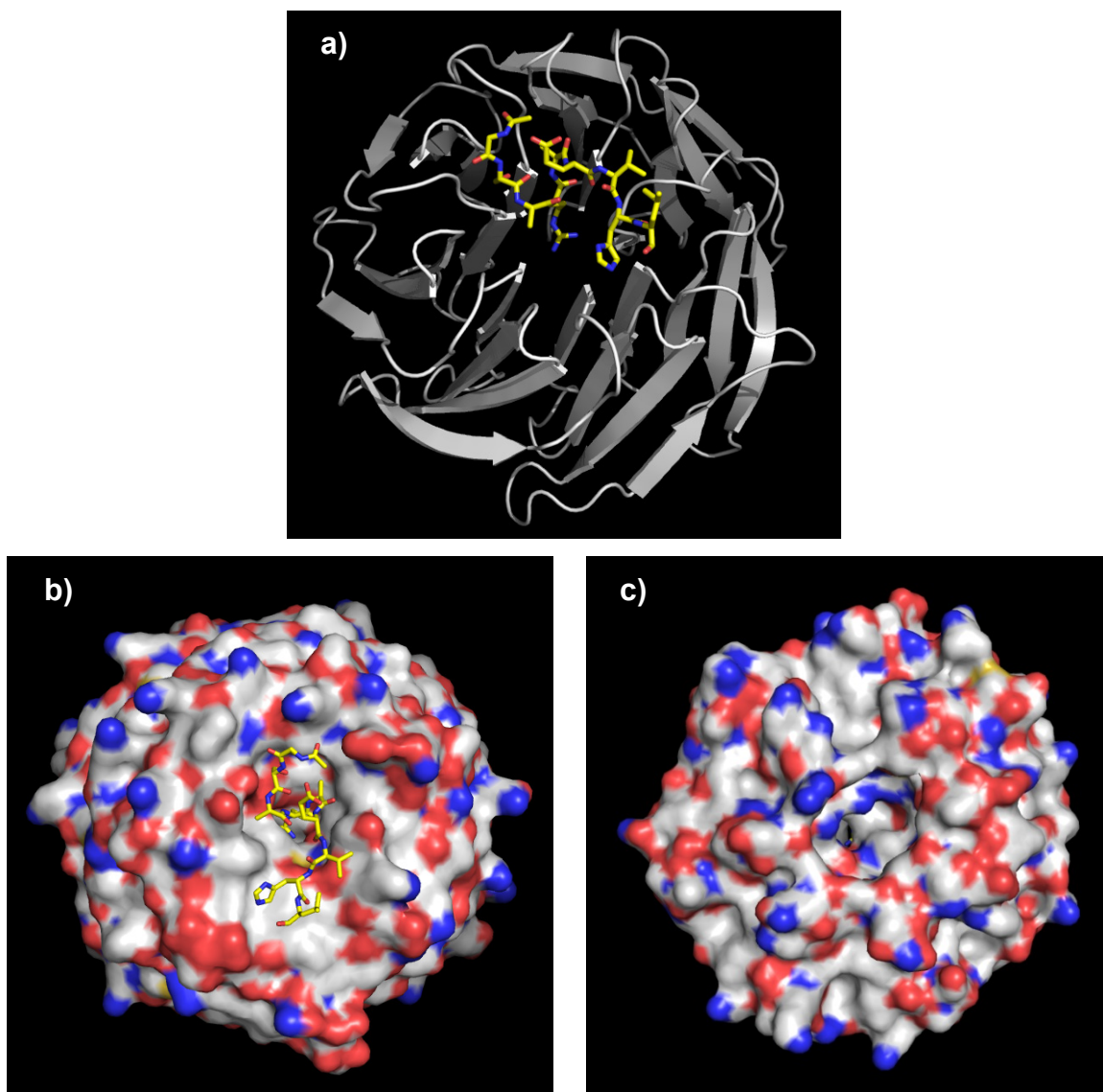
Figure 5: Schematic representation of leukemic transformation with MLL1 fusion proteins and wild-type MLL1 complex.

## 1.6 Targeting the MLL1-WDR5 Interaction

A conserved Arg residue (R3765) in MLL1 mediates the interaction of MLL1 with WDR5, and Ala mutation of this residue abolishes H3K4 methylation of the core complex *in vitro*.<sup>54</sup> WDR5 knockdown in HEK 293 cells results in a decrease in H3K4 trimethylation at the *HoxA9* and *HoxC8* gene promoters.<sup>55</sup> Therefore, inhibition of the MLL1-WDR5 interaction might be a successful strategy with which to target MLL1 activity in leukemia.

WDR5 contains an interior cavity (Figure 6a) and the beginning and the end of this cavity are sites where protein-protein interactions occur.<sup>56,57</sup> A shallow hydrophobic pocket, near the bottom binding pocket (Figure 6c) is used to interact with RbBP5.<sup>58</sup> It is not known if the bottom binding pocket is essential to the MLL1 complex. Initially, WDR5 had been shown to interact with the *N*-terminal tail of H3 using top binding pocket, arginine binding pocket, and it was therefore believed to function by presenting K4 to the catalytic SET domain for methylation.<sup>57,59</sup> Subsequently, two separate groups showed that the conserved region at the N-SET domain of MLL1 binds to WDR5 with a higher binding affinity than the H3 peptide.<sup>54,60</sup> Both H3 and MLL1 peptides use an ARX motif to bind WDR5 which explains the similar binding modes. A detailed analysis of both interactions is presented in Chapter 3.

A 12 aa sequence (residues 3762-3773, GSARAEVHLRKS) from MLL1, named WIN (WDR5 Interacting motif) by Patel *et al.*, has been shown to interact with WDR5 as shown in Figure 6 and can dissociate complexes formed between MLL1-WDR5 and MLL1-WDR5-RbBP5-ASH2L.<sup>54,61</sup> The WIN peptide therefore represents a promising starting point for the design of inhibitors of the MLL1-WDR5 interaction.



**Figure 6: Top and bottom binding pockets of WDR5 (PDB:3EG6). Top (Arginine) binding pocket is ligated with MLL1 WIN peptide (C-terminal residues RKS are not resolved).**

The design of peptidomimetic inhibitors of MLL1-WDR5 interaction is presented in this study. Initially, a competitive binding assay was developed to test the affinities of inhibitors for WDR5. Next, the minimal motif in MLL1 for WDR5 binding was determined by a truncation study using the WIN peptide. Further modifications to improve binding affinity led to the design of peptidomimetics that bind to WDR5 with sub-nanomolar  $K_i$  and which can efficiently inhibit the catalytic activity of the MLL1

core complex *in vitro*. These inhibitors however have undetectable permeability in an *in vitro* permeability assay and efforts to improve cellular permeability yielded two lead compounds, MM-101 and MM-102, both of which can inhibit MLL1<sup>C</sup>-WDR5 interaction *in vitro*. MM-102 reduces *HoxA9* and *Meis-1* expression in *MLL1-AF9* transduced bone marrow cells and shows specificity to inhibit growth of leukemia cell lines with MLL1 fusion proteins, suggesting that targeting MLL1-WDR5 interaction could be a potential strategy in acute leukemia with MLL1 fusion proteins. The crystal structures of both MM-101 and MM-102 complexed with WDR5 confirm the design strategy and provide insight for further inhibitor design.

## CHAPTER 2

### Development of FP-Based Binding Assay

The quantitative Fluorescent Polarization (FP)-based assay is valuable for accurate evaluation of the binding affinities of the compounds under investigation. The FP assay is based on the principle that when a compound or tracer containing a fluorescent chromophore (tracer) is exposed to polarized light, it absorbs the energy and emits high level of polarized fluorescence if it is stationary (Figure 7). Thus when the tracer is bound to a protein, a high level of emitted fluorescence measurement will be observed. If, on the other hand, binding inhibitors are present the tracer will be free and mobile in solution, and the level of emitted fluorescence will be decreased.

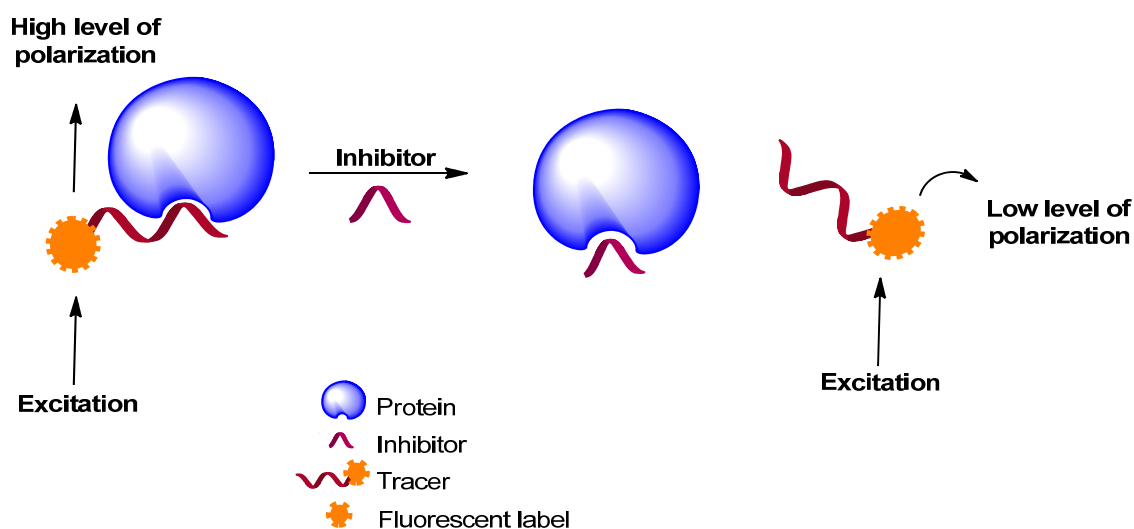
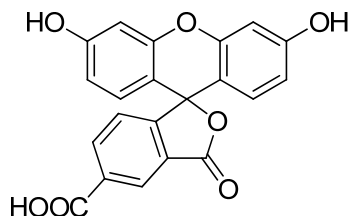


Figure 7: Schematic representation of principle of FP-based competitive binding assay.

## 2.1 Design and Optimization of Fluorescently Tagged Peptides for Assay Development

Initially two tracers WIN-FAM-1 and WIN-FAM-2, tagged with 5-carboxyfluorescein (5-FAM, Figure 8) were synthesized using the WIN sequence with two different linkers, as shown in Table 1. The 5-carboxyfluorescein was introduced to the side chain of C-terminal lysine residue as described in the experimental section (Appendix A). These two tracers were found to have similar  $K_d$  values and dynamic ranges in the WDR5 saturation experiments (Table 1 and Figure 9).



**5-Carboxy Fluorescein (5-FAM)**

Figure 8: Structure of 5-Carboxy Fluorescein.

Table 1: The 5-FAM labeled tracers designed in this study.

Ac-Amino acid sequence-Linker-K(5-FAM)-NH <sub>2</sub>			
Tracer Name	Amino acid sequence	Linker	$K_d \pm SD$ ( $\mu\text{M}$ )
WIN-FAM-1	GSARAEVHLRKS	$\beta\text{A}-\beta\text{A}-\beta\text{A}^*$	$0.86 \pm 0.15$
WIN-FAM-2	GSARAEVHLRKS	Ahx-Ahx**	$0.94 \pm 0.15$
10mer-Ala-FAM	ARAEVHLRKS	Ahx-Ahx	$0.014 \pm 0.002$
10mer-Thr-FAM	ARTEVHLRKS	Ahx-Ahx	$0.001 \pm 0.0003$

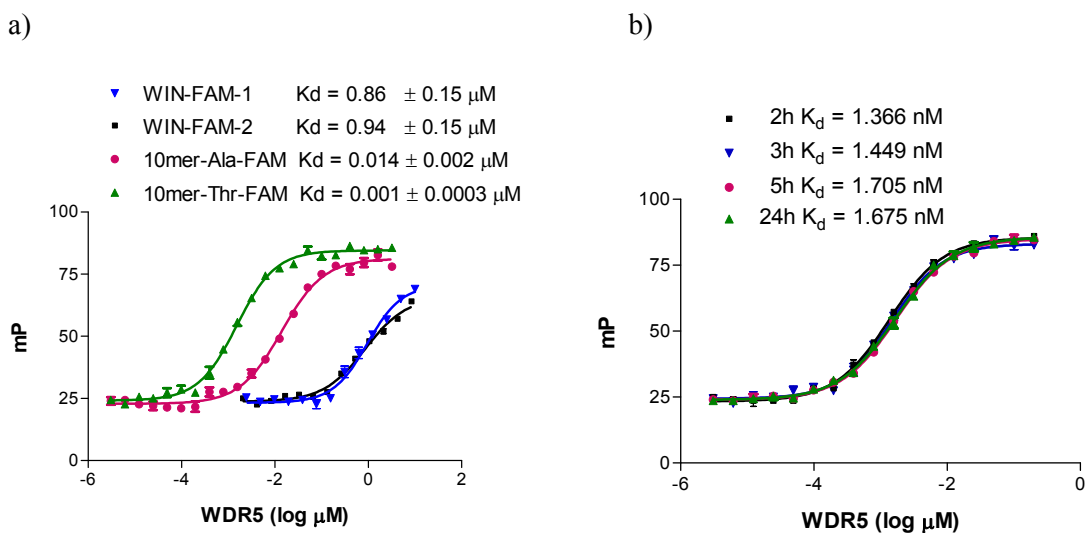
\* $\beta\text{A}$  = Beta alanine \*\*Ahx = 6-Amino hexanoic acid

An FP-based competitive binding assay was developed with WIN-FAM-1, and screening of the designed MLL1 peptides with this initial assay revealed that removal of Gly and Ser residues from N-terminal of the WIN peptide improves the binding affinity significantly, which led to the design of 10mer-Ala-FAM (Table 1). Screening of designed H3 peptides also suggested that substitution of Ala3 with Thr in MLL1 peptides

can further improve the binding affinity to WDR5, and this led to the design of 10mer-Thr-FAM (Table 1). Saturation experiments showed that while 10mer-Ala-FAM and 10mer-Thr-FAM have similar dynamic ranges ( $\Delta mP$ ), both peptides have higher affinities for WDR5 than WIN-FAM-1 and WIN-FAM-2, and the affinity of 10mer-Thr-FAM is 10 times higher than that of 10mer-Ala-FAM (Table 1 and Figure 9a).

## 2.2 Development and Optimization of Competitive Binding Assay Conditions

With the highest binding affinity for WDR5 in the saturation experiments (Figure 9a) 10mer-Thr-FAM was selected for development of an optimized FP-based competitive binding assay. First the minimum concentration of 10mer-Thr-FAM necessary to produce a total fluorescence intensity of 100,000 units was determined in the competitive binding assay. It was found that this fluorescence intensity was achieved at the concentrations of 0.6 nM or higher, and accordingly, this was selected as the tracer concentration for further evaluations of the assay conditions. Next the millipolarization (mP) values were measured at different time points in order to determine equilibrium duration and stability.



**Figure 9: Saturation binding experiments with 0.6 nM of the tracers** (a) WIN-FAM-1, WIN-FAM-2, 10mer-Thr-FAM and 10mer-Ala-FAM were titrated with WDR5 separately. (b) Stability of the saturation binding experiment with 10mer-Thr-FAM over 24 h. mP values are measured at the indicated time points.



The equilibrium between the tracer and protein was reached at 2 h and was stable for over 24 h (Figure 9b).

Higher protein concentrations can increase the dynamic range of the assay, but for the sake of assay sensitivity and accuracy, the protein concentration should not exceed the linear range of the saturation curve.<sup>62</sup> Accordingly, the optimal protein concentration for the competitive assay was investigated. WDR5 (2, 3, and 4 nM) with 0.6 nM of 10mer-Thr-FAM was evaluated in competitive binding assays and the binding affinities of Ac-10mer (Table 3) were determined under these assay conditions. Although very similar  $IC_{50}$  values were obtained with these three WDR5 protein concentrations, the dynamic range increased from 31 to 40 mP when the protein concentration was increased from 2 to 4 nM and 4 nM was chosen as the optimal WDR5 protein concentration together with 0.6 nM of 10mer-Thr-FAM tracer in the competitive binding assay that was used in this study for determination of the  $IC_{50}$  values of the peptides. All  $K_i$  values were calculated using the equation and the associated software developed previously for FP-based assays.<sup>62</sup> Representative examples of competitive binding curves are shown in Figure 10 for peptides with varying binding affinities to WDR5. The structures of the peptides are discussed in Chapter 3.

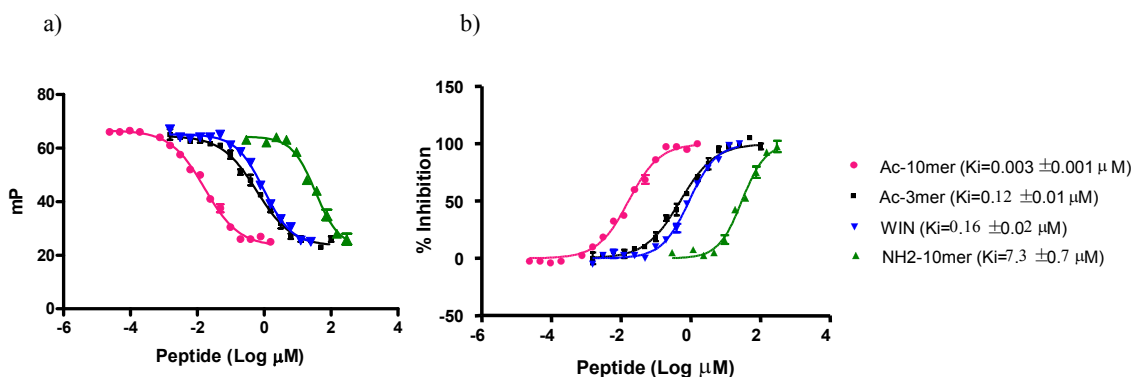


Figure 10: Competitive binding curves for Ac-10mer, Ac-3mer, WIN and H<sub>2</sub>N-10mer as determined using a fluorescence polarization based assay.

## CHAPTER 3

### Analysis of the MLL1 and Histone 3 (H3) Peptides Binding to WDR5

#### 3.1 Determination of the Minimal Motif in MLL1 for High-Affinity Binding to WDR5

The MLL1 peptide containing the WIN sequence was shown to bind to WDR5 with  $K_d = 0.12 \mu\text{M}$ .<sup>54</sup> To identify the residues critical to the high-affinity binding of the WIN peptide to WDR5, the WIN-peptide residues, whose numbering is given in Table 2, were systematically deleted from either its *N*-terminal or *C*-terminal end. Numbering assigned here allows comparison of the residues in WIN and Histone 3 (H3) two peptides.

**Table 2: Sequence of WIN peptide and *N*-terminal of H3 peptide. Residues 1-10 in H3 and 3762-3773 in MLL1 are shown.**

<b>WIN</b>	G	S	A	R	A	E	V	H	L	R	K	S
<b>N-term of H3</b>			A	R	T	K	Q	T	A	R	K	S
Numbering used here	-2	-1	1	2	3	4	5	6	7	8	9	10

All the peptides produced, unless stated otherwise, were acetylated at the *N*-terminus and capped with an amide at the *C*-terminus. Solid phase syntheses of all the analogs are described in Appendix A. The binding affinity of each peptide to WDR5 was measured with the optimized FP-based competitive binding assay (described in Chapter 2).

**Table 3: Binding affinities of truncated MLL1 peptides to WDR5.**

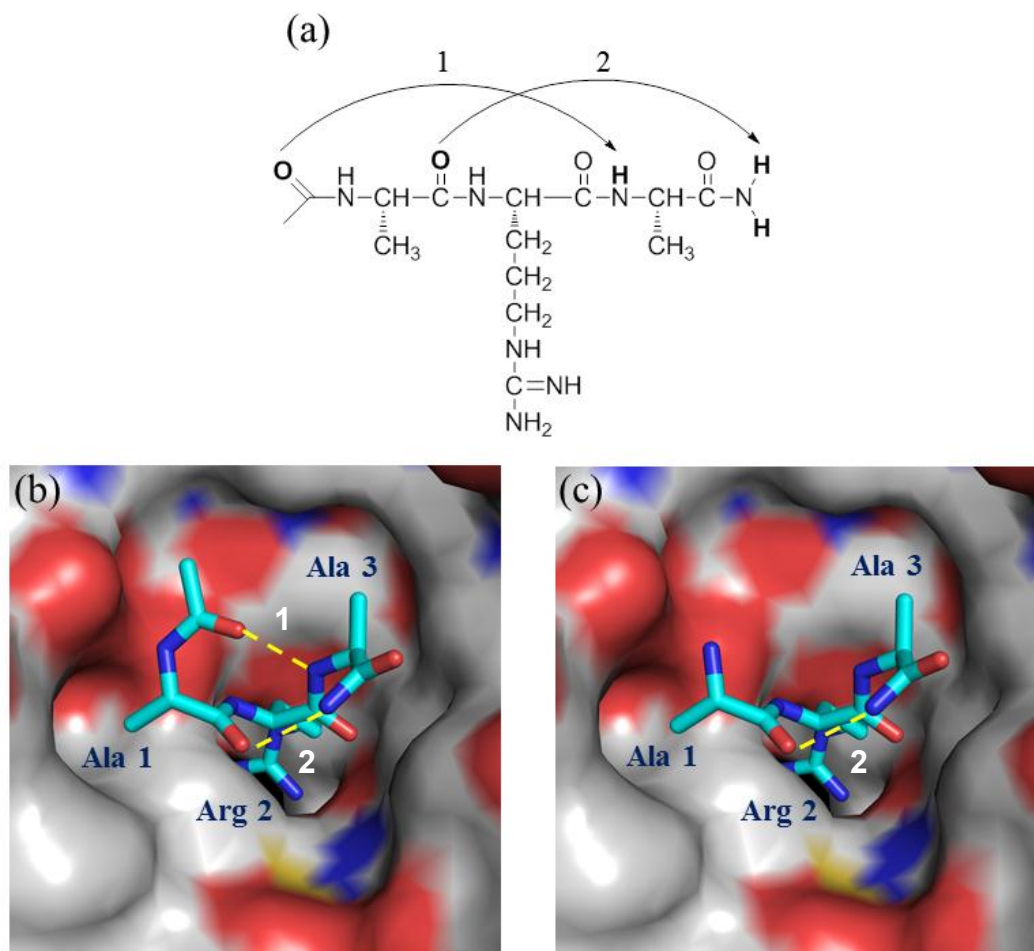
Peptide	Formula	IC <sub>50</sub> ± SD (μM)	K <sub>i</sub> ± SD (μM)
WIN	Ac-GSARAEVHLRKS-NH <sub>2</sub>	0.75 ± 0.10	0.16 ± 0.02
Ac-11mer	Ac-SARAEVHLRKS-NH <sub>2</sub>	1.04 ± 0.14	0.20 ± 0.03
Ac-10mer	Ac-ARAEVHLRKS-NH <sub>2</sub>	0.020 ± 0.004	0.003 ± 0.001
H <sub>2</sub> N-11mer	H <sub>2</sub> N-SARAEVHLRKS-NH <sub>2</sub>	0.08 ± 0.01	0.020 ± 0.002
Ac-9mer	Ac-RAEVHLRKS-NH <sub>2</sub>	29 ± 4	6.30 ± 0.80
Ac-7mer	Ac-ARAEVHL-NH <sub>2</sub>	0.16 ± 0.03	0.03 ± 0.01
Ac-6mer	Ac-ARAEVH-NH <sub>2</sub>	0.40 ± 0.10	0.09 ± 0.02
Ac-5mer	Ac-ARAEV-NH <sub>2</sub>	0.75 ± 0.10	0.16 ± 0.03
Ac-4mer	Ac-ARAE-NH <sub>2</sub>	0.40 ± 0.05	0.08 ± 0.01
Ac-3mer	Ac-ARA-NH <sub>2</sub>	0.54 ± 0.03	0.12 ± 0.01
Ac-2mer	Ac-AR-NH <sub>2</sub>	125 ± 6	27 ± 1

As can be seen in Table 3, the 12-residue WIN peptide has a K<sub>i</sub> value of 0.16 μM, similar to the reported values.<sup>54,60</sup> Removal of the Gly from the -2 position does not affect the binding significantly. Interestingly, further deletion of Ser from the -1 position in the 11-residue peptide results in a highly potent 10-residue peptide (Ac-10mer), with K<sub>i</sub> = 3 nM, 50 times that of the WIN peptide. The *N*-terminal acetyl group in Ac-11mer was found to be detrimental to its binding to WDR5 and the H<sub>2</sub>N-11mer peptide with a free *N*-terminus is 10 times more potent than Ac-11mer. Further deletion of Ala1 from Ac-10mer, giving Ac-9mer, decreases the binding affinity by a factor of 1500.

Truncation of the sequence from the C-terminus of Ac-10mer was investigated next. Simultaneous deletion of Arg8, Lys9, and Ser10 residues unresolved in the co-crystal structure of WIN-WDR5 complex,<sup>61</sup> led to Ac-7mer, which has a 10-fold lower binding affinity than Ac-10mer. Further stepwise deletions from the C-terminus generated Ac-6mer, Ac-5mer, Ac-4mer, and Ac-3mer, all of which have binding affinities similar to the 12-residue WIN peptide. However, removal of Ala3 from the Ac-3mer peptide results in >200-fold loss of binding affinity to WDR5. It is concluded consequently that the Ac-3mer (Ac-ARA-NH<sub>2</sub>) is the shortest MLL1 peptide to achieve high-affinity binding to WDR5.

### **3.2 Role of Two Intramolecular Hydrogen Bonds in MLL1 Peptides for High-Affinity Binding to WDR5**

In the crystal structure of the WDR5-WIN complex, two intramolecular hydrogen bonds can be seen in the main chain of the WIN peptide.<sup>61</sup> The first is between the Ser carbonyl oxygen at the -1 position and the amide proton of Ala3 and the second is between the Ala1 carbonyl oxygen and the Glu4 amide proton. These intramolecular hydrogen bonds cause the peptide to adopt a 3<sub>10</sub>-helical secondary structure and possibly contribute to the affinity of the WIN peptide for WDR5. Ac-ARA-NH<sub>2</sub> with a binding affinity similar to that of the 12mer WIN peptide, maintains these two intramolecular hydrogen bonds and thus was used to explore the modifications (Figure 11a and 11b) described in this part of the study.



**Figure 11: Intramolecular hydrogen bonds.**

(a) Hydrogen bonds 1 and 2 and the atoms involved in Ac-ARA-NH<sub>2</sub> are shown.  
 (b) Ac-ARA-NH<sub>2</sub> and,  
 (c) H<sub>2</sub>N-ARA-NH<sub>2</sub>, modeled in the Arg binding pocket of WDR5 based on PDB entry 3EG6. The intramolecular hydrogen bonds are shown as yellow dots. Carbon atoms are shown in cyan in the peptide and grey in WDR5. The nitrogen and oxygen atoms are colored in blue and red, respectively.

First, hydrogen bond 1 was eliminated by removing the acetyl group from Ala1 or by methylating the Ala3 nitrogen. Removal of the acetyl group from the *N*-terminal Ala1 of the Ac-3mer peptide yields H<sub>2</sub>N-3mer, which does not bind to WDR5 up to the concentrations tested (Table 4). To further confirm the critical importance of this hydrogen bond, the acetyl group from the most potent Ac-10mer peptide was removed, leading to a >1500-fold decrease in binding affinity. A similar reduction in binding

affinity was observed when the *N*-terminal acetyl group was removed from the Ac-7mer, Ac-6mer, and Ac-5mer peptides. Methylation of the Ala3 nitrogen, giving peptide  $\Delta 1$ , in which hydrogen bond 1 is destroyed, led to a complete loss of binding to WDR5.

**Table 4: Removal of intramolecular hydrogen bonds in Ac-ARA-NH<sub>2</sub>.**

Peptide	Formula	IC <sub>50</sub> ± SD (μM)	K <sub>i</sub> ± SD (μM)
Ac-10mer	Ac-ARAEVHLRKS-NH <sub>2</sub>	0.020 ± 0.004	0.003 ± 0.001
H <sub>2</sub> N-10mer	H <sub>2</sub> N-ARAEVHLRKS-NH <sub>2</sub>	34 ± 3	7.30 ± 0.70
Ac-3mer	Ac-ARA-NH <sub>2</sub>	0.54 ± 0.03	0.12 ± 0.01
H <sub>2</sub> N-3mer	H <sub>2</sub> N-ARA-NH <sub>2</sub>	> 300	> 50
CHO-3mer	CHO-ARA-NH <sub>2</sub>	14.9 ± 1.4	3.20 ± 0.30
$\Delta 1$	Ac-AR-(N-Me)A-NH <sub>2</sub>	> 300	> 50
$\Delta 2a$	Ac-ARA-CONHMe	0.70 ± 0.14	0.15 ± 0.03
$\Delta 2b$	Ac-ARA-CONMe <sub>2</sub>	30 ± 5	6.50 ± 1.20
$\Delta 2c$	Ac-ARA-COOCH <sub>3</sub>	7.30 ± 0.80	1.60 ± 0.20

Next the methyl group from the *N*-terminal acetyl was removed, yielding CHO-ARA-NH<sub>2</sub> peptide, in order to explore the contribution of the carbonyl in the absence of methyl. Replacement of the acetyl by a formyl group decreases the binding affinity by a factor of 25, suggesting that the methyl group in the *N*-terminal acetyl contributes to the increase in binding affinity, albeit to a smaller extent. Together, these data show that hydrogen bond 1 plays a vital role in maintaining the high binding affinities of the potent MLL1 peptides to WDR5, presumably through stabilization of the bound conformation. To perturb hydrogen bond 2, first the *C*-terminal amide in Ac-3mer (Table 3) was mono-

or dimethylated. The monomethylated derivative, peptide  $\Delta 2a$ , shown by modeling to be capable of maintaining hydrogen bond 2 in its bound conformation has  $K_i = 0.15 \mu\text{M}$ , similar to that of Ac-3mer, but the dimethylated derivative (peptide  $\Delta 2b$ ) is 50 times less potent than Ac-3mer. Replacement of the C-terminal amide group with a methyl ester gave peptide  $\Delta 2c$ , which is 10 times less potent than Ac-3mer. These data indicate that while hydrogen bond 2 makes an important contribution to the binding affinity of Ac-3mer, increasing it by perhaps an order of magnitude, it is less critical than hydrogen bond 1.

Molecular dynamics (MD) simulations of Ac-ARA-NH<sub>2</sub> and H<sub>2</sub>N-ARA-NH<sub>2</sub> peptides were performed to further investigate hydrogen bonds 1 and 2. As shown in Figure 12a, the probability associated with the distance between the nitrogen and oxygen atoms in hydrogen bond 1 in Ac-ARA-NH<sub>2</sub> has a narrow distribution and a maximum around 3 Å, indicating a very stable and strong hydrogen bond. In comparison, the probability for the distance between the nitrogen and oxygen atoms in hydrogen bond 2 in Ac-ARA-NH<sub>2</sub> while also having a maximum around 3 Å has a broad distribution suggesting that hydrogen bond 2 is the weaker of the two hydrogen bonds. The

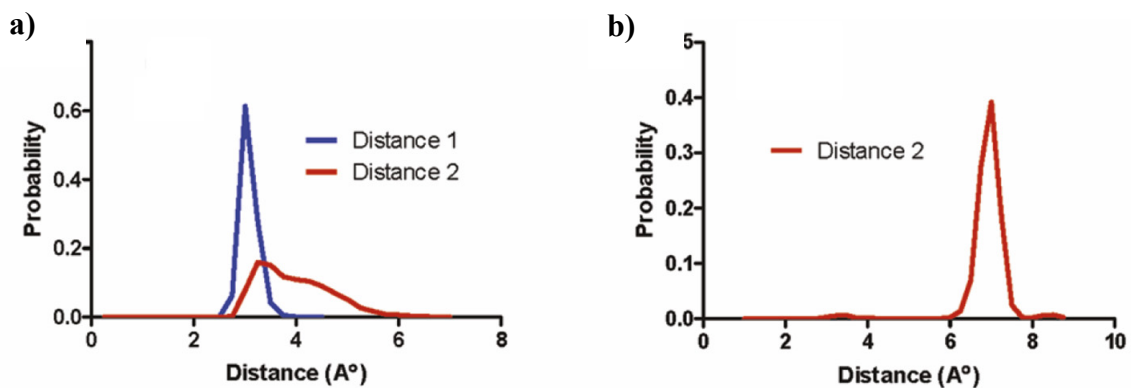


Figure 12: MD simulations of (a) Ac-ARA-NH<sub>2</sub> and, (b) H<sub>2</sub>N-ARA-NH<sub>2</sub> peptides in Amber comparing probability of intramolecular hydrogen bond formation and the length of the bonds.

probability for the distance between the nitrogen and oxygen atoms in the deacetylated peptide NH<sub>2</sub>-ARA-NH<sub>2</sub> (Figure 12b) has a narrow distribution but a maximum around 7 Å, indicating the absence of a hydrogen bond. Thus these simulations suggest that hydrogen bond 1 is stronger than hydrogen bond 2 and is also more critical in maintaining the proper bound conformation of the peptide for interaction with WDR5 and it was concluded that -CO-ARA-NH- is the minimal motif within the WIN peptide for high affinity binding to WDR5.

### 3.3 Binding of H3 Peptides to WDR5

While H3 and MLL1 peptides have similar binding modes to WDR5, the H3 peptides show much weaker affinities than MLL1 peptides.<sup>63</sup> The H3 peptides have an ART binding motif in place of the ARA binding motif in the MLL1 peptides but possess a free amino group at the Ala1 residue. To investigate if this free amino group is responsible for their weaker binding affinities, H3-3mer and H3-10mer peptides were acetylated (Table 5). In both cases, acetylation of this free amino group increases binding affinity to WDR5 significantly (1,500 times for Ac-H3-3mer and >10,000 times for Ac-H3-10mer).

The Ac-H3-3mer and Ac-H3-10mer peptides have  $K_i$  values with WDR5 of 20 nM and <1 nM, respectively, and are both more potent than the corresponding MLL1 peptides Ac-3mer and Ac-10mer (Tables 4 and 5). These data show that the primary feature underlying the weaker binding affinities of H3 peptides to WDR5 is the free amino group of Ala1 and the resulting absence of intramolecular hydrogen bond 1.

Next, the binding of H3-10mer to WDR5 was examined to learn if methylation of Lys4 (K4) significantly changes this binding. Mono-, di-, or tri-methylation of K4 led to



no significant difference in the binding affinity to WDR5 compared to that of H3-10mer (Table 5). This is consistent with previous experiments using isothermal titration curve measurements.<sup>59</sup>

**Table 5: H3 binding to WDR5.**

<b>Peptide</b>	<b>Formula</b>	<b>IC<sub>50</sub> ± SD (μM)</b>	<b>K<sub>i</sub> ± SD (μM)</b>
H3-10mer	H <sub>2</sub> N-ARTKQTARKS-NH <sub>2</sub>	70 ± 6	15.1 ± 1.3
Ac-H3-10mer	Ac-ARTKQTARKS-NH <sub>2</sub>	0.006 ± 0.002	< 0.001
H3-3mer	H <sub>2</sub> N-ART-NH <sub>2</sub>	127 ± 12	27.3 ± 2.5
Ac-H3-3mer	Ac-ART-NH <sub>2</sub>	0.08 ± 0.01	0.02 ± 0.001
H3-10mer-K4Me	H <sub>2</sub> N-ARTK(Me)QTARKS-NH <sub>2</sub>	69 ± 7	15.0 ± 1.6
H3-10mer-K4Me <sub>2</sub>	H <sub>2</sub> N-ARTK(Me <sub>2</sub> )QTARKS-NH <sub>2</sub>	42 ± 6	9.0 ± 1.3
H3-10mer-K4Me <sub>3</sub>	H <sub>2</sub> N-ARTK(Me <sub>3</sub> )QTARKS-NH <sub>2</sub>	73 ± 6	15.6 ± 1.2

### 3.4 Conclusion

To facilitate the design of small-molecule inhibitors of the MLL1-WDR5 interaction, critical elements required for high-affinity binding to WDR5 and the structural features responsible for the large difference in binding affinities of the MLL1 and H3 peptides to WDR5 were investigated. Through systematic analysis of peptides derived from the 12mer MLL1 WIN peptide, the minimal binding motif in the MLL1 peptides required for high binding affinity to WDR5 was found to be -CO-ARA-NH-. The tripeptide Ac-ARA-NH<sub>2</sub>, containing this minimal binding motif, has  $K_i = 0.12 \mu\text{M}$  with WDR5 in the FP-based competitive binding assay, essentially the same as that of the 12-residue WIN peptide ( $K_i = 0.16 \mu\text{M}$ ) determined under the same assay conditions.

The residues RKS at the C-terminus of the WIN peptide, which were not resolved in the crystal structure of the WIN peptide complexed with WDR5,<sup>51</sup> appear to enhance the binding affinity to WDR5 by a factor of 10. The most potent peptide derived from the MLL1 peptide sequence is Ac-10mer (Ac-ARAEVHLRKS) which, with  $K_i = 3 \text{ nM}$ , is 50 times more potent than the original 12-residue WIN peptide.

A dramatic increase was observed in binding affinities of the MLL1 peptides upon *N*-terminal acetylation of Ala1, which results in formation of the intramolecular hydrogen bond 1. Examination of Ac-ARA-NH<sub>2</sub> as the template molecule showed that the hydrogen bond 1 is essential for this high-affinity binding to WDR5 and in addition, MD simulations suggest that hydrogen bond 1 is required for the stability of hydrogen bond 2. Disruption of hydrogen bond 2 while maintaining hydrogen bond 1 decreases the binding affinity by only 10-fold. The methyl group of the *N*-terminal acetyl also contributes to the binding affinity and it was concluded that both of the intramolecular

hydrogen bonds and the methyl of the acetyl group contribute to the improvement in binding affinity upon *N*-terminal acetylation.

Although H3 peptides contain an ART motif, corresponding to the ARA motif in the MLL1-based peptides, they have a free amino group at their *N*-terminus and are thus incapable of forming hydrogen bond 1 that is observed in the MLL1 peptides. It was hypothesized that the absence of hydrogen bond 1 in the H3 peptides underlies their much reduced binding affinities to WDR5 compared to the MLL1 peptides. The wild-type H3 peptide (ARTKQTARKS), with a free *N*-terminal amino group, has  $K_i = 15 \mu\text{M}$  to WDR5 in the FP-based competitive binding assay, but introduction of an acetyl group at its *N*-terminus to establish the missing intramolecular hydrogen bond 1 improves the binding affinity by a factor of  $>10,000$ . Furthermore, Ac-ART-NH<sub>2</sub> binds to WDR5 with  $K_i = 20 \text{ nM}$  and is 6 times more potent than Ac-ARA-NH<sub>2</sub> whose design is based upon the MLL1 peptide sequence.

Acetylation of the *N*-terminal amino group of the MLL1 peptides and the 3mer H3 peptide (ART), improves their binding affinities to WDR5 by a factor of  $\sim 1,500$ , but  $>10,000$  times improvement is observed upon the acetylation of H3-10mer. Ac-ARTKQTA (Ac-H3-7mer) similarly shows a  $>10,000$  increase in binding affinity to WDR5 upon *N*-terminal acetylation. Therefore, it is likely that one or more of the residues (KQTA) in Ac-H3-10mer or Ac-H3-7mer, which are not present in the MLL1 peptides and Ac-ART, contribute to the further increase in binding affinity.

## CHAPTER 4

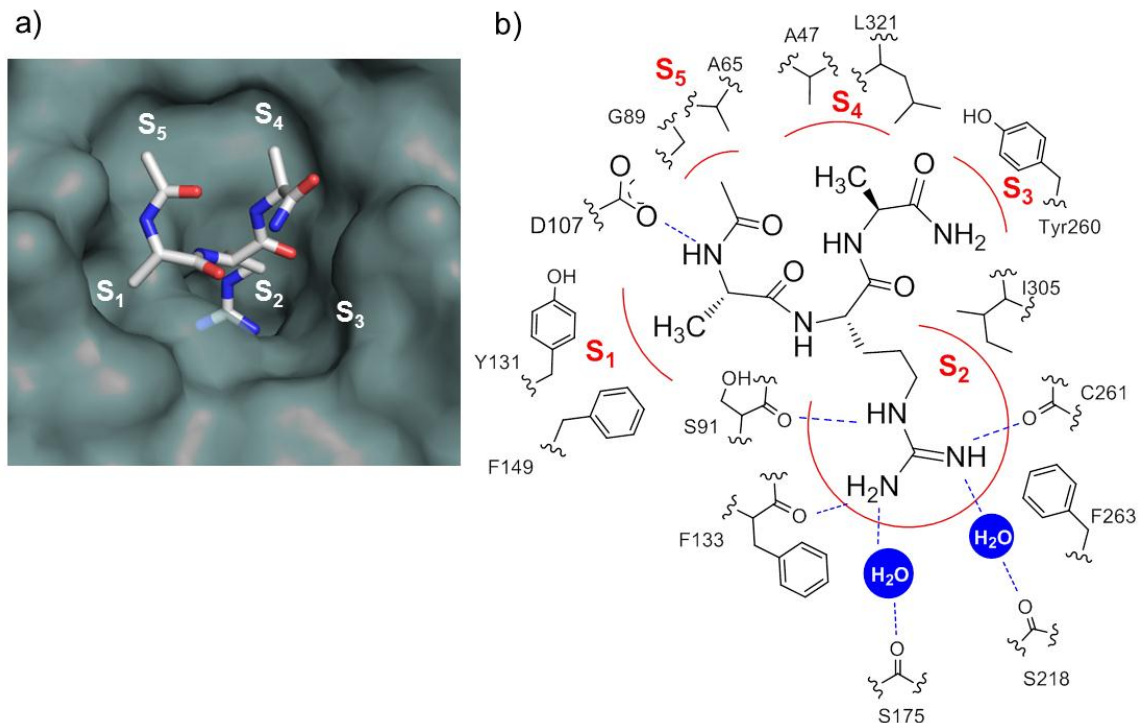
### SAR Studies of Ligand-WDR5 Interaction

The truncation study described in Chapter 3 revealed that -CO-ARA-NH- motif within MLL1 is necessary and sufficient for high-affinity interaction with WDR5.<sup>64</sup> The Ac-ARA-NH<sub>2</sub> tripeptide (Figure 2), which retains this minimal motif, was identified as a promising lead structure for further optimization. In this part of the study extensive modifications of Ac-ARA-NH<sub>2</sub> were performed in order to define the detailed structure-activity relationship for binding to WRD5.

#### 4.1 Determination of Favorable Residues for Binding to WDR5 at Ala1, Arg2 and Ala3 Positions in Ac-ARA-NH<sub>2</sub>

Based upon the crystal structure of MLL1 peptide in a complex with WDR5, a binding model of Ac-ARA-NH<sub>2</sub> in a complex with WDR5 was predicted (Figure 13a). Analysis of this binding model suggests that the key interactions between Ac-ARA-NH<sub>2</sub> and WDR5 may be broadly divided into five sub-sites (S1-S5 in Figure 13a-b). The methyl group of Ala1 interacts with a small binding pocket (S1) formed by Y131 and F149 (Figure 13b). To probe this pocket, Ala1 was replaced with residues of different sizes, shapes and hydrophobicities (Table 6). Replacement of Ala1 with Gly (**1a**) decreases the binding affinity by a factor of >100. In contrast, substitution of Ala1 with either 2-aminobutyric acid (2-Abu) (**1b**) or Val (**1c**) improves binding affinity by a factor of 2. However, residues with a side chain larger than the isopropyl in Val decrease the

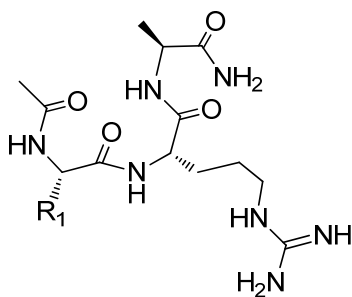
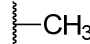
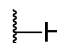
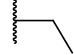
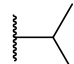
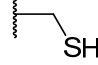
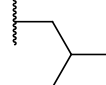
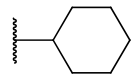
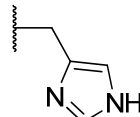
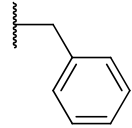
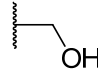
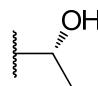
binding affinity significantly, as evident from the much reduced binding affinities of **1e** and **1f**.



**Figure 13: (a) Interaction of WDR5 with Ac-ARA-NH<sub>2</sub> peptide in the predicted binding model. (b) Binding pockets (S1-S5) in WDR5 and their interaction with Ac-ARA-NH<sub>2</sub>.**

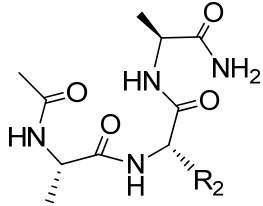
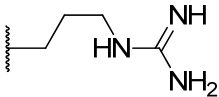
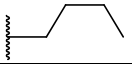

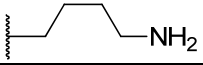
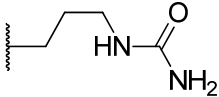
Residues with a polar side chain in this position such as Ser (**1i**) and Thr (**1j**) in this position also weaken the binding by 5 times as compared to Ala and by approximately 10 times as compared to Val and 2-Abu. A hydrophobic aromatic residue Phe (**1h**) or a polar aromatic residue His (**1g**) decreases the binding by 3-6 times as compared to Ala. Hence, the most favorable residues for binding in the S1 pocket are either 2-Abu or Val.

**Table 6: Binding affinities of Ac-ARA-NH<sub>2</sub> analogs designed to investigate WDR5-ligand interaction through the S1 pocket.**

				
Peptide		R <sub>1</sub>	IC <sub>50</sub> ± SD (μM)	K <sub>i</sub> ± SD (μM)
ARA			0.54 ± 0.03	0.12 ± 0.01
<b>1a</b>	GRA		77.4 ± 13.2	16.7 ± 2.8
<b>1b</b>	AbuRA		0.28 ± 0.02	0.060 ± 0.001
<b>1c</b>	VRA		0.24 ± 0.03	0.050 ± 0.005
<b>1d</b>	CRA		1.83 ± 0.30	0.4 ± 0.6
<b>1e</b>	LRA		10.8 ± 0.4	2.3 ± 0.3
<b>1f</b>	ChgRA		8.7 ± 0.6	1.9 ± 0.1
<b>1g</b>	HRA		1.7 ± 0.3	0.40 ± 0.03
<b>1h</b>	FRA		3.1 ± 0.3	0.7 ± 0.1
<b>1i</b>	SRA		2.9 ± 0.6	0.6 ± 0.1
<b>1j</b>	TRA		2.9 ± 0.4	0.6 ± 0.1

Next Arg2 was modified. In the crystal structures of WDR5 bound to either MLL1 or H3 peptides<sup>60,65</sup> and in the predicted binding model of Ac-ARA-NH<sub>2</sub> with WRD5, the Arg side chain inserts into a deep cavity in WDR5 and has extensive interactions with the S2 channel of WDR5 (Figure 13a-b). The guanidino group in Arg forms  $\pi$ -cation interactions with F133 and F263 *via* its two  $\omega$ -nitrogen atoms. These two  $\omega$ -nitrogen atoms also form hydrogen bonds directly with the backbone carbonyl groups of F133 and C261 and, *via* two water molecules, with S175 and S218. The  $\delta$ -nitrogen in Arg forms a hydrogen bond with the backbone carbonyl group of S91. There are also hydrophobic contacts between the hydrophobic portion in the side chain of Arg2 and I305 side chain. Since the S2 channel is narrow, only a number of residues with linear side chains to probe this site were selected (Table 7).

**Table 7: Binding affinities of Ac-ARA-NH<sub>2</sub> analogs designed to investigate WDR5-ligand interaction through the S2 channel.**

				
Peptide		R <sub>2</sub>	IC <sub>50</sub> ± SD (μM)	K <sub>i</sub> ± SD (μM)
ARA			0.54 ± 0.03	0.12 ± 0.01
2a	ANleA		> 300	> 65
2b	AOrnA		> 300	> 65
2c	AKA		> 300	> 65
2d	ACitA		> 300	> 65
Nle (Nor-leucine), Orn (Ornithine), Cit (citrulline)				

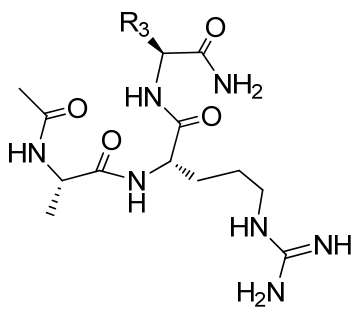
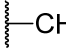
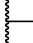
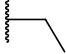
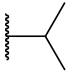
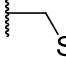
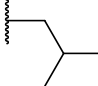
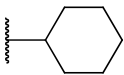
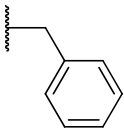
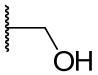
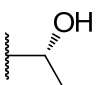
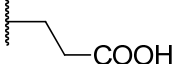
Replacement of the guanidino of Arg2 with a methyl group (**2a**) or removal of the amidine portion of guanidino group (**2b**) leads to complete loss of binding. Replacement of Arg2 with Lys (**2c**) yields another inactive compound. Finally, replacement of the Arg guanidino with urea yields **2d**, which also fails to bind to WDR5. These results clearly show that the side chain of Arg2 is essential for binding to WDR5, consistent with the extensive interactions between Arg2 and WDR5 observed in the predicted binding model.

Next, Ala3 was modified. The Ala3 side chain is projected to a hemispherical hydrophobic S4 pocket formed mainly by side chains of A47 and L321 in WDR5 (Figure 13a-b). Replacement of the methyl in Ala3 with hydrogen (**3a**) decreases the binding by >10-fold. Changing this methyl group to ethyl (**3b**), however, improves the binding affinity by a factor of 20.

Further increase in the size of the ethyl to isopropyl (**3c**) reduces the binding affinity 3-fold as compared to **3b**, although **3c** is still 5 times more potent than the ARA peptide. Peptides with a side chain larger than isopropyl, for example ARL (**3e**), ARChg (**3f**) and ARF (**3g**) all have much weaker affinities than the ARA peptide. Replacement of Ala3 with Cys (**3d**) or Thr (**3i**) leads to 5-fold enhancement in binding affinity, similar to that achieved by Val. Finally, replacement of Ala3 with Ser (**3h**) reduces the binding by 3 times as compared to ARA, but Glu at this position (**3j**) decreases the binding by >100 times.



**Table 8: Binding affinities of Ac-ARA-NH<sub>2</sub> analogs designed to investigate WDR5-ligand interaction through S4 pocket.**

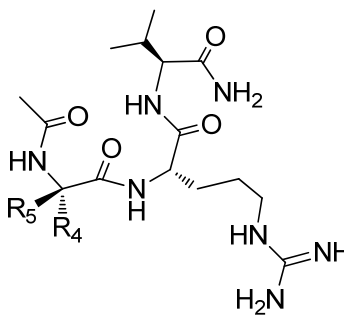
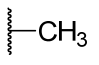

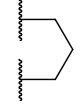
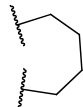
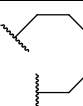
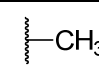
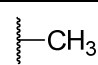
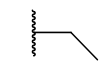
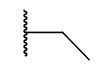

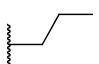
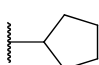
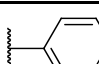
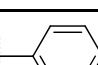
				
Peptide		R <sub>3</sub>	IC <sub>50</sub> ± SD (μM)	K <sub>i</sub> ± SD (μM)
ARA			0.54 ± 0.03	0.12 ± 0.01
3a	ARG		10.3 ± 1.2	2.2 ± 0.3
3b	ARAbu		0.030 ± 0.008	0.006 ± 0.002
3c	ARV		0.11 ± 0.02	0.020 ± 0.003
3d	ARC		0.08 ± 0.01	0.020 ± 0.003
3e	ARL		34 ± 6	7.3 ± 1.2
3f	ARChg		280 ± 70	61 ± 16
3g	ARF		280 ± 40	60 ± 8
3h	ARS		1.8 ± 0.1	0.40 ± 0.07
3i	ART		0.08 ± 0.01	0.020 ± 0.001
3j	ARE		> 100	> 20

## 4.2 Further Modifications Using Constrained Hydrophobic Side Chains to Target S1 and S4 Pockets

The modifications described above showed that small hydrophobic groups at the Ala1 and Ala3 positions are highly desirable for achieving high affinity binding to WDR5. These positions were further explored using a series of unnatural amino acids with small and constrained hydrophobic side chains. The tripeptides VRA and ARV were used as template for these modifications, since Val is favorable at both positions. The results are summarized in Tables 9 and 10.

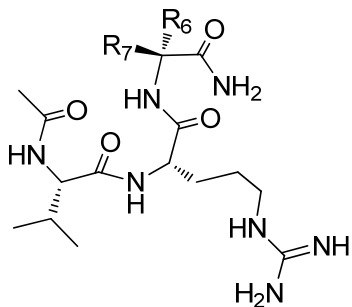
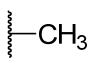

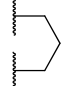

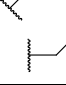
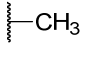
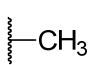
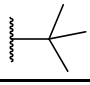
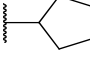
Similar binding affinities were observed when the Ala in ARV is replaced with either *tert*-Leu (Tle) (**4g**) or norvaline (Nva) (**4h**) (Table 9). Cyclopentylglycine (Cpg) (**4i**) at this position decreases the binding affinity by 15 times, whereas phenylglycine (**4j**) reduces the affinity by a factor of 50. Changing the chiral center in **4j**, yielding **4k**, further decreases the binding by >10-fold. Introduction of another methyl group in the C $\alpha$  carbon (**4e**), however, improves the affinity by 10-fold and therefore a series of compounds using conformationally constrained cyclopropyl, cyclobutyl, cyclopentyl and cyclohexyl groups were synthesized. While **4a** with a cyclopropyl group, is only 2 times less potent than ARV peptide, the other three compounds have improved binding affinities. Compound **4b** with a cyclobutyl group, for example, is 10 times more potent than ARV and as potent as **4e**.

Table 9: Binding affinities of Ac-XRV-NH<sub>2</sub> analogs designed to further investigate S1 pocket.

					
Compound		R <sub>4</sub>	R <sub>5</sub>	IC <sub>50</sub> ± SD (μM)	K <sub>i</sub> ± SD (μM)
3c	ARV		-H	0.11 ± 0.02	0.020 ± 0.003
4a	ACPC-RV			0.26 ± 0.06	0.06 ± 0.01
4b	CycVal-RV			0.010 ± 0.008	0.002 ± 0.001
4c	CycLeu-RV			0.040 ± 0.003	0.009 ± 0.001
4d	homocycloLeu-RV			0.04 ± 0.01	0.007 ± 0.002
4e	α-MeAla-RV			0.010 ± 0.002	0.002 ± 0.0005
4f	Deg-RV			0.02 ± 0.01	0.004 ± 0.002
4g	Tle-RV		-H	0.18 ± 0.04	0.040 ± 0.005
4h	Nva-RV		-H	0.18 ± 0.01	0.040 ± 0.002
4i	Cpg-RV		-H	1.56 ± 0.30	0.34 ± 0.06
4j	Phg-RV		-H	5.4 ± 1.1	1.20 ± 0.25
4k	D-Phg-RV	-H		68 ± 4	14.6 ± 0.80

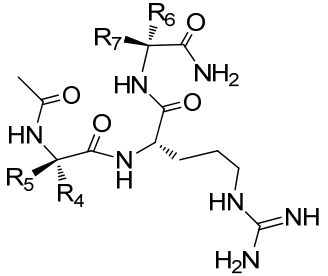
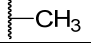
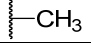
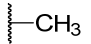
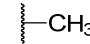
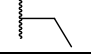


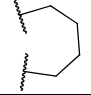
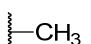
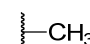
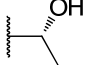
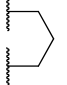
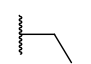
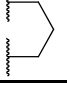
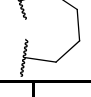
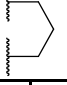
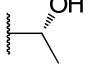
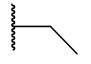
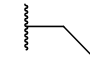
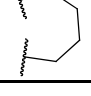
Next, similar modifications at the Ala3 position in VRA peptide were performed giving the results shown in Table 10. Compound **5c** with a constrained cyclopentyl side chain is 2 times more potent than VRA, while **5d** with a cyclohexyl group is 2 times less potent than VRA. All the other modifications resulted in a decrease in binding affinity of at least an order of magnitude.

**Table 10: Binding affinities of Ac-VRX-NH<sub>2</sub> analogs designed to further investigate S4 pocket.**

					
Compound		R <sub>6</sub>	R <sub>7</sub>	IC <sub>50</sub> ± SD (μM)	K <sub>i</sub> ± SD (μM)
<b>1c</b>	VRA	-H		0.24 ± 0.03	0.050 ± 0.005
<b>5a</b>	VR-ACPC			2.71 ± 0.34	0.6 ± 0.1
<b>5b</b>	VR-CycVal			2.43 ± 0.55	0.52 ± 0.12
<b>5c</b>	VR-CycLeu			0.09 ± 0.01	0.018 ± 0.001
<b>5d</b>	VR-homocycloLeu			0.44 ± 0.15	0.44 ± 0.15
<b>5e</b>	VR-α-MeAla			7.44 ± 0.15	1.6 ± 0.2
<b>5f</b>	VR-Tle	-H		41 ± 7	8.7 ± 1.5
<b>5g</b>	VR-Cpg	-H		41 ± 5	8.8 ± 1.1

Finally, the most favorable modifications identified at Ala1 and Ala3 positions were combined. For Ala1 position, those used in **4b**, **4e** and **4f** and for the Ala3 position, those used in **3b**, **3i** and **5c** were selected. These led to compounds **6a-6g** (Table 11). Compounds **6a**, **6c**, **6d** and **6f** have  $IC_{50}$  values of 5-9 nM with  $K_i$  values of  $\leq 1$  nM. In direct comparison, compounds **6a** and **6d** are 100 times more potent than the initial ARA tripeptide ( $K_i = 120$  nM).

**Table 11: Binding affinities and effective permeability of the trimeric peptidomimetics combining favorable groups at Ala1 and Ala3 positions.**

							
Compound	R <sub>4</sub>	R <sub>5</sub>	R <sub>6</sub>	R <sub>7</sub>	IC <sub>50</sub> ± SD (nM)	K <sub>i</sub> ± SD (nM)	P <sub>e</sub> (x10 <sup>-6</sup> cm <sup>2</sup> /s)
ARA		-H	-H		540 ± 30	120 ± 10	< 0.01
<b>6a</b>			-H		5 ± 1	< 1	< 0.01
<b>6b</b>					36 ± 5	8 ± 2	< 0.01
<b>6c</b>			-H		6 ± 1	< 1	NT*
<b>6d</b>			-H		5 ± 1	< 1	< 0.01
<b>6e</b>					32 ± 7	6 ± 2	NT*
<b>6f</b>			-H		9 ± 1	1.0 ± 0.3	< 0.01
<b>6g</b>					80 ± 14	16 ± 3	< 0.01
							*Not tested

### 4.3 Evaluation of Permeability of Peptides and Peptidomimetics

Many peptides and peptidomimetics have low cell permeability. Therefore the permeability of ARA peptide and a number of potent peptidomimetics in Table 11 (**6a**, **6b**, **6e** and **6g**) was evaluated using a Parallel Artificial Membrane Permeability Assay (PAMPA), which measures the passive diffusion permeability *in vitro*. The data showed that peptidomimetics **6a**, **6b**, **6e** and **6g** and ARA peptide all have a permeability coefficient ( $P_e$ ) value of  $< 0.01$  (Table 11), suggesting that these compounds may have poor passive cell permeability.

### 4.4 Further Modifications at the *N*- and *C*-terminus to Improve Cell Permeability

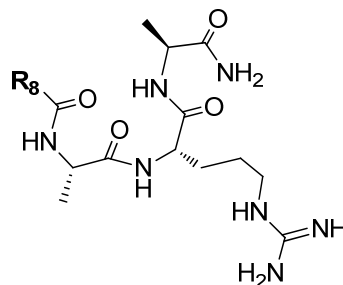
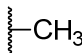
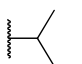
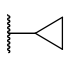

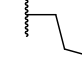
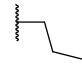
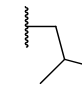
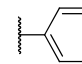
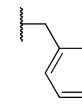
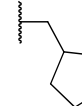
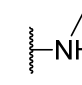
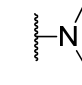
The PAMPA data with potent peptidomimetics **6a**, **6b**, **6e** and **6g** show that these compounds are likely to have very poor passive cell permeability, which suggested that additional optimization to improve the permeability of the peptidomimetics is necessary.

One of the commonly used methods to improve cell permeability is to increase hydrophobicity of the compounds. Therefore further modifications were performed at both the *N*- and *C*-terminals of ARA peptide with a goal of identifying additional modifications that would increase the overall hydrophobicity without detrimental effect on binding to WDR5.

Based upon the predicted binding model of Ac-ARA-NH<sub>2</sub> peptide with WDR5, *N*-terminal portion of the molecule is projected towards a small hydrophobic pocket (S5 pocket, Figure 13a-b) formed by G89 and A65. Thus the methyl group of the acetyl group was modified with larger hydrophobic groups. As shown in Table 12, small groups such as isopropyl (**7a**,  $K_i = 0.04 \mu\text{M}$ ) and cyclopropyl (**7b**,  $K_i = 0.11 \mu\text{M}$ ) are much preferred over large (**7g**,  $K_i = > 65 \mu\text{M}$ ) or branched (**7f**,  $K_i = 4.7 \mu\text{M}$ ) groups. The most

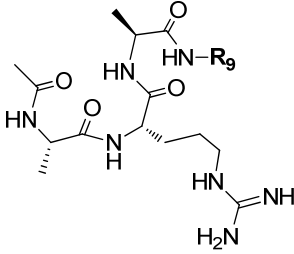
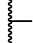
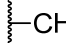
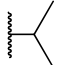
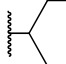
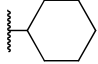
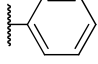
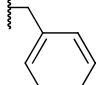
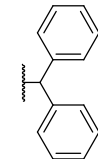
favorable group at this position is isopropyl (**7a**,  $K_i = 0.04 \mu\text{M}$ ), which improves the binding affinity by 3 times compared to methyl in Ac-ARA-NH<sub>2</sub>.

**Table 12: Binding affinities of the ARA peptides with *N*-terminal modifications.**

			
Compound	R <sub>8</sub>	IC <sub>50</sub> ± SD (μM)	K <sub>i</sub> ± SD (μM)
ARA		0.54 ± 0.03	0.12 ± 0.01
<b>7a</b>		0.17 ± 0.06	0.04 ± 0.01
<b>7b</b>		0.5 ± 0.03	0.11 ± 0.01
<b>7c</b>		5.1 ± 0.5	1.1 ± 0.1
<b>7d</b>		0.7 ± 0.02	0.16 ± 0.01
<b>7e</b>		23.4 ± 1.7	5.1 ± 0.4
<b>7f</b>		22 ± 2	4.7 ± 0.5
<b>7g</b>		> 300	> 65
<b>7h</b>		> 100	> 5
<b>7i</b>		> 100	> 20
<b>7j</b>		2.5 ± 0.4	0.54 ± 0.09
<b>7k</b>		17.4 ± 0.3	3.74 ± 0.06

The C-terminal amide in Ac-ARA-NH<sub>2</sub> is projected close to a small hydrophobic patch (the S3 pocket) formed by Y260 and K259 side chains (Figure 13a-b). Similar to the N-terminal modifications, this part of the molecule was substituted with different hydrophobic groups and the binding data are summarized in Table 13. All the modifications larger than methyl (**8b-8g**) improve the binding affinity. In particular, the biphenylmethyl group in **8g** enhances the binding affinity by >10-fold.

Table 13: Binding affinities of the ARA peptides with C-terminal amide modifications.

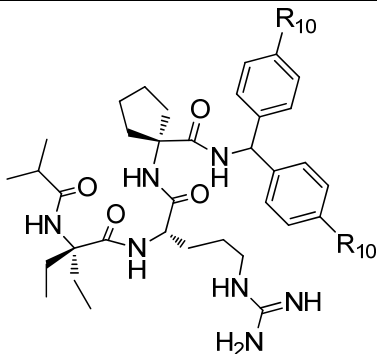
			
Compound	R <sub>9</sub>	IC <sub>50</sub> ± SD (μM)	K <sub>i</sub> ± SD (μM)
ARA	 -H	0.54 ± 0.03	0.12 ± 0.01
<b>8a</b> ( <b>Δ2a</b> )	 -CH <sub>3</sub>	0.70 ± 0.14	0.15 ± 0.03
<b>8b</b>		0.16 ± 0.1	0.05 ± 0.01
<b>8c</b>		0.10 ± 0.06	0.02 ± 0.01
<b>8d</b>		0.28 ± 0.06	0.06 ± 0.01
<b>8e</b>		0.34 ± 0.08	0.06 ± 0.02
<b>8f</b>		0.12 ± 0.02	0.03 ± 0.004
<b>8g</b>		0.04 ± 0.01	0.007 ± 0.002



#### 4.5 Design of Potent and Cell Permeable Peptidomimetics (MM-101 and MM-102)

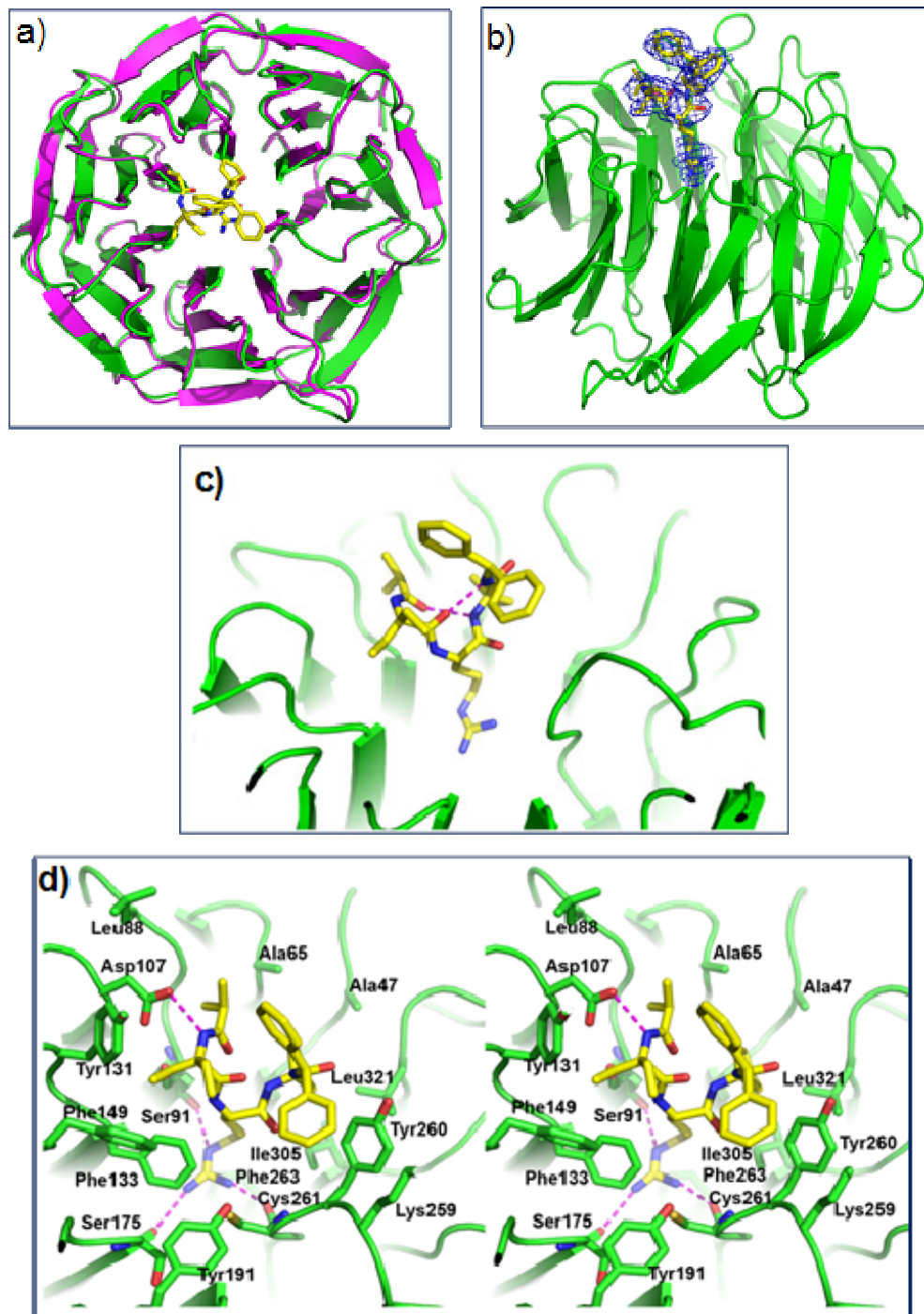
The favorable groups for *N*- and *C*-terminals were combined with those of Ala1 and Ala3 positions to produce a potent peptidomimetic with improved cellular permeability. For *N*- and *C*-terminal modifications isopropyl and biphenylmethyl groups were chosen, respectively, diethyl glycine (Deg) for Ala1 and cycloleucine (CycLeu) for Ala3 positions were preferred. Combination of all the modifications led to design of MM-101 (MLL1 mimetic 101), which binds to WDR5 with an IC<sub>50</sub> value of < 5 nM and a K<sub>i</sub> value of < 1 nM. Moreover, fluoro (MM-102) and chloro (MM-103) analogs were designed, and found that both of the compounds have similar sub-nanomolar binding affinity to WDR5. On the other hand, due to low solubility profile of the chloro analog (MM-103), this compound was not studied further.

Table 14: Structures and binding affinities of MM-101 and analogs.

				
Compound	R <sub>10</sub>	IC <sub>50</sub> ± SD (nM)	K <sub>i</sub> (nM)	P <sub>e</sub> (x10 <sup>-6</sup> cm <sup>2</sup> /s)
MM-101	-H	2.9 ± 1.4	< 1	0.52 ± 0.14
MM-102	-F	2.4 ± 1.7	< 1	0.05 ± 0.01
MM-103	-Cl	4.5 ± 0.6	< 1	ND*
				*Not determined

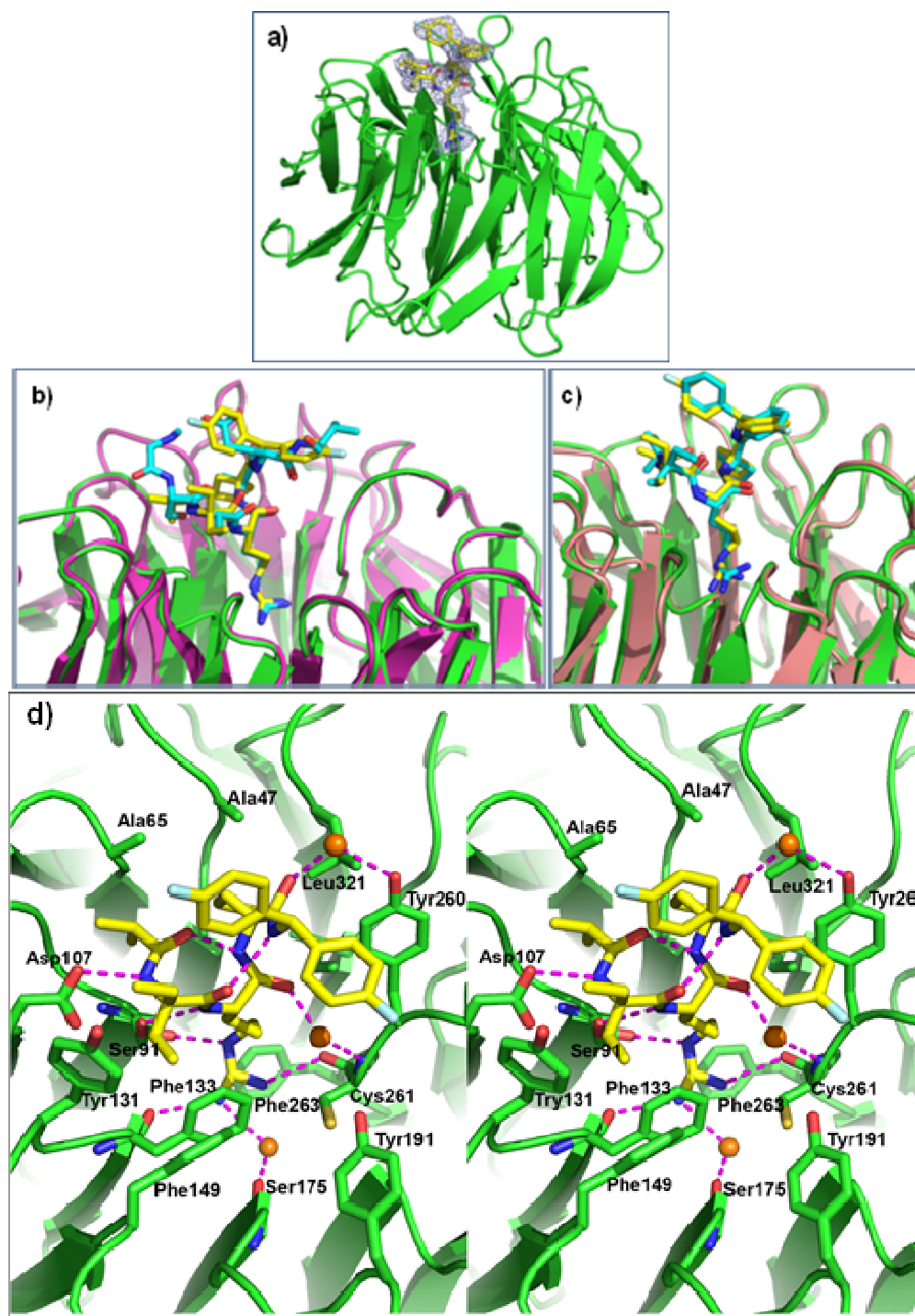
#### 4.6 Determination of Crystal Structures of MM-101 and MM-102 in Complex with WDR5

To provide a structural basis for high affinity binding of MM-101 and MM-102 to WDR5 and for further structure-based optimization, crystal structures of these inhibitors complexed with WDR5 were determined at a resolution of 3.4 Å and 2.6 Å, respectively. As compared to the previously published apo-structure<sup>59</sup>, WDR5 adopts an almost identical configuration, with a RMSD value of 0.58 Å for 303 C $\alpha$  atoms (Figure 14a). Consistent with the design strategy, MM-101 binds to the central channel of the WD40 propeller where MLL1 peptides bind (Figure 14b). Similar to that observed in the WIN peptide two intramolecular hydrogen bonds are formed in MM-101 that stabilizes the molecule in a short  $3_{10}$ -helix conformation (Figure 14c). Interaction network between MM-101 and WDR5 is also similar to that of MLL1 peptides. The Arg side chain of MM-101 penetrates deeply into the central channel of WDR5, and is sandwiched between the two aromatic rings of F133 and F263. The guanidinium group forms hydrogen bonds with the main chain carbonyls of C261, S175 and S91. Additionally, the *N*-terminal amide hydrogen bonds to D107, which has been shown to be a critical residue for binding to WDR5. Besides electrostatic interactions, MM-101 makes extensive hydrophobic packing against hydrophobic pockets surrounded by Y131, F149, F133, Y191, I305, Y260, K259, L88, L321, A47 and A65 from WDR5.



**Figure 14: Crystal structure of WDR5-MM-101 complex.**

WDR5 in the complex is colored in green. Carbon atoms in MM-101 are shown in yellow, nitrogen and oxygen atoms are colored in blue and red, respectively. (a) WDR5 in the complex shows the identical configuration as apo WDR5 (PDB:2H14), colored in magenta. (b) The overall structure of WDR5-MM-101 complex. The electron density ( $2F_o - F_c$ ) map, contoured to  $1\delta$  is shown for MM-101. (c) The MM-101 occupies the same pocket as MLL1 and exhibits a  $3_{10}$ -helical configuration. The intermolecular hydrogen bonds in compound A are shown in magenta dotted lines. (d) Stereo view of the interface between MM-101 (yellow) and WDR5 (green). MM-101 and WDR5 pack across an extensive interface, involving both hydrophobic packing and hydrogen bonds (shown in magenta dotted lines).



**Figure 15: Crystal structure of WDR5-MM-102 complex.**

(a) The overall structure of WDR5-MM-102 complex. WDR5 is colored in green and MM-102 is colored in yellow. The electron density ( $2F_o - F_c$ ) map, contoured to  $1\delta$  is shown for MM-102. (b) MM-102 occupies the same pocket as MLL1 and also exhibits a  $3_{10}$ -helical configuration. MLL1 and WDR5 from WDR5-MLL1 complex (PDB: 3EG6) is shown in cyan and magenta respectively. (c) The comparison of MM-101 and MM-102 in WDR5 complexes. In WDR5-MM-102 complex, WDR5 is colored in green and MM-102 is colored in yellow. In WDR5-MM-101 complex, WDR5 is colored in salmon and MM-101 is in cyan. (d) Stereo view of the interface between compound MM-102 (yellow) and WDR5 (green). MM-102 and WDR5 pack across an extensive interface, involving both hydrophobic packing and hydrogen bonds (shown in magenta dotted lines). Water molecules are shown in orange spheres.

MM-102 occupies the arginine binding pocket in WDR5 in the same manner as MM-101 and the WIN peptide (Figure 15a). Both backbone and side chain orientations are also very similar to those in the WIN peptide (Figure 15b) and MM-101 (Figure 15c). A higher resolution (2.6 Å) structure of WDR5-MM-102 complex compared to that of WDR5-MM-101 (3.4 Å) reveals the detailed map of the interaction network (Figure 15d). All the nitrogen atoms in the molecule engage in either intra- or intermolecular hydrogen bonds. The *N*-terminal amide nitrogen and the Arg backbone nitrogen interact with D107 and S91, respectively. The guanidino group hydrogen bonds with S91, F133, and C261 directly and with S175 through a water molecule. The remaining amide nitrogen atoms at the *C*-terminal of Arg residue form intramolecular hydrogen bonds, similar to those in WIN peptide and MM-101. Two *C*-terminal main chain carbonyls in MM-102 take part in water-mediated hydrogen bonds with C261 and Y260, while the *N*-terminal carbonyls engage in intramolecular hydrogen bonds. The hydrophobic packing is similar to that of MM-101.

#### **4.7 Conclusion**

The initial modification study described in Chapter 3 revealed that -CO-ARA-NH- in MLL1 is the minimal motif for high affinity binding to WDR5. In this part of the study, the MLL1 binding site in WDR5 was further probed with the goal of establishing an extensive structure activity relationship and obtaining highly potent peptides and peptidomimetics. Therefore modifications on Ala1, Arg2 and Ala3 were performed using both natural and unnatural amino acids. Modifications of Ala1 showed that small hydrophobic residues are preferred for high affinity binding to WDR5 and introduction of an additional methyl group into the *C* $\alpha$  position enhances the binding affinity by >10

times. Of all the residues examined, unnatural amino acids with dimethyl, diethyl or a cyclobutyl group appear to be the best for enhancing the binding affinity. All the modifications on Arg2 residues led to complete loss of the binding affinity, indicating the essential role of this residue. For Ala3, as with Ala1, residues with small hydrophobic groups are also preferred for binding. Residues with an ethyl or a cyclopentyl side chain are the most preferred.

Based upon these SAR data, a number of highly potent peptidomimetics have been designed. These include compounds **6a** and **6d**. Both compounds have IC<sub>50</sub> values of 5 nM with estimated  $K_i$  values of < 1 nM. In direct comparison, **6a** and **6d** are 100 times more potent than the initial Ac-ARA-NH<sub>2</sub> peptide derived from MLL1.

In the next step, efforts were focused on improvement of cellular permeability of these potent peptidomimetics. Both *N*- and *C*-terminal modifications with hydrophobic groups helped not only to improve the permeability but also to increase binding affinity. Therefore, MM-101 and MM-102 were designed by combining the most favorable groups for binding and cell permeability. Consistent with the design, MM-101 has an improved cell-permeability based upon the *in vitro* permeability assay.

Finally, the crystal structures of both MM-101 and MM-102 complexed with WDR5 were determined, and showed that they indeed bind to WDR5 with a similar binding mode as MLL1 peptides. These co-crystal structures also provide the solid foundation for further structure based design to further optimize MM-101/MM-102 toward developing a new class of anticancer therapy for the treatment of acute leukemia harboring MLL1 fusion protein.

## CHAPTER 5

### **Biochemical and Biological Evaluation MLL1-WDR5 Interaction Inhibitors**

In Chapter 4 the design of inhibitors (**6a-6f**, MM-101, MM-102, MM-103) with high binding affinities for WDR5 was described. It is critical to show that binding of these inhibitors to WDR5 can block the interaction between MLL1 and WDR5. Therefore, initially MM-101 and MM-102 were examined whether they inhibit MLL1-WDR5 interaction using recombinant proteins and nuclear fractions of cell lysate, respectively. Next, whether inhibition of MLL1-WDR5 interaction could impair the catalytic activity of MLL1 core complex with MM-101 was addressed. Importantly, selected compounds were analyzed for their inhibition of *HoxA9* and *Meis-1* expression in *MLL1-AF9* transduced murine bone marrow cells and for the inhibition of cell growth in cells with and without MLL1 fusion protein. In order to interpret the experimental results correctly it is essential to show if the selected inhibitors are soluble and stable in the assay conditions. Therefore, initially MM-101 was tested for its solubility and stability.

## **5.1 Solubility Analysis of MM-101**

Thermokinetic solubility of MM-101 in PBS (phosphate buffered saline, pH 7.4) and H<sub>2</sub>O was tested. PBS or H<sub>2</sub>O was added to serial dilutions of MM-101 in DMSO, and shook for 1.5-24 h at room temperature. Absorbance at 485 nm was measured for any precipitation. At 2 mM and lower concentrations the compound is soluble for both solvents. Next 4 mM, 2 mM and 1.5 mM solutions of MM-101 in H<sub>2</sub>O were prepared from powder form, in order to compare the thermokinetic and thermodynamic solubilities of the compound. MM-101 precipitates in both 4 mM and 2 mM H<sub>2</sub>O solutions, while completely dissolves in 1.5 mM solution of H<sub>2</sub>O. Therefore it was concluded that MM-101 has 1.5 mM solubility in H<sub>2</sub>O and this is satisfactory for the experiments described below.

## **5.2 Stability Analysis of MM-101 against Trypsin Degradation**

One of the main disadvantages of peptides for drug development is their susceptibility to proteolytic degradation, which causes their low bioavailability profile. Introducing unnatural amino acids would help to increase peptide stability since the proteases recognizes natural amino acids. To address this issue, MM-101 was tested for its trypsin stability at physiological pH. Trypsin is a serine protease and cleaves peptides from the C-terminus of lysine or arginine residues. Because MM-101 and the analogs described here contain an arginine residue it was important to assess the stability against trypsin degradation. The tested compound, tryptophan (internal standard) and trypsin were incubated in PBS at 37 °C. At the indicated time point a sample from this solution was withdrawn and mixed with equal volume of 20% trifluoroacetic acid to stop the



enzymatic activity of trypsin. This sample was then analyzed with analytical RP-HPLC for AUC using tryptophan as the internal control. Initially ARV (**3c**) peptide was tested as a control since this peptide would be cleaved by trypsin. 100% of ARV is cleaved in 1h showing that trypsin is active under the assay conditions (Figure 16). Next MM-101 was analyzed using the same conditions. Only 20% of MM-101 is cleaved in 24 h (1 day) and 50% of the compound is still stable after 4 days of incubation (Figure 16). This shows that combination of *N*- and *C*-terminal modifications with unnatural amino acids in the molecule improves the enzymatic stability significantly.

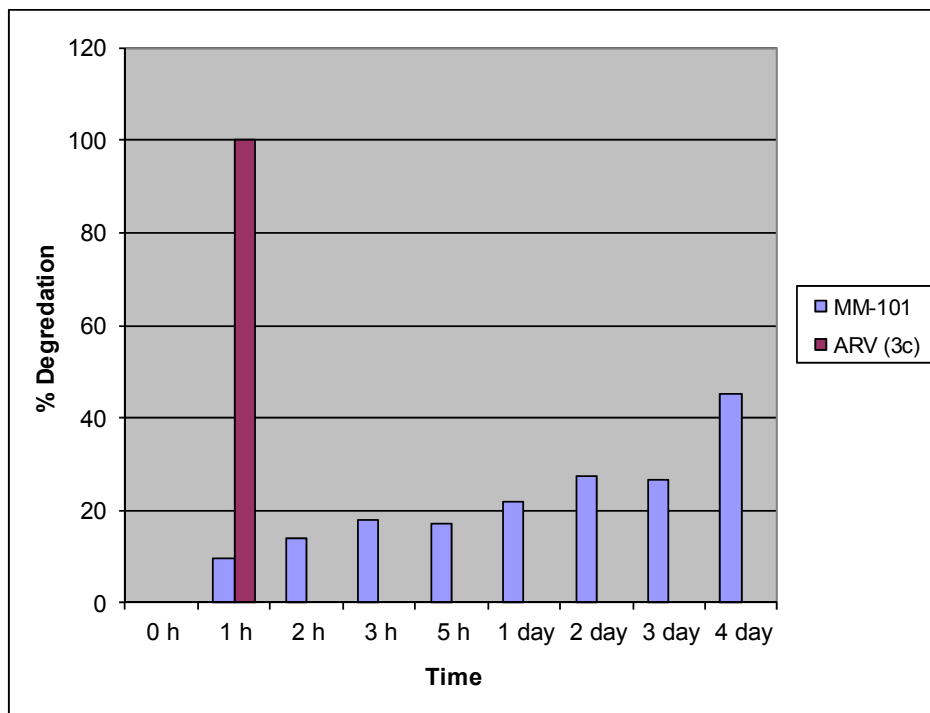


Figure 16: Trypsin stability of MM-101 and ARV peptide.

### 5.3 Stability Analysis of MM-101 in Cell Culture Media

Before testing the inhibitors activity in cell lines, it was important to confirm their stability in culture media used for these cell lines. Therefore three different concentrations (100, 50, 10  $\mu$ M) of MM-101 were incubated in RPMI-1640 media containing 10% fetal bovine serum (FBS) up to 12 days at 37  $^{\circ}$ C. Samples at the indicated time points were analyzed in analytical RP-HPLC. As shown in Figure 17, MM-101 is stable under the assay conditions. No significant decrease in the concentration of MM-101 was observed during the experiment.

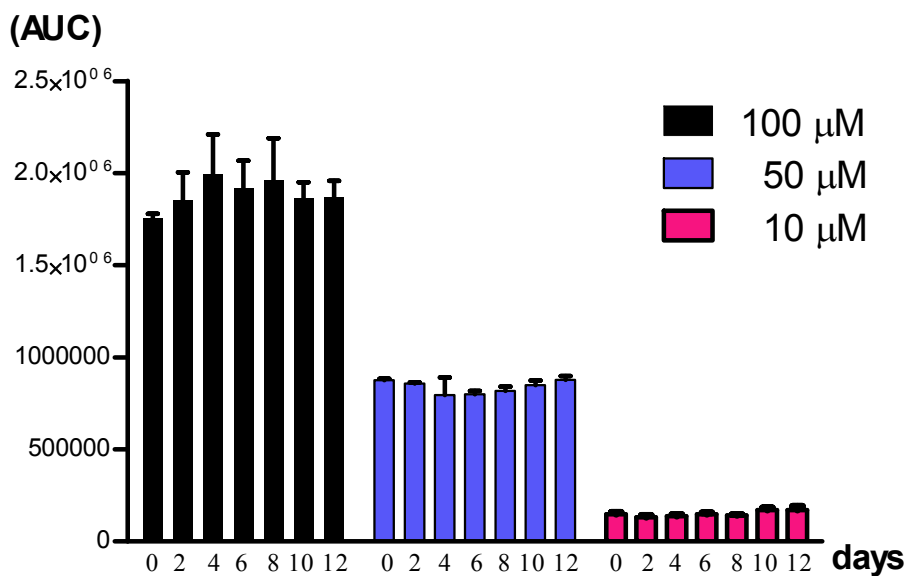
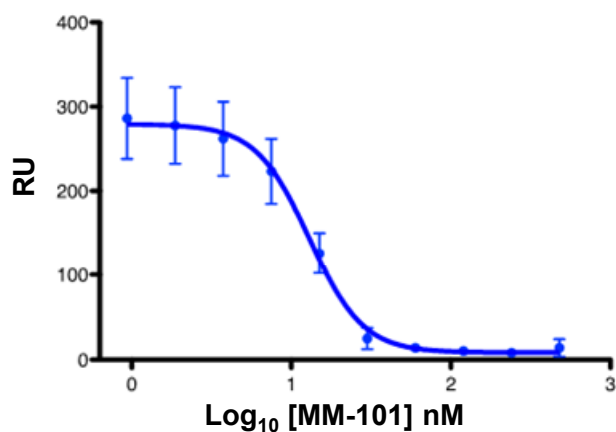


Figure 17: Stability of MM-101 in RPMI-1640 Media measured by analytical RP-HPLC at the indicated time points.

#### 5.4 Inhibition of MLL1-WDR5 Interaction

MM-101 was tested to inhibit MLL1<sup>C</sup>-WDR5 interaction using Biacore assay, which uses Surface Plasmon Resonance (SPR) to monitor the interaction between molecules. MLL1<sup>C</sup> was attached to the sensor chip and WDR5, pre-equilibrated with MM-101, was injected.

MM-101 disrupts the interaction of MLL1<sup>C</sup> and WDR5 in this Biacore assay with an IC<sub>50</sub> of 13 nM (Figure 18), which is in agreement with its binding affinity to WDR5 (IC<sub>50</sub> = 2.9 nM and  $K_i < 1$ ) as measured with the competitive binding assay (Table 14).



**Figure 18: Inhibition curve of MLL1<sup>C</sup> and WDR5 interaction with MM-101 using SPR experiment.**

Next MM-102 activity to block MLL1<sup>C</sup>-WDR5 interaction in the nuclear fractions of cell lysates was analyzed. Flag-WDR5 transduced HEK-293T cells were lysed and

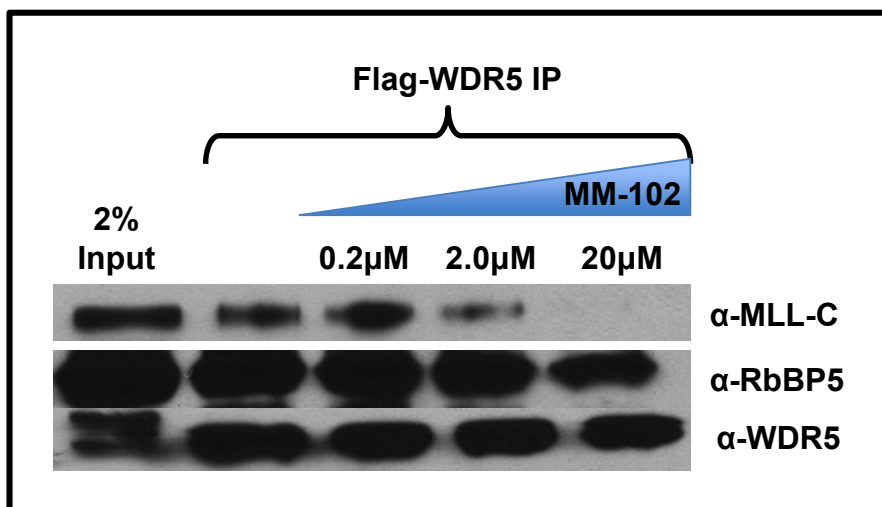


Figure 19: Inhibition of MLL1<sup>C</sup>-WDR5 interaction in HEK-293T nuclear fractions.

fractionated. Nuclear fractions were treated with increasing concentrations of MM-102 and immunoprecipitated with Flag-antibody followed by blotting individually with MLL1<sup>C</sup>, WDR5 or RbBP5 antibodies. As shown in Figure 19, increasing concentrations (i.e. 0.2, 2 and 20 μM) of MM-102 disrupts the interaction of WDR5 with MLL1<sup>C</sup> *in vitro*. However, interaction of WDR5 with RbBP5 is not effected by MM-102, proving that the designed inhibitors are specifically targeting the top binding pocket in WDR5, which is used for MLL1 interaction.

### 5.5 Inhibition of H3K4 Methyltransferase Activity of the MLL1 Core Complex

Since the interaction of WDR5 and MLL1 is critical for H3K4 methyltransferase activity of the MLL1 complex, it was predicted that small-molecule inhibitors designed to block this interaction could effectively inhibit the catalytic activity.

To directly test this hypothesis, a fully reconstituted *in vitro* functional assay was developed using recombinant MLL1<sup>C</sup>, WDR5, RbBP5 and ASH2L proteins to form the core complex, an H3-10mer peptide as the substrate, and radio-labeled <sup>3</sup>H-S-adenosyl methionine as the methyl donor. H3K4 methyltransferase activity is monitored by incorporation of the radioactivity (<sup>3</sup>H-labeled methyl) into Lys4 residue of H3 peptide determined with a scintillation counter. Using this assay, initially the inhibitory activity for a number of compounds with different ranges of binding affinities to WDR5 as determined in the FP-based assay were evaluated. The results are shown in Figure 20.

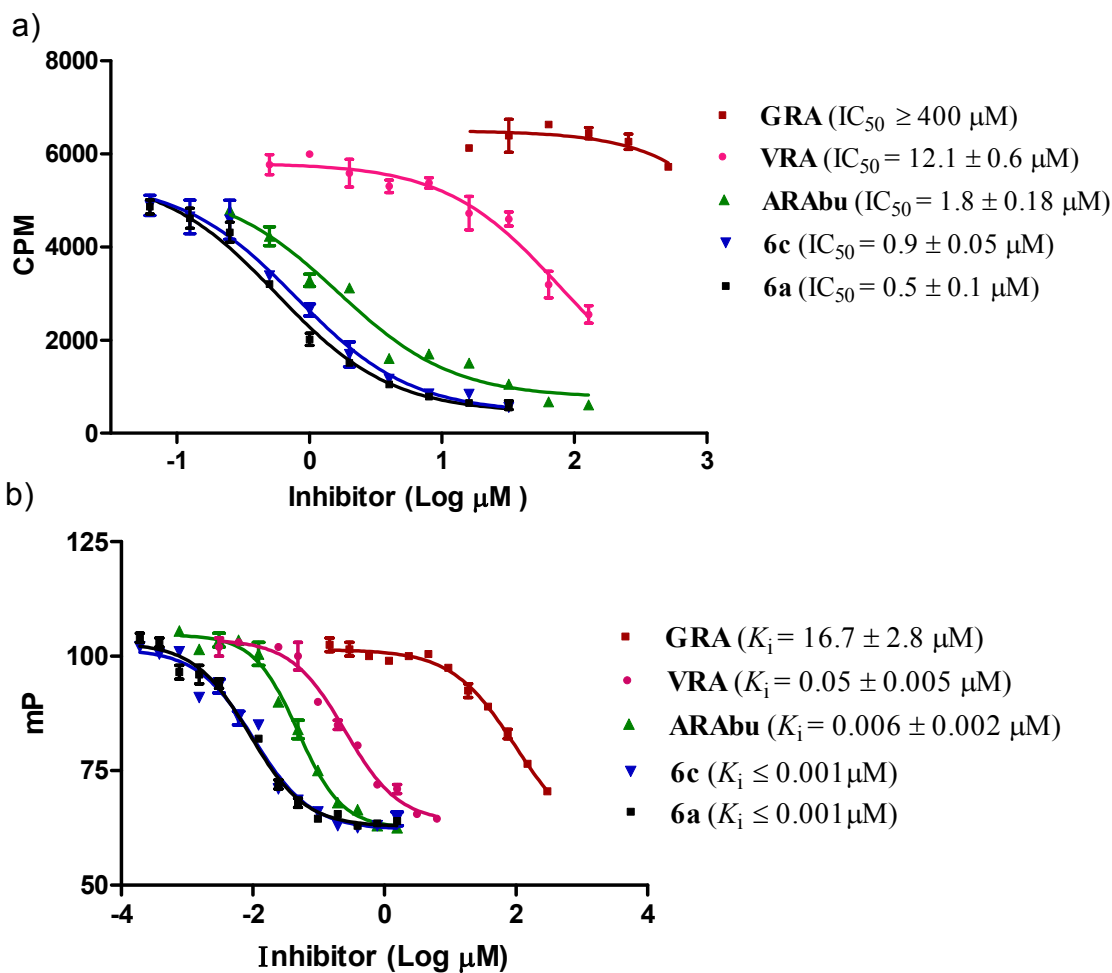


Figure 20: Comparison of activities of selected compounds in HMTase and competitive binding assays. (a) Inhibition of HMTase activity of reconstituted MLL1 core complex as measured with scintillation counter assay in the presence of selected inhibitors. (b) Competitive binding curves of the same inhibitors for WDR5.

Compounds **6a** and **6c**, which have the highest binding affinities to WDR5 ( $IC_{50} = 5$  nM and  $K_i < 1$  nM for both compounds), also show the most potent inhibitory activity in the functional assay with  $IC_{50}$  values of  $0.5$   $\mu$ M and  $0.9$   $\mu$ M, respectively. Compound **3b** (ARAbu), which binds to WDR5 with an  $IC_{50} = 30$  nM ( $K_i = 6$  nM), has an  $IC_{50}$  value of  $1.8$   $\mu$ M to inhibit H3K4 methyltransferase activity of the core complex and is thus 2-3 times less potent than **6a** and **6c**. VRA, which binds to WDR5 with an  $IC_{50}$  value of  $0.24$   $\mu$ M ( $K_i = 0.05$   $\mu$ M), has an  $IC_{50} = 12.1$   $\mu$ M in the functional assay. Finally, GRA, which has an  $IC_{50}$  value of  $77.4$   $\mu$ M to WDR5 ( $K_i = 16.7$   $\mu$ M) in the binding assay, fails to inhibit the HMTase activity at concentrations as high as  $100$   $\mu$ M. Therefore, this data show that peptides or peptidomimetics with high-affinity for WDR5 can effectively inhibit the H3K4 methyltransferase activity of the reconstituted MLL1 core complex in the *in vitro* functional assay. The rank-order of the inhibitory activity of these compounds in the functional assay is in an excellent agreement with that of their affinities to WDR5, as compared in Figure 20a and Figure 20b. Of note, the apparent discrepancy between the  $IC_{50}$  values in the binding and HMTase assays for each compound is due to the fact that 125-fold higher WDR5 protein ( $500$  nM) was used in the functional assay than that ( $4$  nM) in the binding assay.

MM-101 and MM-102 were also tested in this functional assay, and inhibited the HMTase activity of the core complex with  $IC_{50} = 5$  nM and  $3$  nM, respectively.

## 5.6 Inhibition of MLL1 Target Gene Expression

The ability of MM-102 to inhibit expression of *HoxA9* and *Meis-1*, two key genes regulated by MLL1 activity, was investigated. *MLL1-AF9* transduced murine bone marrow cells were treated with MM-102 for 7 days, followed by gene expression analysis with qRT-PCR. Results are shown in Figure 21. *HoxA9* expression decreases with MM-102 treatment in a dose dependent manner. Approximately 40% and 60% reduction in gene expression was observed with 25 and 50  $\mu$ M, respectively, when compared with the non-treated (NT) control. A decrease in *HoxA9* expression with DMSO treatment was

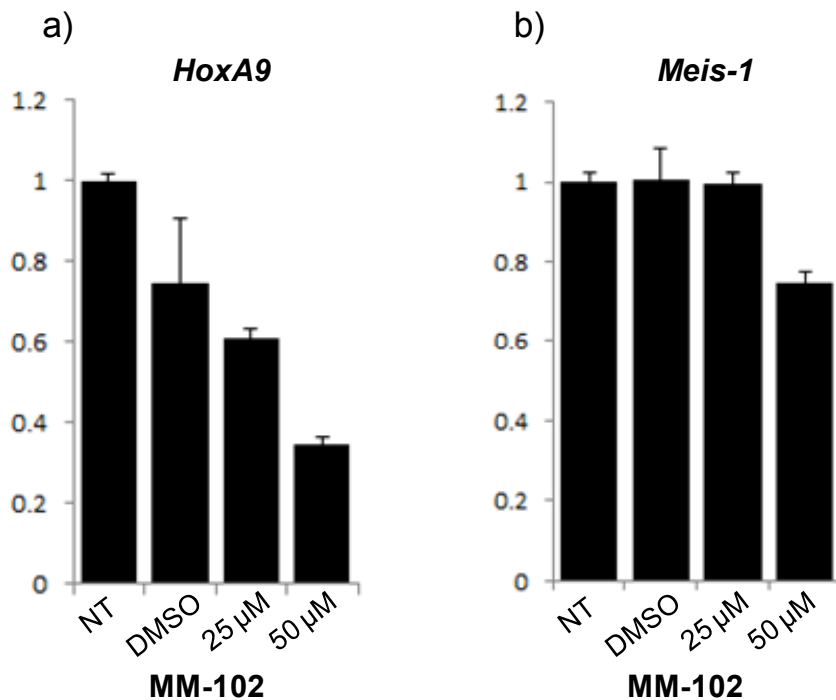


Figure 21: qRT-PCR analysis of *MLL1-AF9* transduced cells upon MM-102 treatment.

observed in the experiment shown in Figure 21a. This observation is due to high error bar and was not observed in an independent experiment. *Meis-1* expression decreases moderately with the highest concentration (50  $\mu$ M) of MM-102 treatment (Figure 21b).

MM-101 was also tested in the same assay. However, no significant inhibition of gene expression was observed, which might be due to lower permeability profile of the compound and therefore not selected for further studies.

These data show that MM-102 can reduce expression levels of two critical MLL1 target genes required for leukemogenesis, strongly supporting the hypothesis that inhibition of MLL1-WDR5 interaction can be used to regulate expression levels of MLL1 target genes.

## 5.7 Inhibition of Cell Growth

*HoxA9* expression is essential for the self-renewal of both hematopoietic stem cells and leukemia cells. shRNA knockdown of *HoxA9* in a panel of acute leukemia cell lines with and without MLL1 fusion proteins has been shown to differentially inhibit growth of cells with MLL1 translocation.<sup>66</sup> Therefore, it was predicted that growth of cell lines with chimeric MLL1 proteins would be inhibited with MM-102. Leukemia cell lines with MLL1 fusion proteins, MV4:11 and KOPN8, or without MLL1 fusion proteins, K562, were treated with MM-102 for 2, 4 or 7 days. Cell growth inhibition was analyzed with CellTiter-Glo® Luminescent Cell Viability Assay. As shown in Figure 22, MM-102

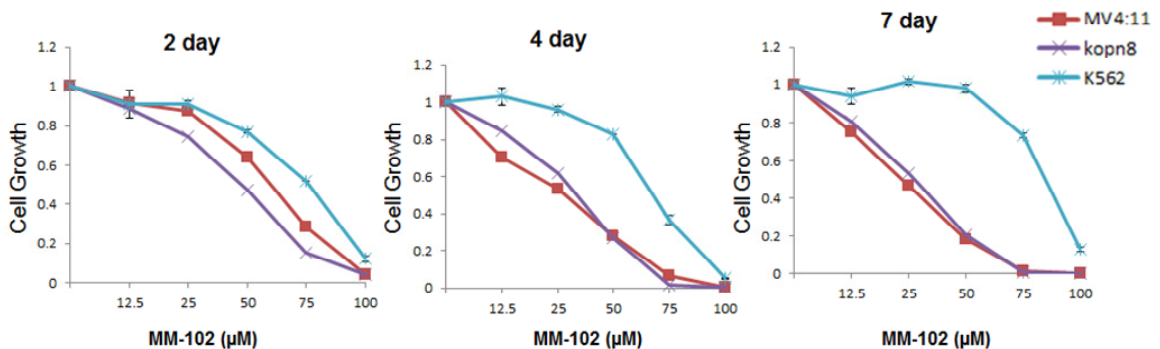


Figure 22: Growth inhibition of selected leukemia cell lines with MM-102 normalized to DMSO control.



differentially inhibits growth of MV4:11 and KOPN8 cells in time and dose dependent manners when compared to that of K562 cells. These findings suggest that the selective inhibition of cell growth with MM-102 is through targeting function of MLL1 activity.

## 5.8 Conclusion

This part of the study is aimed to investigate whether the inhibitors that can block MLL1-WDR5 interaction can successfully downregulate expression of crucial MLL1 target genes, *HoxA9* and *Meis-1*, and selectively inhibit self-renewal of leukemia cell lines with MLL1 fusion proteins. MM-101 and MM-102 was selected for these studies. Before testing the inhibitors in cellular and cell free assays, it was necessary to show if they are soluble and stable under the assay conditions. Therefore, MM-101 was tested for thermodynamic and thermokinetic solubility and found to have over 1 mM solubility, which is sufficient for the studies described here. Significant improvement with MM-101 against trypsin stability was observed when compared to ARV peptide showing the success of peptidomimetic design in this study.

Next, the hypothesis to inhibit MLL1 fusion protein activity in leukemia through blocking the wild-type MLL1 activity and inhibiting MLL1-WDR5 interaction was tested. Initially, inhibition of protein-protein interaction in *in vitro* systems was investigated. MM-101 can block recombinant MLL1<sup>C</sup>-WDR5 interaction with an IC<sub>50</sub> of 13 nM and MM-102 prevents MLL1<sup>C</sup> binding to WDR5 in nuclear fractions of HEK-293T. Moreover, association of WDR5 with RbBP5 is not effected by MM-102, showing the specific binding of the designed compounds to MLL1 binding pocket, consistent with the crystal structure analysis.

To determine if compounds that bind to WDR5 protein with high affinities in the FP-based competitive binding assays will effectively inhibit the H3K4 methyltransferase activity of MLL1, a fully reconstituted *in vitro* functional assay have been developed and optimized using recombinant MLL1, WDR5, RbBP5 and ASH2L proteins, a H3 peptide, and a radio-labeled co-factor <sup>3</sup>H-S-adenosyl methionine. Using this functional assay, the inhibitory activities of several peptides and peptidomimetics with a large range of binding affinities to WRD5 were evaluated. These experiments showed that peptides and peptidomimetics with high binding affinities to WDR5 can indeed effectively inhibit the MLL1 H3K4 methyltransferase activity in this fully reconstituted functional assay, while compounds with lower binding affinities show less potent activity. Furthermore, their rank-order in inhibition of the MLL1 methyltransferase activity in the functional assay for these compounds is in a good agreement with that obtained from the WDR5 binding assay.

Analysis of *HoxA9* and *Meis-1* expression in *MLL1-AF9* transduced murine bone marrow cells treated with MM-102 revealed that expression of *HoxA9* can be reduced with the inhibitor significantly (60%), while a moderate decrease is observed for *Meis-1* expression (20%). These data show that MM-102 can reduce expression levels of two critical MLL1 target genes required for leukemogenesis, strongly supporting the hypothesis that inhibition of MLL1-WDR5 interaction can be used to regulate expression levels of MLL1 target genes. However, lack of effect with MM-101 in the same conditions suggests that MM-101 has lower cellular permeability compared to MM-102.

The specificity of MM-102 to inhibit cell growth in AML and ALL cell lines with and without MLL1 translocation was evaluated. MV4:11 and KOPN8 cell lines, with

MLL1-AF4 and MLL1-ENL fusion proteins respectively, are more sensitive to MM-102 when compared with K562 cell line without MLL1 abnormality and the differential effect appears after 4 day treatment.

## CHAPTER 6

### Summary and Future Directions

#### 6.1 Rationale and Design of the Study

Acute leukemia is a disease of the hematopoietic system characterized by abnormal proliferation of immature white blood cells (leukocytes) which do not execute their normal function. MLL1, a protein associated with leukemogenesis, is one of the most frequently misregulated proteins in acute leukemia. Translocations of the chromosome 11q23 lead to highly leukemogenic chimeric MLL1 proteins, which exert their function through upregulation of *HoxA9* and *Meis-1* genes.<sup>9,10</sup> The HoxA9 protein induces self-renewal of leukemic stem cells, and Meis-1 is a co-factor for HoxA9 function.<sup>4,5</sup> Recent research has shown the significance of co-expression of wild type MLL1 with MLL1 fusion protein in leukemogenesis<sup>53</sup> and accordingly, the research described here had the aim of suppressing the MLL1 function in leukemia by targeting the catalytic activity of wild type MLL1 (Figure 23). Our hypothesis was that blocking MLL1-WDR5 interaction could inhibit H3K4 methyltransferase activity of MLL1, resulting in decrease in target gene expression. Downregulation of *HoxA9* and *Meis-1* would suppress self-renewal and induce differentiation of the leukemia cells, which eventually inhibit transforming capacity of the leukemia cells.

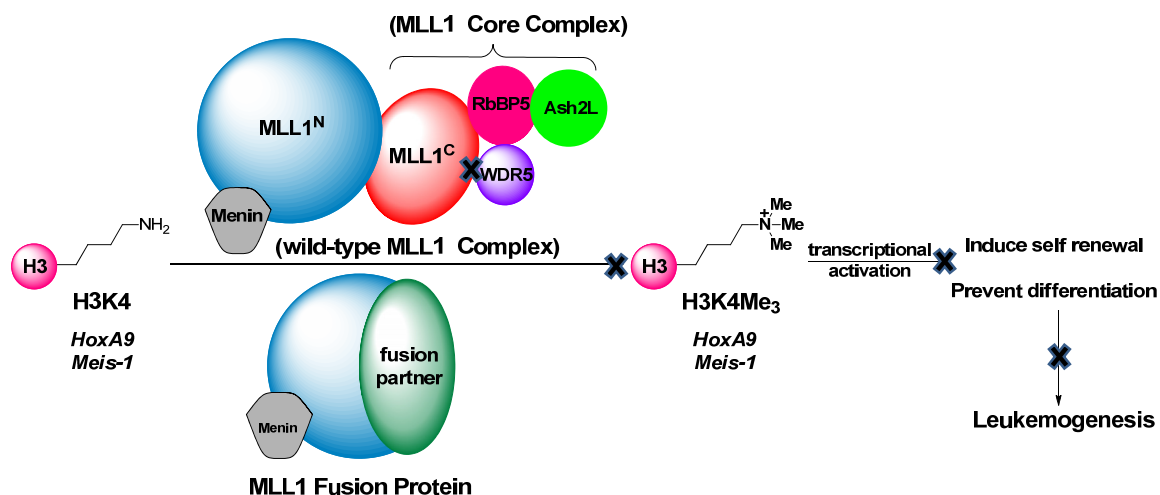


Figure 23: The strategy and rationale to inhibit the function of the MLL1 fusion protein in leukemogenesis.

To design potent MLL1 mimetics, inhibitors of MLL1-WDR5 interaction, the 12mer WIN peptide was used as a starting point. The minimal structure required for interaction with the top binding site of WDR5 was investigated and the tripeptide motif -CO-ARA-NH- was identified as the minimal motif necessary for high affinity binding to WDR5. A modification study was performed using Ac-ARA-NH<sub>2</sub>, a peptide that contains this minimal motif. Modifications at the arginine site invariably resulted in complete loss of binding, and were therefore not pursued. Both alanine residues were replaced with polar and hydrophobic amino acids of increasing size and it was found that small hydrophobic amino acids at these positions are preferred for ligand binding to WDR5 and unnatural amino acids with constrained side chains at the Ala1 and Ala3 positions were also analyzed. Combination of the most favorable groups led to the design of peptidomimetics which have sub-nanomolar  $K_i$  for WDR5 and block the catalytic activity of MLL1 core complex in a functional assay. Efforts to improve the permeability and cellular function of the inhibitors by substituting *N*- and *C*-terminal of the peptidomimetics with hydrophobic groups led to the design of two lead compounds,

MM-101 and MM-102. Crystal structure information confirmed that the compounds bind to the top binding pocket in WDR5 and provided information for the structure based design of further generations of inhibitors. Both MM-101 and MM-102 inhibit the interaction of MLL1<sup>C</sup> with WDR5 and the catalytic activity of the core complex *in vitro*. Two subsequent questions were addressed; can inhibition of MLL1-WDR5 interaction suppress *HoxA9* and *Meis-1* expression and is it capable of inhibiting self-renewal of the leukemia cells? It was successfully shown that MM-102 decreases expression of both *HoxA9* and *Meis-1* in *MLL1-AF9* transduced bone marrow cells and differentially inhibits growth of cells with MLL1 fusion protein.

## **6.2 Significance of the Study**

This research validates a new target in leukemia therapy; compounds with high binding affinities for WDR5 can block the MLL1 binding to WDR5 and can inhibit the catalytic activity of MLL1 core complex leading to reduction in target gene expression and inhibition of growth of cells expressing MLL1 fusion proteins. These findings strongly suggest that small-molecule inhibitors of WDR5-MLL1 interaction can block the misregulated cellular function of MLL1. Therefore, targeting MLL1-WDR5 interaction has the potential to develop a new class of therapy for the treatment of leukemia and other types of cancer, in which MLL1 activity plays a role.

This study showed for the first time, that a potent inhibitor of the MLL1-WDR5 interaction can reduce the expression of *HoxA9* and *Meis-1*, and can selectively inhibit growth of cells with MLL1 fusion proteins. These findings support the earlier studies suggesting the essential role of wild type MLL1 in the function of MLL1 fusion proteins.<sup>52,53</sup>

SAR studies and crystal structure information of inhibitor-WDR5 complexes revealed a detailed map of ligand-WDR5 interaction. Therefore this study can be the basis for the development of non-peptidic small molecule inhibitors of MLL1-WDR5 interaction.

### 6.3 Future Directions

#### Improving Cellular Permeability of the MLL1 Mimetics

In an FP-based competitive binding assay, both MM-101 and MM-102 have sub-nanomolar affinities for WDR5, and the latter inhibits MLL1<sup>C</sup>-WDR5 interaction with  $K_i = 13$  nM. However, 25-50  $\mu$ M of MM-102 is required to inhibit *HoxA9* expression and no inhibition was observed with MM-101 at the same concentrations. These observations suggest that those designed MLL1 mimetics may suffer from low cellular permeability, a common problem of peptide-based inhibitors stemming from the amide bonds they contain. Peptides make extensive hydrogen bonding with the surrounding water through their amide bonds resulting in high energy cost for desolvation during membrane transport. Cyclization constrains such molecules and promotes intramolecular hydrogen bond formation, which would decrease the interaction with the surrounding water. Moreover, the number and the polarity of amide bonds can be decreased to improve permeability. Methylation of the backbone nitrogen atoms has been shown to contribute to the permeability and it is also possible to replace the amide bond with isosteres. In addition to their contribution to permeability these proposed modifications would be expected to enhance the resistance to metabolism of MLL1-mimetics.

Non-peptidic small molecules are less susceptible to permeability and metabolism problems. As shown in Chapter 4, high affinity binding to WDR5 requires extensive

interaction with the protein and these interactions must be considered when designing small molecule non-peptidic inhibitors.

### **Further Studies to Support the Target Validation**

- **H3K4 methylation of target genes:** Although MM-102 was shown to inhibit *HoxA9* expression, it is necessary to show that this effect is due to specifically inhibition of H3K4 methyltransferase activity of the wild type MLL1 in cells. The CHIP assay could be used to detect the change in H3K4Me<sub>3</sub> levels of *HoxA9* loci in response to MM-102 treatment.
- **Differentiation:** *HoxA9* prevents differentiation and induces self-renewal in leukemic cells. Therefore, whether the decrease in *HoxA9* level with MLL1 mimetics could lead to cell differentiation can be addressed.
- **Testing MLL1-Mimetics in animal models:** A next step would be testing cell permeable and metabolically stable potent MLL1 mimetics in animal leukemia models both to prevent onset of the disease and to develop a treatment for the disease.
- **Effects of MLL1-Mimetics on the other targets:** Although the critical role of WDR5 in MLL1 complex is well established, its role in other H3K4 methyltransferases has not been studied in detail. Similar to MLL1, the MLL2-4 and hSet1a/b enzymes form a complex with WDR5, RbBP5 and ASH2L and it is essential to address the effect of MLL1 mimetics on the activity of these enzymes. WDR5 has been shown to be involved in the larger MLL1-MOF protein complex. MOF acetylates H4K16, which is a histone modification critical for *HoxA9* expression, and MLL1 has been shown to be essential for this activity. MLL1



mimetics could be used to investigate the role of WDR5 and/or the MLL1-WDR5 interaction in the MLL1-MOF complex.

### **Alternative Targets to Suppress MLL1 Activity in Leukemia**

The catalytic activity of wild-type MLL1 can be also targeted through RbBP5 or ASH2L both of which are necessary for the activity. The interaction surfaces between WDR5 and RbBP5, RbBP5 and ASH2L, MLL1 and RbBP5 are all potential sites for the inhibitor design. Alternatively, catalytic activity of MLL1 could be blocked through inhibiting the H3 substrate or *S*-adenosyl methionine (SAM) binding to the SET domain. Mimetics of substrate or cofactor could be designed based on the crystal structure of MLL1 SET domain in complex with H3 peptide and *S*-adenosyl homocysteine (SAH).<sup>67</sup> However, mimetics of SAM would lack in specificity since all the other methyltransferases use the same cofactor. In order to achieve specificity, compounds containing both the substrate and cofactor moieties could be designed based on the crystal structure information of MLL1 SET domain.

Another approach for targeting wild type MLL1 activity could be inhibition of the proteolytic cleavage of MLL1 by Taspase 1 whose crystal structure is known.<sup>68</sup> However, there are other substrates for Taspase 1 and thus, blocking MLL1 cleavage by Taspase 1 will probably be an approach lacking in specificity.

Alternatively, MLL1 fusion protein activity could be targeted. It has been shown that several MLL1 fusion proteins associate with Dot1L, the only known H3K79 methyltransferase, and recruit Dot1L to up-regulate *HoxA9* expression. Successful inhibition of MLL1 fusion protein activity in model cells and cell lines with a Dot1L inhibitor has already been demonstrated.<sup>69</sup>

Targeting both the wild-type and fusion proteins of MLL1 through their interaction with Menin could be another approach. Menin is a critical binding partner of MLL1<sup>N</sup> and is essential for *HoxA9* expression.<sup>70</sup> Menin interacts with *N*-terminus of MLL1 and this interaction is preserved within the fusion proteins.<sup>30,71</sup> Therefore, dual targeting of MLL1 could be achieved and this would lead to a robust inhibition compared to the inhibition achieved by targeting only wild type or fusion protein activity.

Inhibition of the interaction of HoxA9 with DNA is another approach. HoxA9 uses a hexapeptide to interact with the minor groove and this hexapeptide might be starting point of another class of inhibitors.<sup>72</sup>

## Appendices

## Appendix A

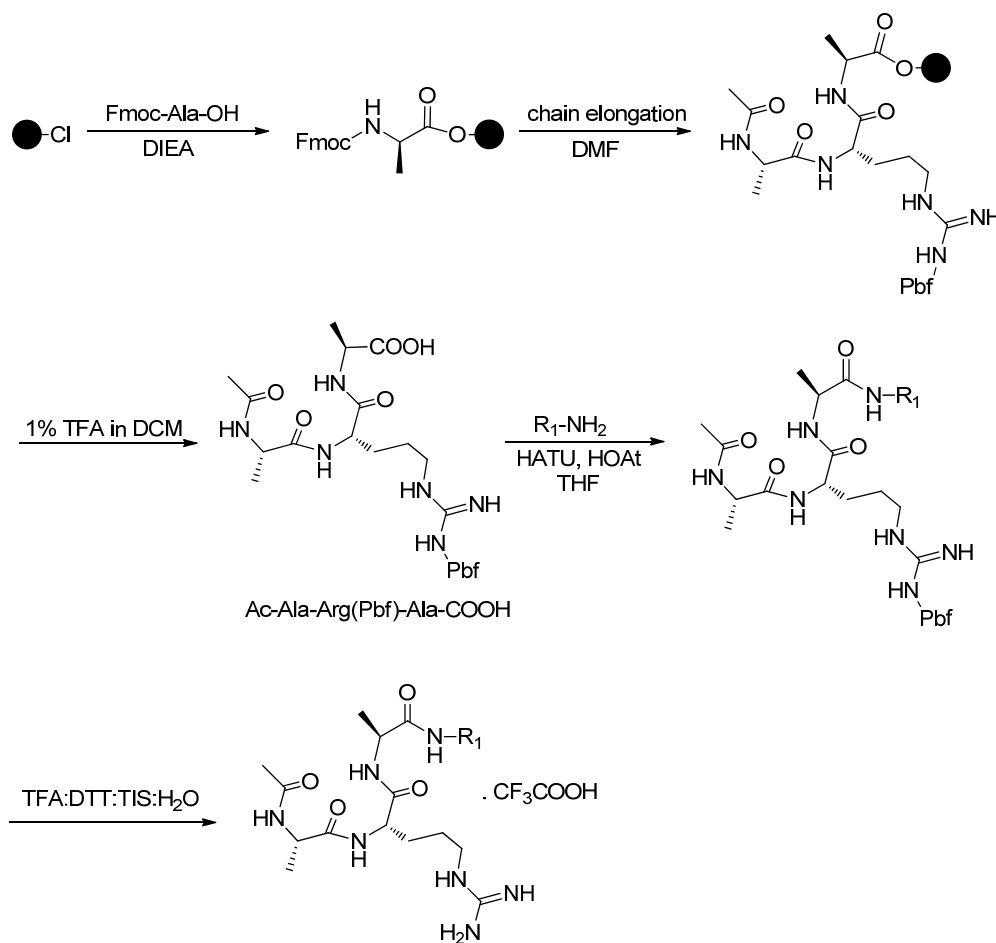
### Experimental

#### 1) Solid Phase Synthesis of the Peptides

Peptides were synthesized manually or with an ABI 433 peptide synthesizer using Fmoc chemistry. Rink amide resin was used as the solid support. To avoid side reactions, amino acid residues were protected as follows: Glu (OtBu), His (Trt), Lys (Boc or Mtt), Gln (Trt), Arg (Pbf), Ser (OtBu), Thr (OtBu). HOBt/HBTU or DIC/HOAt was used as the coupling reagent. HCOOH/DIC/HOAt in DMF was used for on-bead formylation where the reaction was carried out in a flask rotated overnight at room temperature using rotavapor without applying vacuum. All the peptides were cleaved from the resin using a TFA:DTT:TIS:H<sub>2</sub>O (17.5ml:0.5g:0.5ml:1ml) cleavage cocktail which also led to removal of the protecting groups. The cleavage solution was evaporated and the crude product was precipitated with diethyl ether followed by HPLC purification using a C18 reversed phase column (Waters, Sunfire Prep C18, 19 mm × 150 mm, 5 μm). All the purified final peptides were analyzed by analytical RP-HPLC (Waters, Sunfire C18, 4.6 mm × 150 mm, 5 μm) for purity, and the characterization of the peptides was determined by electrospray ionization mass spectroscopy (ESI-MS).

## 2) Synthesis of C-terminally Modified Compounds ( $\Delta$ 2a-b, 8a-g)

Ac-Ala-Arg(Pbf)-Ala-COOH peptide was synthesized using Fmoc-solid phase chemistry and 2-chlorotrityl chloride resin as the solid support (Scheme 1). Fmoc-Ala-OH (3 eq.) was loaded overnight in dichloromethane and in the presence of 3 eq. DIEA. Then, methanol was added to this mixture to and shaken for 30 min to endcap unreacted 2-chlorotrityl group. Next, classical chain elongation was carried out with Fmoc chemistry. The carboxylic acid intermediate was cleaved from the resin by treatment with

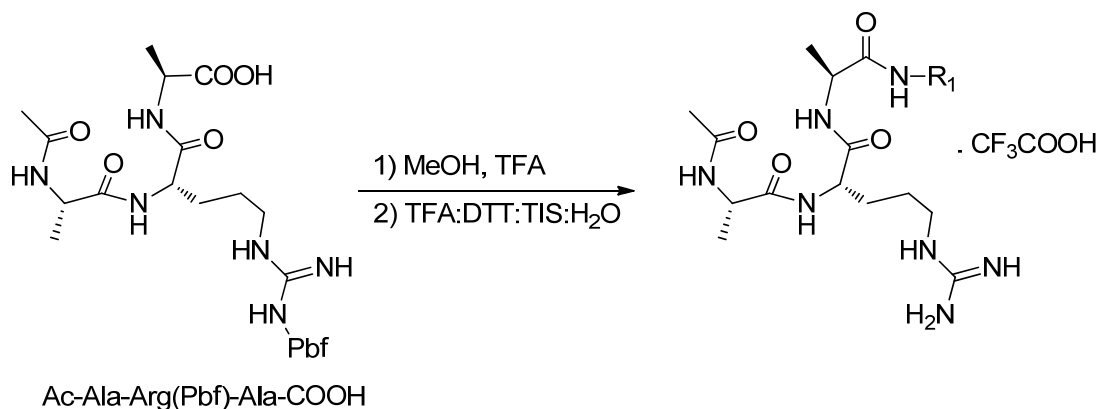


Scheme 1: Synthesis of C-terminally modified peptides.

4 ml of 1% trifluoroacetic acid in dichloromethane (3×10 min). The filtrate was evaporated and purified over the HPLC using the C18 reverse phase column. The Ac-

AR(Pbf)A-COOH (0.2 mmol) was dissolved in 10 ml of THF, and 3 eq. HATU, 3 eq. HOAt, 5 eq. DIEA, and 3 eq. of the corresponding amine was added. The reaction mixture was stirred at room temperature for 24h, the solvent was evaporated and the crude product was purified by RP-HPLC. The Pbf protected group from the arginine was removed by treatment with the cleavage cocktail TFA:DTT:TIS:H<sub>2</sub>O (17.5ml:0.5g:0.5ml:1ml), followed by HPLC purification (Waters, Sunfire™ Prep C18, 19×150 mm, 5 μm).

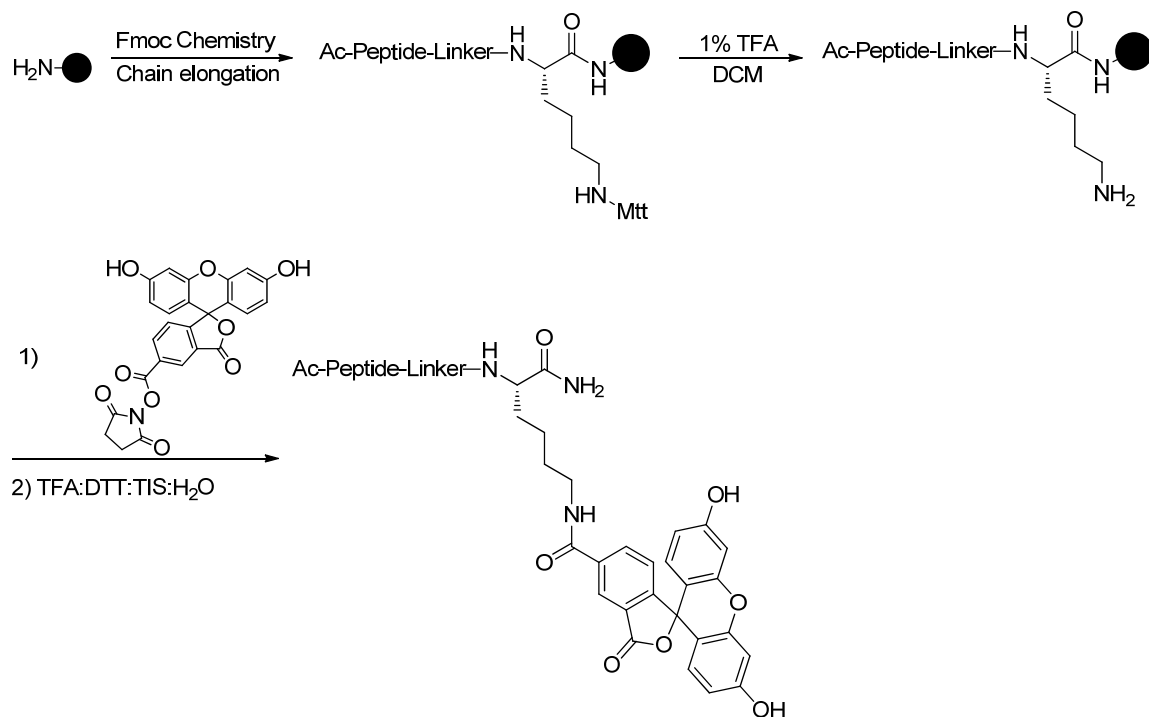
### 3) Synthesis of Δ2c



Scheme 2: Synthesis of Δ2c

The Ac-AR(Pbf)A-COOH intermediate (0.2 mmol) was dissolved in absolute methanol, and 0.5 ml of trifluoroacetic acid was added. The reaction mixture was stirred at room temperature for three days, the solvent was evaporated, and the Pbf protecting group was removed by treatment with the cleavage cocktail to give the final product which was purified by RP-HPLC (Waters, Sunfire™ Prep C18, 19×150 mm, 5 μm).

#### 4) Synthesis of the Tracers



**Scheme 3: Synthesis of the tracers**

The peptide was synthesized as described above with an Mtt protecting group on the C-terminal lysine residue. The fluorescein label, 5-FAM, was introduced to the side chain of C-terminal lysine group by removal of the Mtt protecting group with 5 ml of 1% trifluoroacetic acid in dichloromethane (4 × 10 min) followed by overnight treatment with 1.5 eq. of 5-carboxy fluorescein succinimide ester (5-FAM, SE) and 4 eq. of DIEA. The peptide was cleaved from the resin and purified over HPLC as described above.

#### 5) Binding Assay

All the FP-based experiments were performed in Microfluor 2 Black, “U” Bottom, 96-well microtiter plates (Thermo Scientific) and FP was measured as mP units in a microplate reader (Tecan Ultra) with excitation at 485 nm and emission at 530 nm.

The  $K_d$  of the tracers and the  $IC_{50}$  value of the inhibitors were calculated using GraphPad Prism 4 software.

**a) Protein Expression and Purification for the Binding Assay (by Elizabeth C. Townsend)**

*N*-terminal His-tagged WDR5 $\Delta$ 23 (residues 24-334) was cloned into pET28A-MHL vector by ligation independent cloning. This construct was gifted by A. Ruthenburg.<sup>65</sup> It was expressed in Rosetta2-(DE3) pLysS cells (Novagen). Cells were grown to  $OD_{600}=0.4-0.6$  in 4 L of 2XTY at 30 °C, induced with 0.1mM IPTG at 16 °C for 16h and harvested in 20 mM HEPES pH 7.5, 500 mM KCl, 10% glycerol, 0.1 mg/ml PMSF, and 0.05% NP40. Cells were lysed by addition of 0.2 mg/ml hen egg white lysozyme followed by sonication and clarification (by centrifuging for 30 min at 15000 rpm). The resin was washed 3 times for 10 min with 40 ml of lysis buffer. His-WDR5 $\Delta$ 23 was eluted from the resin by 315 min elutions with 20 mM HEPES pH 7.5, 100 mM KCl, 10% glycerol, 250 mM imidazole, pH 7.5. Eluates were clarified by centrifugation at 2000 rpm for 1 min, syringe-filtered through a 0.45  $\mu$ M membrane (Millipore), and then loaded onto two 5 ml SP-Sepharose Hi-Trap columns using the AKTA purifier (GE Healthcare). Fractions were eluted in 20 mM HEPES pH 7.5, 10% glycerol with a KCl gradient from 0 to 1000 mM, and peak fractions were pooled and concentrated to 64  $\mu$ M using an Amicon Ultra centrifugal filter, 10000 MWCO (Amicon). Concentrated protein was aliquoted and samples were frozen on dry ice and stored at -80 °C.



**b) Saturation Binding Experiment to Determine Dissociation Constant ( $K_d$ ) of the Tracers**

To dilutions of WDR5 $\Delta$ 23 (2.2-0  $\mu$ M) in 100  $\mu$ l of assay buffer (0.1 M phosphate, 25 mM KCl, 0.01% Triton, pH 6.5), 20  $\mu$ l of a fixed concentration of the tracer in the assay buffer was added, followed by an addition of 5  $\mu$ l of DMSO to give 125  $\mu$ l of total volume. Each assay had two controls: blank (without protein and tracer) and tracer only (without protein). The plates were incubated on a shaker at room temperature to reach equilibrium, and mP values were measured at the 3 h time point.

**c) Competitive Binding Experiments**

A preincubated complex solution of WDR5 $\Delta$ 23 and the tracer in 120  $\mu$ l of assay buffer were added to dilutions of the test compound in 5  $\mu$ l of DMSO, giving final concentrations of WDR5 $\Delta$ 23 and the tracer of 4 and 0.6 nM, respectively. Three control wells were included in each plate: blank (without protein and tracer), 100% inhibition (tracer only), and 0% inhibition (complex solution only). The plates were incubated with shaking at room temperature. The mP values were measured after five hours of incubation, and  $K_i$  values were calculated using the equation described previously.<sup>62</sup>

**6) Molecular Dynamics (MD) Simulation (by Denzil Bernard, Ph.D.)**

The crystal structure of WDR5 in complex with the WIN peptide (PDB: 3EG6) was used to construct the models of the peptides using Sybyl (Tripos, Inc.) with minimization of any mutation introduced. MD simulations were performed with Amber for 3 ns using explicit TIP3P solvent. After initial minimization of the solvent, the system was further relaxed with constraints on the backbone before final minimization. MD simulations involved a gradual increase in temperature to 300 K over 30 ps, while holding the solute constrained, followed by another 30 ps of simulation with the

constraint only on the backbone. Further equilibration was performed for 40 ps before the production run. SHAKE was applied to all bonds involving hydrogen atoms to permit a time step of 0.002 ps. Structures were saved every 1 ps for analysis.

### 7) Parallel Artificial Membrane Permeability Assay (PAMPA) (by Liu Liu, Ph.D.)

1% Lecithin solution (w/v) in dodecane was prepared and sonicated for 1 min with Fisher/Branson 500 probe sonicator to ensure complete dissolution. 5  $\mu$ l of the lecithin/dodecane solution was carefully loaded on the PVDF (polyvinylidene fluoride) filter membrane of each acceptor plate well immediately followed by adding 150  $\mu$ l of PBS (pH = 7.4) to each well of the acceptor plate. 300  $\mu$ l of compound solution in PBS was loaded to the PTFE (polytetrafluoroethylene) donor plate in which controls were loaded as well to verify membrane integrity. The complete donor-acceptor assembly was incubated at room temperature for 16h in sealed container with humidity controlled. After incubation, concentrations of compounds and controls in both the donor and acceptor plates were determined by UV/Vis absorption spectrometry.  $P_e$  was calculated using the equation below;

$$P_e = \left\{ -\ln \left( 1 - \frac{[drug]_{acceptor}}{[drug]_{equilibrium}} \right) \right\} \times C \text{ where}$$

$$C = \frac{V_D \times V_A}{(V_D + V_A) \times Area \times time}$$

$V_D$  = Volume of donor compartment

$V_A$  = Volume of acceptor compartment

Area = Active surface area of membrane

Time = Incubation time

$[drug]_{acceptor}$  = Conc. of compound in the acceptor compartment after incubation

$[drug]_{equilibrium}$  = Conc. of compound at theoretical equilibrium (the resulting concentration if the donor and acceptor solution were simply mixed)

## **8) Determination of Crystal Structure of MM-101 and MM-102 in Complex with WDR5 (by Yong Chen, Ph.D.)**

### **a) Protein Preparation**

WDR5 ( $\Delta 23aa$ , NP\_060058.1) was cloned into a pET28b-based vector with a 6xHis-SUMO tag fused at the *N*-terminus. *E. coli* BL21(DE3) cells bearing expression plasmids were induced for 16h with 0.1 mM IPTG at 25 °C. The protein was purified by Ni-NTA affinity resin and on-bead digestion using Ulp1 protease, followed by the gel filtration chromatography on HiloadSuperdex 75 equilibrated with 25 mM Tris-HCl pH 8.0 and 150 mM NaCl. The purified protein was concentrated to 30 mg per ml and stored at -80 °C for crystallization.

### **b) Crystallization and Structural Determination**

WDR5-MM-101 binary complex was obtained by mixing WDR5 and MM-101 at molar ratio 1: 3 right before crystallization. The complex was crystallized at 25% PEG 4000, 0.1M sodium acetate, pH 4.6, 0.2M ammonium sulfate. The crystals were harvested in the same buffer with 20% glycerol. The 3.4 Å data set was collected at Advanced Photon Source beamline 21ID-F and was processed by HKL2000.<sup>73</sup> The crystal belongs to P1 space group. The structure was solved by molecular replacement by Phaser<sup>74</sup> using the previously published WDR5 structure (2H14). Iterative cycles of refinement and modeling were carried out using Phenix and Coot.<sup>75,76</sup>

WDR5-MM-102 binary complex was obtained by mixing WDR5 and MM-102 at molar ratio 1: 3 before crystallization. The complex was crystallized at 30% PEG8000, 0.2M ammonium sulfate. The crystals were harvested in the same buffer with 20% glycerol. The 2.6 Å dataset was collected at Advanced Photon Source beamline 21ID-D and was processed by HKL2000. The crystal belongs to P21 space group. The structure

was solved by molecular replacement by Phaser using the previously published WDR5 structure (2H14). There are four WDR5 molecules in one asymmetric unit. Iterative cycles of refinement and modeling were carried out using Phenix and Coot.

**Table 15: Data collection and refinement statistics for WDR5-MM-101 and WDR5-MM-102 complexes by molecular replacement.**

	<b>WDR5-MM-101</b>	<b>WDR5-MM-102</b>
<b>Data collection</b>		
Space group	<i>P</i> 1	<i>P</i> 21
Cell dimensions		
a, b, c (Å)	48.943,105.985, 20.907	48.861,106.478,120.719
$\alpha$ , $\beta$ , $\gamma$ (°)	90.002, 89.758, 90.034	90, 90.352, 90
Wavelength(Å)	0.9785	0.9785
Resolution (Å)	100-3.40	100-2.60
R <sub>merge</sub>	0.08 (0.129)*	0.134 (0.399)*
I / $\sigma$ I	8.0(4.5)	8.0(4.5)
Completeness (%)	90.5(68.9)	93.8(94.2)
Redundancy	1.9(1.8)	2.7(2.3)
<b>Refinement</b>		
Resolution (Å)	48-3.40	48.8-2.6
No. reflections	30243	32146
R <sub>work</sub> / R <sub>free</sub>	19.5/22.6	19.3/24.9
<b>No. Atoms</b>		
Protein	18856	9309
Ligand(165b)	368	192
Water		304
<b>B-factors</b>		
Protein	61.1	26.2
Ligand	52.3	25.9
Water		23.9
<b>r.m.s deviations</b>		
Bond lengths (Å)	0.018	0.008
Bond angles (°)	1.912	1.200

\*Values in parentheses are for highest-resolution shell.

## 9) Solubility Analysis of MM-101

PBS (phosphate buffered saline, pH 7.4) or H<sub>2</sub>O was added to serial dilutions of MM-101 in DMSO and shook for 1.5-24 h at room temperature in 98-well cell culture plates. Absorbance at 485 nm was measured for any precipitation.

## **10) Stability Analysis of MM-101**

### **a) Stability Analysis of MM-101 against Trypsin Degradation**

Tested compound (200  $\mu$ M), tryptophan (200  $\mu$ M) and trypsin (10 nM) were incubated in PBS at 37 °C. At the indicated time point 100  $\mu$ l from this solution was withdrawn and mixed with equal volume of 20% trifluoroacetic acid solution. The sample was analyzed with analytical RP-HPLC for AUC (area under curve) using tryptophan as internal control.

### **b) Stability Analysis of MM-101 in Cell Culture Media**

100, 50 and 10  $\mu$ M solutions of MM-101 were prepared in RPMI-1640 media. The solutions were incubated in a 6-well tissue culture plate for up to 12 days at 37 °C under 5% CO<sub>2</sub>. At the certain time point 200  $\mu$ l of the solution was withdrawn and centrifuged at 13,000 rpm for 5 min at 4 °C to remove serum proteins. The supernatant was collected and analyzed using analytical RP-HPLC for AUC.

## **11) Inhibition of MLL1-WDR5 Interaction (by Elizabeth C. Townsend)**

### **a) Biacore Assay**

Purified MLL1<sup>3762</sup> was immobilized on the CM5 chip (GE Healthcare) using standard amide coupling chemistry. To monitor binding, purified WDR5 was diluted in HBS buffer, 10 mM HEPES pH 7.4, 150 mM NaCl, P20 0.005%, at concentrations ranging from 16 nM to 1000 nM. WDR5 dilutions were injected at a flow rate of 60  $\mu$ l for 120s and allowed to dissociate for 480s. Binding data was fit to the Drifting Fit baseline model using the Bioanalysis software. For inhibition, WDR5 at 60nM was combined with varying concentrations of MM-101, ranging from 0.9 to 240 nM. Dilutions of WDR5 plus inhibitor were injected over the MLL1 chip as in the binding

experiments. Binding was monitored at 110s and plotted against inhibitor concentration using GraphPad Prism 5.0 and fit to determine the IC<sub>50</sub>.

#### **b) FLAG-Immunoprecipitation**

HEK-293T cells, stably transfected with a FLAG-WDR5 construct, were lysed and fractionated according to Dou *et al.*<sup>77</sup> Nuclear fractions were combined with concentrations of MM-102 at 0.2, 2.0 and 20  $\mu$ M and immunoprecipitated using M2 agarose as described.<sup>77</sup> WDR5, RbBP5 and MLL1<sup>C</sup> were detected by western blotting.

### **12) Inhibition of H3K4 Methyltransferase Activity of the MLL1 Core Complex (by Elizabeth C. Townsend)**

#### **a) Protein Expression**

MLL1<sup>3762-C'</sup>, WDR5<sup>23-C'</sup>, RbBP5 and ASH2L<sup>SPRY</sup> were expressed as His-SUMO fusions from the pET28A-SUMO vector (expression vectors were a generous gift from the Lei Lab). Proteins were expressed from BL21 DE3 pLyss codon (+) at 16 °C overnight after induction with 0.1 mM IPTG in mid-log phase of bacterial growth. Cells were harvested and protein was purified by the His-tag on Ni-NTA resin (Qiagen) as described previously. The SUMO tag was removed from RbBP5, ASH2L and MLL1 by incubation with the ULP1 protease at 4 °C overnight. The protease and cleaved SUMO-His tag were collected by batch binding with the Ni-NTA resin for 1h.

#### **b) *In vitro* Methyltransferase Assay**

Assays were performed in 50 mM HEPES pH 7.8, 100 mM NaCl, 1.0 mM EDTA and 5% glycerol at room temperature (approximately 22 °C). Each reaction contained 1.5  $\mu$ Ci of the co-factor, <sup>3</sup>H-S-adenosyl methionine (Perkin Elmer). H3 10mer was used as the substrate at 50  $\mu$ M. Inhibitors were added at concentrations ranging from 0.125-128

$\mu\text{M}$  and incubated with the pre-assembled WDR5, RbBP5, ASH2L complex at a final concentration of  $0.5 \mu\text{M}$ . 3-component complex for 2-5 min. Reactions were initiated by addition of the MLL1<sup>3762-C'</sup> fragment at a final concentration of  $0.5 \mu\text{M}$  and allowed to proceed for 30 min before preparing for scintillation counting. To count samples, reactions were spotted on separate squares of P81 filter paper (Whatman) and precipitated by submerging in freshly prepared 50 mM sodium bicarbonate buffer, pH 9.0. After washing and drying, samples were vortexed in Ultima Gold scintillation fluid and counted. As a negative control, assays were performed using  $0.5 \mu\text{M}$  MLL1 complex assembled with the non-interacting mutant, WDR5<sup>D107A</sup>.

### **13) Inhibition of MLL1 Target Gene Expression (by Fang Cao, Ph.D.)**

#### **qRT-PCR Analysis of *HoxA9* and *Meis-1* Genes**

Total RNA was isolated from *MLL1-AF9* transduced cells using RNEASY® from QIAGEN. 1  $\mu\text{g}$  of total RNA was treated with RNase-free DNase I, and applied for reverse transcription using SuperScript III First-Strand Synthesis system (Invitrogen, Cat18080-051) according to manufacturer's protocol. The resulting cDNA was used as template for PCR amplification of *HoxA9* genes using SYBR PCR kit (Applied Biosystem).

HoxA9-F: ccgggttattgggatcgat,  
HoxA9-R:gcgccttctccgaaaaca,  
Meis-1-F: aaggtgatggcttgacaac,  
Meis-1 R: tgtccaactgcttttctg

#### **14) Inhibition of Cell Growth (by Fang Cao, Ph.D.)**

##### **CellTiter-Glo® Luminescent Cell Viability Assay**

MV4:11, KOPN8, and K562 cells were cultured in RPMI 1640 medium (ATCC) supplemented with 10% fetal bovine serum, 100 U/L penicillin-streptomycin, and incubated at 37 °C under 5% CO<sub>2</sub>. Cells were seeded into 12-well plates for suspension at a density of 5×10<sup>5</sup> per well (1ml) and treated with the following: vehicle control (DMSO), MM-102 for 2, 4, or 7 days. Cells were given fresh medium with each application of the compound every two days.

The CellTiter-Glo® Luminescent Cell Viability Assay kit (Promega) was used following the manufacturer's instruction. 100 µl of the assay reagent was added into each well and the content was mixed for 2 min on an orbital shaker to induce cell lysis. After 10 min incubation in room temperature, the luminescence was read on a Microplate Reader (SpectraMax M5, Molecular Devices).



## Appendix B

### Spectral Data

Spectral data for the compounds designed in the study are shown in Table 16 and

Table 17.

**Table 16: ESI-Mass characterization and HPLC analysis of the compounds in Chapters 2 and 3.**

Peptide	% Purity (analytical RP- HPLC) *	Calculated	Observed (ESI-MS)**
		$(M+2H)^{2+}$	
WIN-FAM-1	> 99	1026.009	1026.20
WIN-FAM-2	99	1032.538	1032.60
		$(M+H)^+$	
10mer-Ala-FAM	98	1920.013	1919.87
10mer-Thr-FAM	99	1950.024	1949.87
WIN	95	1351.756	1351.73
Ac-11mer	> 99	1294.734	1294.80
Ac-10mer	90	1207.702	1207.73
NH <sub>2</sub> -11mer	> 99	1252.724	1252.80
Ac- 9mer	98	1136.665	1136.73
Ac-7mer	96	836.474	836.53
Ac-6mer	97	723.390	723.53
Ac-5mer	99	586.331	586.47
Ac-4mer	93	487.263	487.40

Ac-3mer (ARA)	96	358.220	358.33
Ac-2mer	> 99	287.183	287.27
NH <sub>2</sub> -10mer	98	1165.692	1165.73
NH <sub>2</sub> -3mer	> 99	316.210	316.27
CHO-ARA	> 99	344.205	344.27
Δ1	> 99	372.236	372.33
Δ2a	95	372.236	372.33
Δ2b	> 99	386.252	386.33
Δ2c	95	373.220	373.33
H3-10mer	> 99	1145.687	1145.80
Ac-H3-10mer	> 99	1187.697	1187.73
H3-3mer	93	346.220	346.27
Ac-H3-3mer	95	388.231	388.33
H3-10mer-K4Me	> 99	1159.702	1159.80
H3-10mer-K4Me <sub>2</sub>	> 99	1173.718	1173.80
H3-10mer-K4Me <sub>3</sub>	> 99	1188.741	1187.80
* Waters, Sunfire™ C18, 4.6×150mm, 5μm.			
** Finnigan LCQ Deca (Thermoquest).			

Table 17: ESI-Mass characterization and <sup>1</sup>H-NMR spectra of the compounds in Chapter 4.

Peptide	Calculated (M+H) <sup>+</sup>	Observed (M+H) <sup>+</sup> ESI-MS)*	<sup>1</sup> H-NMR** Chemical Shifts (D <sub>2</sub> O)
<b>1a</b>	344.20	344.33	4.39 (dd, J <sub>1</sub> = 5.6 Hz, J <sub>2</sub> = 8.1 Hz, 1H), 4.34 (q, J= 7.3 Hz, 1H), 3.96 (s, 2H), 3.25 (t, J= 6.8 Hz, 2H), 2.09 (s, 3H), 1.98-1.61 (m, 4H), 1.44 (d, J= 7.3 Hz, 3H).
<b>1b</b>	372.24	372.33	4.43-4.27 (m, 2H), 4.17 (t, J= 7.1 Hz, 1H), 3.25 (t, J= 6.5 Hz, 2H), 2.06 (s, 3H), 1.99-1.62 (m, 6H), 1.43 (d, J= 7.3 Hz, 3H), 0.98 (t, J= 7.4 Hz, 3H).
<b>1c</b>	386.25	386.42	4.44-4.28 (m, 2H), 4.08 (d, J= 7.4 Hz, 1H), 3.25 (t, J= 6.7 Hz, 2H), 2.12-2.03 (m, 4H), 1.97-1.76 (m, 2H), 1.75-1.61 (m, 2H), 1.43 (d, J= 7.2 Hz, 3H), 0.98 (m, 6H).
<b>1d</b>	390.19	390.33	4.45 (t, J= 6.3 Hz, 1H), 4.40-4.33 (m, 1H), 4.28 (q, J= 7.2 Hz, 1H), 3.20 (t, J= 6.7 Hz, 2H), 2.89 (d, J= 6.3 Hz, 2H), 2.04 (s, 3H), 1.96-1.57 (m, 4H), 1.39 (d, J= 7.2 Hz, 3H).
<b>1e</b>	400.27	400.42	4.42-4.26 (m, 3H), 3.24 (t, J= 6.6 Hz, 2H), 2.05 (s, 3H), 1.97-1.51 (m, 7H), 1.42 (d, J= 7.1 Hz, 3H), 0.97 (d, J= 5.8 Hz, 3H), 0.92 (d, J= 5.8 Hz, 3H).
<b>1f</b>	426.28	426.42	4.40 (dd, J <sub>1</sub> = 5.7 Hz, J <sub>2</sub> = 8.3 Hz, 1H), 4.32 (q, J= 7.2 Hz, 1H), 4.09 (d, J= 7.7 Hz, 1H), 3.24 (t, J= 6.9 Hz, 2H), 2.06 (s, 3H), 1.95-1.54 (m, 9H), 1.43 (d, J= 7.2 Hz, 3H), 1.31-0.99 (m, 6H).
<b>1g</b>	424.24	424.42	8.66 (s, 1H), 7.33 (s, 1H), 4.68 (t, J= 7.2 Hz, 1H), 4.41-4.25 (m, 2H), 3.32-3.10 (m, 4H), 2.02 (s, 3H), 1.93-1.58 (m, 4H), 1.43 (d, J= 7.2 Hz, 3H).
<b>1h</b>	434.25	434.42	7.40-7.20 (m, 5H), 4.50 (t, J= 7.7 Hz, 1H), 4.28-4.11 (m, 2H), 3.14 (t, J= 6.8 Hz, 2H), 3.07-2.98 (m, 2H), 1.96 (s, 3H), 1.83-1.60 (m, 2H), 1.59-1.44 (m, 2H), 1.38 (d, J= 7.2 Hz, 3H).

<b>1i</b>	374.22	374.33	4.43-4.34 (m, 2H), 4.27 (q, J= 7.3 Hz, 1H), 3.89-3.78 (m, 2H), 3.20 (t, J= 6.7 Hz, 2H), 2.05 (s, 3H), 1.97-1.57 (m, 4H), 1.38 (d, J= 7.3 Hz, 3H).
<b>1j</b>	388.23	388.33	4.46-4.14 (m, 4H), 3.25 (t, J= 6.7 Hz, 2H), 2.19-1.62 (m, 7H), 1.43 (d, J= 7.3 Hz, 3H), 1.25 (d, J= 6.3 Hz, 3H).
<b>2a</b>	315.20	315.08	4.38-4.25 (m, 3H), 2.05 (s, 3H), 1.92-1.68 (m, 4H), 1.47-1.29 (m, 8H), 0.92 (t, J= 6.3 Hz, 3H).
<b>2b</b>	316.20	316.17	4.45-4.23 (m, 3H), 3.06 (t, J= 6.8 Hz, 2H), 2.05 (s, 3H), 2.01-2.69 (m, 4H), 1.48-1.35 (m, 6H).
<b>2c</b>	330.21	330.25	4.41-4.24 (m, 3H), 3.04 (t, J= 7.3 Hz, 2H), 2.05 (s, 3H), 1.96-1.65 (m, 4H), 1.57-1.35 (m, 8H).
<b>2d</b>	359.20	359.08	4.39-4.24 (m, 3H), 3.15 (t, J= 6.6 Hz, 2H), 2.04 (s, 3H), 1.95-1.67 (m, 2H), 1.66-1.50 (m, 2H), 1.46-1.35 (m, 6H).
<b>3a</b>	344.20	344.33	4.32 (dd, J <sub>1</sub> = 5.8Hz, J <sub>2</sub> = 8.3 Hz, 1H), 4.25 (q, J= 7.2 Hz, 1H), 3.90 (d, J= 4.0 Hz, 2H), 3.20 (t, J= 6.7 Hz, 2H), 2.00 (s, 3H), 1.96-1.53 (m, 4H), 1.35 (d, J= 7.2 Hz, 3H).
<b>3b</b>	372.24	372.33	4.39 (t, J= 7.0 Hz, 1H), 4.34-4.18 (m, 2H), 3.25 (t, J= 6.7 Hz, 2H), 2.07-1.57 (m, 9H), 1.40 (d, J= 7.2 Hz, 3H), 0.98 (t, J= 7.4 Hz, 3H).
<b>3c</b>	386.25	386.42	4.41 (t, J= 7.1 Hz, 1H), 4.29 (q, J= 7.2 Hz, 1H), 4.14 (d, J= 7.5 Hz, 1H), 3.25 (t, J= 6.7 Hz, 2H), 2.15-1.96 (m, 4H), 1.94-1.54 (m, 4H), 1.39 (d, J= 7.2 Hz, 3H), 0.99 (d, J= 6.6 Hz, 6H).
<b>3d</b>	390.19	390.33	4.53-4.47 (m, 1H), 4.41-4.34 (m, 1H), 4.26 (q, J= 7.2 Hz, 1H), 3.22 (t, J= 6.8 Hz, 2H), 3.01-2.85 (m, 2H), 2.01 (s, 3H), 1.94-1.59 (m, 4H), 1.37 (d, J= 7.2 Hz, 3H).
<b>3e</b>	400.27	400.42	4.43 (m, 3H), 3.25 (t, J= 6.7 Hz, 2H), 2.05 (s, 3H), 1.98-1.54 (m, 7H), 1.39 (d, J= 7.2 Hz, 3H), 0.97 (d, J= 4.4 Hz, 3H), 0.91 (d, J= 5.13 Hz, 3H).
<b>3f</b>	426.28	426.42	4.40 (t, J= 7.0 Hz, 1H), 4.29 (q, J= 7.2 Hz, 1H), 4.17 (d, J= 7.5 Hz, 1H), 3.25 (t, J= 6.8 Hz, 2H), 2.07-1.54 (m, 13H), 1.43-0.95 (m, 8H).

<b>3g</b>	434.25	434.42	7.45 (m, 5H), 4.67 (dd, $J_1= 6.0$ Hz, $J_2= 9.0$ Hz, 1H), 4.32-4.20 (m, 2H), 3.25 (dd, $J_1= 5.9$ Hz, $J_2= 14.0$ Hz, 1H), 3.16 (t, $J= 6.9$ Hz, 2H), 3.03 (dd, $J_1= 9.3$ Hz, $J_2= 14$ Hz, 1H), 2.05 (s, 3H), 1.77-1.62 (m, 2H), 1.56-1.40 (m, 2H), 1.34 (d, $J= 7.2$ Hz, 3H).
<b>3h</b>	374.22	374.33	4.49-4.39 (m, 2H), 4.30 (q, $J= 7.2$ Hz, 1H), 3.93-3.85 (m, 2H), 3.26 (t, $J= 6.6$ Hz, 2H), 2.07-1.62 (m, 7H), 1.41 (d, $J= 7.2$ Hz, 3H).
<b>3i</b>	388.23	388.33	4.46 (dd, $J_1= 5.6$ Hz, $J_2= 8.5$ Hz, 1H), 4.38-4.23 (m, 3H), 3.26 (t, $J= 6.7$ Hz, 2H), 2.09-1.61 (m, 7H), 1.41 (d, $J= 7.2$ Hz, 3H), 1.24 (d, $J= 6.3$ Hz, 3H).
<b>3j</b>	416.23	416.42	4.43-4.24 (m, 3H), 3.25 (t, $J= 6.7$ Hz, 2H), 2.51 (t, $J= 7.1$ Hz, 2H), 2.23-1.61 (m, 9H), 1.39 (d, $J= 7.2$ Hz, 3H).
<b>4a</b>	398.25	398.20	4.44 (dd, $J_1= 5.9$ Hz, $J_2= 8.5$ Hz, 1H), 4.13 (d, $J= 7.4$ Hz, 1H), 3.24 (t, $J= 6.8$ Hz, 2H), 2.16-2.04 (m, 4H), 1.98-1.51 (m, 5H), 1.49-1.40 (m, 1H), 1.26-1.11 (m, 2H), 0.99 (d, $J= 6.7$ Hz, 6H).
<b>4b</b>	412.27	412.20	4.42 (dd, $J_1= 5.5$ Hz, $J_2= 8.6$ Hz, 1H), 4.14 (d, $J= 7.3$ Hz, 1H), 3.23 (t, $J= 6.8$ Hz, 2H), 2.73-2.50 (m, 2H), 2.32-1.55 (m, 12H), 1.00 (d, $J= 6.7$ Hz, 6H).
<b>4c</b>	426.28	426.24	4.43-4.35 (m, 1H), 4.13 (d, $J= 7.2$ Hz, 1H), 3.23 (t, $J= 6.5$ Hz, 2H), 2.29-1.54 (m, 16H), 0.99 (d, $J= 6.6$ Hz, 6H).
<b>4d</b>	440.30	440.24	4.43-4.35 (m, 1H), 4.13 (d, $J= 7.3$ Hz, 1H), 3.24 (t, $J= 6.7$ Hz, 2H), 2.20-1.41 (m, 17H), 1.40-1.21 (m, 1H), 1.00 (d, $J= 6.7$ Hz, 6H).
<b>4e</b>	400.27	400.20	4.42-4.34 (m, 1H), 4.12 (d, $J= 7.2$ Hz, 1H), 3.24 (t, $J= 6.7$ Hz, 2H), 2.20-2.06 (m, 1H), 2.02 (s, 3H), 1.98-1.56 (m, 4H), 1.47 (s, 6H), 1.00 (d, $J= 6.7$ Hz, 6H).
<b>4f</b>	428.30	428.42	4.42 (dd, $J_1= 5.5$ Hz, $J_2= 8.8$ Hz, 1H), 4.11 (d, $J= 7.5$ Hz, 1H), 3.24 (t, $J= 6.8$ Hz, 2H) 2.20-1.55 (m, 12H), 1.00 (d, $J= 6.8$ Hz, 6H), 0.81 (t, $J= 7.4$ Hz, 6H).

<b>4g</b>	428.30	428.24	4.46 (t, J= 7.0 Hz, 1H), 4.17-4.10 (m, 2H), 3.24 (t, J= 6.5 Hz, 2H), 2.16-2.02 (m, 4H), 1.93-1.55 (m, 4H), 1.08-0.95 (m, 15H).
<b>4h</b>	414.28	414.24	4.45 (dd, J <sub>1</sub> = 6.0 Hz, J <sub>2</sub> = 8.2 Hz, 1H), 4.25 (t, J= 7.2 Hz, 1H), 4.14 (d, J= 7.4 Hz, 1H), 3.25 (t, J= 6.8 Hz, 2H), 2.16-2.02 (m, 4H), 1.96-1.57 (m, 6H), 1.49-1.29 (m, 2H), 0.99 (dd, J <sub>1</sub> = 2.4 Hz, J <sub>2</sub> = 6.8 Hz, 3H), 0.94 (t, J= 7.4 Hz, 3H).
<b>4i</b>	440.30	440.24	4.46 (t, J= 7.1 Hz, 1H), 4.13 (d, J= 7.5 Hz, 1H), 4.07 (d, J= 9.3 Hz, 1H), 3.25 (t, J= 6.8 Hz, 2H), 2.24-2.02 (m, 5H), 1.95-1.51 (m, 10H), 1.42-1.23 (m, 2H), 0.99 (d, J= 6.6 Hz, 6H).
<b>4j</b>	448.27	448.33	7.52-7.44 (m, 5H), 5.39 (s, 1H), 4.46 (dd, J <sub>1</sub> = 6.0 Hz, J <sub>2</sub> = 8.5 Hz, 1H), 4.05 (d, J= 7.2 Hz, 1H), 3.22 (t, J= 6.9 Hz, 2H), 2.10 (s, 3H), 2.06-1.95 (m, 1H), 1.94-1.72 (m, 2H), 1.71-1.53 (m, 2H), 0.88 (d, J= 6.8 Hz, 3H), 0.83 (d, J= 6.8 Hz, 3H).
<b>4k</b>	448.27	448.42	7.53-7.44 (m, 5H), 5.39 (s, 1H), 4.42 (dd, J <sub>1</sub> = 5.3 Hz, J <sub>2</sub> = 9.3 Hz, 1H), 4.14 (d, J= 7.3 Hz, 1H), 3.07 (t, J= 7.1 Hz, 2H), 2.17-2.01 (m, 4H), 1.93-1.65 (m, 2H), 1.50-1.33 (m, 2H), 0.97 (d, J= 6.8 Hz, 3H), 0.96 (d, J= 6.8 Hz, 3H).
<b>5a</b>	398.25	398.33	4.19 (t, J= 7.0 Hz, 1H), 4.10 (d, J= 7.2 Hz, 1H), 3.25 (t, J= 6.7 Hz, 2H), 2.16-2.03 (m, J= 4H), 1.91-1.42 (m, 6H), 1.22-1.10 (m, 2H), 1.04-0.93 (m, 6H).
<b>5b</b>	412.27	412.33	4.28 (t, J= 7.2 Hz, 1H), 4.02 (d, J= 7.3 Hz, 1H), 3.22 (t, J= 6.6 Hz, 2H), 2.69-2.49 (m, J= 2H), 2.25-1.91 (m, 8H), 1.87-1.53 (m, 4H), 0.98-0.89 (m, 6H).
<b>5c</b>	426.28	426.33	4.35 (t, J= 7.1 Hz, 1H), 4.07 (d, J= 7.3 Hz, 1H), 3.25 (t, J= 6.6 Hz, 2H), 2.31-1.54 (m, 16H), 1.03-0.93 (m, 6H).
<b>5d</b>	440.30	440.42	4.43 (t, J= 7.1 Hz, 1H), 4.08 (d, J= 7.5 Hz, 1H), 3.26 (t, J= 6.7 Hz, 2H), 2.22-1.28 (m, 18H), 1.05-0.92 (m, 6H).
<b>5e</b>	400.27	400.33	4.33 (t, J= 7.0 Hz, 1H), 4.07 (d, J= 7.3 Hz, 1H), 3.25 (t, J= 6.6 Hz, 2H), 2.14-2.01 (m, 4H), 1.94-1.56 (m, 4H), 1.50 (s, 6H), 1.04-0.92 (m, 6H).

<b>5f</b>	428.30	428.42	4.46 (t, J= 7.1 Hz, 1H), 4.13 (s, 1H), 4.03 (d, J= 7.6 Hz, 1H), 3.19 (t, J= 6.6 Hz, 2H), 2.09-1.93 (m, 4H), 1.89-1.48 (m, 4H), 0.99 (s, 9H), 0.96-0.88 (m, 6H).
<b>5g</b>	440.30	440.42	4.46 (t, J= 7.0 Hz, 1H), 4.13 (d, J= 9.3 Hz, 1H), 4.08 (d, J= 7.4 Hz, 1H), 3.24 (t, J= 6.7 Hz, 2H), 2.32-2.15 (m, 1H), 2.13-1.99 (m, 4H), 1.95-1.52 (m, 10H), 1.43-1.20 (m, 2H), 1.04-0.91 (m, 6H).
<b>6a</b>	386.25	386.33	4.36 (dd, J <sub>1</sub> = 5.4 Hz, J <sub>2</sub> = 8.9 Hz, 1H), 4.20 (t, J= 7.1 Hz, 1H), 2.25 (t, J= 6.7 Hz, 2H), 2.03 (s, 3H), 2.01-1.58 (m, 6H), 1.48 (s, 6H), 0.99 (t, 7.4 Hz).
<b>6b</b>	412.27	412.33	4.31-4.24 (m, 1H), 3.25 (t, J= 6.7 Hz, 2H), 2.26-2.10 (m, 2H), 2.07-2.54 (m, 13H), 1.48 (s, 6H).
<b>6c</b>	402.25	402.42	4.43 (dd, J <sub>1</sub> = 5.0 Hz, J <sub>2</sub> = 9.2 Hz, 1H), 4.37-4.26 (m, 2H), 3.25 (t, J= 6.8 Hz, 2H), 2.03 (s, 3H), 2.00-1.58 (m, 4H), 1.49 (s, 6H), 1.25 (d, J= 6.1 Hz, 3H).
<b>6d</b>	398.25	398.33	4.33(dd, J <sub>1</sub> = 5.4 Hz, J <sub>2</sub> = 8.9 Hz, 1H), 4.19-4.11 (m, 1H), 3.18 (t, J= 6.7 Hz, 2H), 2.66-2.46 (m, 2H), 2.25-1.49 (m, 13H), 0.93 (t, J= 7.3 Hz, 3H).
<b>6e</b>	424.27	424.42	4.25 (dd, J <sub>1</sub> = 5.8 Hz, J <sub>2</sub> = 8.6 Hz, 1H), 3.19 (t, J= 6.8 Hz, 2H), 2.65-2.47 (m, 2H), 2.25-1.49 (m, 19H).
<b>6f</b>	414.25	414.33	4.45 (dd, J <sub>1</sub> = 5.1 Hz, J <sub>2</sub> = 9.3 Hz, 1H), 4.36-4.25 (m, 2H), 3.24 (t, J= 6.9 Hz, 2H), 2.74-2.52 (m, 2H), 2.32-1.87 (m, 8H), 1.86-1.73 (m, 1H), 1.72-1.56 (m, 2H), 1.24 (d, J= 6.3 Hz, 3H).
<b>6g</b>	440.30	440.41	4.28-4.17 (m, 1H), 3.13 (t, J= 6.6 Hz, 2H), 2.25-1.43 (m, 19H), 0.76 (t, J= 7.3 Hz, 6H).
<b>7a</b>	386.25	386.31	4.41-4.24 (m, 3H), 3.25 (t, J= 6.7 Hz, 2H), 2.65-2.50 (m, 1H), 1.96- 1.62 (m, 4H), 1.43 (d, J= 7.3 Hz, 3H), 1.40 (d, J= 7.3 Hz, 3H), 1.12 (d, J= 6.9 Hz, 6H).
<b>7b</b>	384.24	384.30	4.40-4.26 (m, 3H), 3.25 (t, J= 6.8 Hz, 2H), 1.97-1.61 (m, 5H), 1.45-1.39 (m, 6H), 0.94-0.83 (m, 4H).

<b>7c</b>	398.25	398.33	4.41-4.24 (m, 3H), 3.29-3.16 (m, 3H), 2.25-1.16 (m, 10H), 1.44 (d, J= 7.1Hz, 3H), 1.39 (d, J= 6.8 Hz, 3H).
<b>7d</b>	386.25	386.42	4.40-4.26 (m, 3H), 3.25 (t, J= 6.6 Hz, 2H), 2.28 (t, J= 7.1 Hz, 2H) 1.96-1.56 (m, 6H), 1.46-1.37 (m, 6H), 0.93 (t, J= 7.4 Hz, 3H).
<b>7e</b>	400.27	400.34	4.41-4.26 (m, 3H), 3.25 (t, J= 6.5 Hz, 2H), 2.31 (t, J= 7.3 Hz, 2H), 1.97-1.53 (m, 6H), 1.46-1.26 (m, 8H), 0.92 (t, J= 7.3 Hz, 3H).
<b>7f</b>	400.27	400.35	4.40-4.28 (m, 3H), 3.25 (t, J= 6.5 Hz, 2H), 2.18 (d, J= 7.7 Hz, 2H), 2.07-1.62 (m, 5H), 1.47-1.37 (m, 6H), 0.95 (d, J= 6.5 Hz, 6H).
<b>7g</b>	420.24	420.32	7.83 (d, J=7.9 Hz, 2H), 7.67 (m, 1H), 7.57 (m, 2H), 4.53(q, J= 7.1 Hz, 1H), 4.41 (t, J= 6.7 Hz, 1H), 4.33 (q, J= 7.2 Hz, 1H), 3.24 (t, J= 6.7 Hz, 2H), 1.99-1.64 (m, 4H), 1.53 (d, J= 7.1 Hz, 3H), 1.43 (d, J= 7.2 Hz, 3H).
<b>7h</b>	434.25	434.34	7.48-7.33 (m, 5H), 4.37-4.25 (m, 3H), 3.67 (s, 2H), 3.18 (t, J= 6.8 Hz, 2H), 1.87-1.62 (m, 4H), 1.41 (d, J= 7.2 Hz, 3H), 1.38 (d, J= 7.3 Hz, 3H).
<b>7i</b>	426.28	426.36	4.41-4.27 (m, 3H), 3.25 (t, J= 6.4 Hz, 2H), 2.30 (d, J= 7.2 Hz, 2H), 2.23-2.10 (m, 1H), 1.97-1.51 (m, 10H), 1.46-1.37 (m, 6H), 1.26-1.12 (m, 2H).
<b>7j</b>	373.23	373.33	4.41-4.27 (m, 2H), 4.16 (q, J= 7.0 Hz, 1H), 3.25 (t, J= 6.5 Hz, 2H), 2.71 (s, 3H), 2.00-1.63 (m, 4H), 1.44 (d, J= 7.0 Hz, 3H), 1.37 (d, J= 7.0 Hz, 3H).
<b>7k</b>	387.25	387.75	4.39-4.28 (m, 2H), 4.18 (q, J= 7.3 Hz, 1H), 3.25 (t, J= 6.6 Hz, 2H), 2.94 (s, 6H), 1.98-1.63 (m, 4H), 1.44 (d, J=7.3 Hz, 3H), 1.40 (d, J= 7.3 Hz, 3H).
<b>8a</b>	372.24	372.33	4.40-4.23 (m, 3H), 3.25 (t, J= 6.6 Hz, 2H), 2.77 (s, 3H), 2.05 (s, 3H), 1.97-1.59 (m, 4H), 1.39 (d, J= 7.0 Hz, 6H).
<b>8b</b>	400.27	400.42	4.29-4.09 (m, 3H), 3.91-3.77 (m, 1H), 3.16 (t, J= 6.6 Hz, 2H), 1.96 (s, 3H), 1.87-1.53 (m, 4H), 1.30 (d, J=6.3, 6H), 1.10-1.03 (m, 6H).
<b>8c</b>	428.30	428.42	4.38-4.25 (m, 3H), 3.66-3.55 (m, 1H), 3.25 (t, J= 6.5, 2H), 2.05 (s, 3H), 1.96-1.52 (m, 6H), 1.46-1.37 (m, 8H), 0.87 (t, J= 7.3 Hz, 6H).



<b>8d</b>	440.30	440.42	4.38-4.21 (m, 3H), 3.66-3.55 (m, 1H), 3.25 (t, J= 6.7 Hz, 2H), 2.05 (s, 3H), 1.94-1.58 (m, 9H), 1.41-1.14 (m, 11H).
<b>8e</b>	343.25	434.33	7.50-7.44 (m, 4H), 7.36-7.27 (m, 1H), 4.51-4.25 (m, 3H), 3.23 (t, J= 6.6 Hz, 2H), 2.05 (s, 3H), 1.97-1.6 (m, 4H), 1.52 (d, J= 6.7 Hz, 3H), 1.39 (d, 6.9 Hz, 3H).
<b>8f</b>	448.27	448.42	7.47-7.31 (m, 5H), 4.50-4.22 (m, 5H), 3.17 (t, J= 6.6 Hz, 2H), 2.04 (s, 3H), 1.93-1.54 (m, 4H), 1.43 (d, J= 7.0 Hz, 3H), 1.37 (d, J= 7.0 Hz, 3H).
<b>8g</b>	524.30	524.42	7.48-7.31 (m, 10H), 6.09 (s, 1H), 4.48-4.20 (m, 3H), 3.12 (t, J= 6.5 Hz, 2H), 2.04 (s, 3H), 1.89-1.50 (m, 4H), 1.44 (d, J=7.1 Hz, 3H), 1.36 (d, J= 7.2 Hz, 3H).
<b>MM-101 (MeOD)</b>	634.41	634.49	7.42-7.21 (m, 10H), 6.21 (s, 1H), 4.04-3.98 (m, 1H), 3.21 (t, J= 7.0 Hz, 2H), 2.56-2.46 (m, 1H), 2.37-2.09 (m, 4H), 1.94-1.59 (m, 12H), 1.14-1.05 (m, 6H), 0.84-0.71 (m, 6H).
<b>MM-102 (MeOD)</b>	670.39	670.33	7.41-7.28 (m, 4H), 7.07-6.96 (m, 4H), 6.17 (s, 1H), 3.95-3.88 (m, 1H), 3.23-3.16 (m, 2H), 2.55-2.43 (m, 1H), 2.37-2.01 (m, 4H), 1.94-1.52 (m, 12H), 1.07 (dd, J <sub>1</sub> = 5.3 Hz, J <sub>2</sub> = 6.7 Hz 6H), 0.79-0.68 (m, 6H).
* Thermo Scientific LCQ Fleet ** Bruker 300 MHz			

## **Bibliography**

## Bibliography

- (1) Jude, C. D.; Climer, L.; Xu, D.; Artinger, E.; Fisher, J. K.; Ernst, P. *Cell Stem Cell* **2007**, *1*, 324.
- (2) Guenther, M. G.; Jenner, R. G.; Chevalier, B.; Nakamura, T.; Croce, C. M.; Canaani, E.; Young, R. A. *Proc Natl Acad Sci U S A* **2005**, *102*, 8603.
- (3) Wang, P.; Lin, C.; Smith, E. R.; Guo, H.; Sanderson, B. W.; Wu, M.; Gogol, M.; Alexander, T.; Seidel, C.; Wiedemann, L. M.; Ge, K.; Krumlauf, R.; Shilatifard, A. *Mol Cell Biol* **2009**, *29*, 6074.
- (4) Milne, T. A.; Briggs, S. D.; Brock, H. W.; Martin, M. E.; Gibbs, D.; Allis, C. D.; Hess, J. L. *Mol Cell* **2002**, *10*, 1107.
- (5) Argiropoulos, B.; Humphries, R. K. *Oncogene* **2007**, *26*, 6766.
- (6) Slany, R. K. *Hematol Oncol* **2005**, *23*, 1.
- (7) Huret, J. L.; Dessen, P.; Bernheim, A. *Leukemia* **2001**, *15*, 987.
- (8) Hess, J. L. *Trends Mol Med* **2004**, *10*, 500.
- (9) Dou, Y.; Hess, J. L. *Int J Hematol* **2008**, *87*, 10.
- (10) Kroon, E.; Kros, J.; Thorsteinsdottir, U.; Baban, S.; Buchberg, A. M.; Sauvageau, G. *EMBO J* **1998**, *17*, 3714.
- (11) Richmond, T. J.; Davey, C. A. *Nature* **2003**, *423*, 145.
- (12) Davey, C. A.; Sargent, D. F.; Luger, K.; Maeder, A. W.; Richmond, T. J. *J Mol Biol* **2002**, *319*, 1097.
- (13) Bustin, M.; Catez, F.; Lim, J. H. *Mol Cell* **2005**, *17*, 617.
- (14) Luger, K.; Mader, A. W.; Richmond, R. K.; Sargent, D. F.; Richmond, T. J. *Nature* **1997**, *389*, 251.
- (15) Kouzarides, T. *Cell* **2007**, *128*, 693.
- (16) Marmorstein, R. *Nat Rev Mol Cell Biol* **2001**, *2*, 422.
- (17) Sims, R. J., 3rd; Nishioka, K.; Reinberg, D. *Trends Genet* **2003**, *19*, 629.
- (18) Wang, G. G.; Allis, C. D.; Chi, P. *Trends Mol Med* **2007**, *13*, 363.
- (19) Papp, B.; Muller, J. *Genes Dev* **2006**, *20*, 2041.
- (20) Bernstein, B. E.; Kamal, M.; Lindblad-Toh, K.; Bekiranov, S.; Bailey, D. K.; Huebert, D. J.; McMahon, S.; Karlsson, E. K.; Kulbokas, E. J., 3rd; Gingeras, T. R.; Schreiber, S. L.; Lander, E. S. *Cell* **2005**, *120*, 169.
- (21) Santos-Rosa, H.; Schneider, R.; Bannister, A. J.; Sherriff, J.; Bernstein, B. E.; Emre, N. C.; Schreiber, S. L.; Mellor, J.; Kouzarides, T. *Nature* **2002**, *419*, 407.
- (22) Ruthenburg, A. J.; Allis, C. D.; Wysocka, J. *Mol Cell* **2007**, *25*, 15.
- (23) Wysocka, J.; Swigut, T.; Xiao, H.; Milne, T. A.; Kwon, S. Y.; Landry, J.; Kauer, M.; Tackett, A. J.; Chait, B. T.; Badenhorst, P.; Wu, C.; Allis, C. D. *Nature* **2006**, *442*, 86.
- (24) Pena, P. V.; Davrazou, F.; Shi, X.; Walter, K. L.; Verkhusha, V. V.; Gozani, O.; Zhao, R.; Kutateladze, T. G. *Nature* **2006**, *442*, 100.

- (25) Taverna, S. D.; Ilin, S.; Rogers, R. S.; Tanny, J. C.; Lavender, H.; Li, H.; Baker, L.; Boyle, J.; Blair, L. P.; Chait, B. T.; Patel, D. J.; Aitchison, J. D.; Tackett, A. J.; Allis, C. D. *Mol Cell* **2006**, *24*, 785.
- (26) Iwase, S.; Lan, F.; Bayliss, P.; de la Torre-Ubieta, L.; Huarte, M.; Qi, H. H.; Whetstine, J. R.; Bonni, A.; Roberts, T. M.; Shi, Y. *Cell* **2007**, *128*, 1077.
- (27) Shi, Y.; Whetstine, J. R. *Mol Cell* **2007**, *25*, 1.
- (28) Zhu, Q.; Liu, C.; Ge, Z.; Fang, X.; Zhang, X.; Straat, K.; Bjorkholm, M.; Xu, D. *PLoS One* **2008**, *3*, e1446.
- (29) Tahiliani, M.; Mei, P.; Fang, R.; Leonor, T.; Rutenberg, M.; Shimizu, F.; Li, J.; Rao, A.; Shi, Y. *Nature* **2007**, *447*, 601.
- (30) Yokoyama, A.; Wang, Z.; Wysocka, J.; Sanyal, M.; Aufiero, D. J.; Kitabayashi, I.; Herr, W.; Cleary, M. L. *Mol Cell Biol* **2004**, *24*, 5639.
- (31) Shilatifard, A. *Curr Opin Cell Biol* **2008**, *20*, 341.
- (32) Hsieh, J. J.; Ernst, P.; Erdjument-Bromage, H.; Tempst, P.; Korsmeyer, S. J. *Mol Cell Biol* **2003**, *23*, 186.
- (33) Dou, Y.; Milne, T. A.; Ruthenburg, A. J.; Lee, S.; Lee, J. W.; Verdine, G. L.; Allis, C. D.; Roeder, R. G. *Nat Struct Mol Biol* **2006**, *13*, 713.
- (34) Cao, F.; Chen, Y.; Cierpicki, T.; Liu, Y.; Basrur, V.; Lei, M.; Dou, Y. *PLoS One* **2010**, *5*, e14102.
- (35) Chen, Y. X.; Yan, J.; Keeshan, K.; Tubbs, A. T.; Wang, H.; Silva, A.; Brown, E. J.; Hess, J. L.; Pear, W. S.; Hua, X. *Proc Natl Acad Sci U S A* **2006**, *103*, 1018.
- (36) Hombria, J. C.; Lovegrove, B. *Differentiation* **2003**, *71*, 461.
- (37) Monier, B.; Tevy, M. F.; Perrin, L.; Capovilla, M.; Semeriva, M. *Fly (Austin)* **2007**, *1*, 59.
- (38) Svingen, T.; Tonissen, K. F. *Heredity* **2006**, *97*, 88.
- (39) Calvo, K. R.; Sykes, D. B.; Pasillas, M.; Kamps, M. P. *Mol Cell Biol* **2000**, *20*, 3274.
- (40) Ziemin-van der Poel, S.; McCabe, N. R.; Gill, H. J.; Espinosa, R., 3rd; Patel, Y.; Harden, A.; Rubinelli, P.; Smith, S. D.; LeBeau, M. M.; Rowley, J. D.; et al. *Proc Natl Acad Sci U S A* **1991**, *88*, 10735.
- (41) Felix, C. A.; Lange, B. J.; Chessells, J. M. *Hematology Am Soc Hematol Educ Program* **2000**, 285.
- (42) Borkhardt, A.; Wuchter, C.; Viehmann, S.; Pils, S.; Teigler-Schlegel, A.; Stanulla, M.; Zimmermann, M.; Ludwig, W. D.; Janka-Schaub, G.; Schrappe, M.; Harbott, J. *Leukemia* **2002**, *16*, 1685.
- (43) Pakakasama, S.; Kajanachumpol, S.; Kanjanapongkul, S.; Sirachainan, N.; Meekaewkunchorn, A.; Ningsanond, V.; Hongeng, S. *Int J Lab Hematol* **2008**, *30*, 286.
- (44) Pui, C. H.; Relling, M. V. *Br J Haematol* **2000**, *109*, 13.
- (45) Krivtsov, A. V.; Armstrong, S. A. *Nat Rev Cancer* **2007**, *7*, 823.
- (46) Hess, J. L. *Crit Rev Eukaryot Gene Expr* **2004**, *14*, 235.
- (47) Orlovsky, K.; Kalinkovich, A.; Rozovskaia, T.; Shezen, E.; Itkin, T.; Alder, H.; Ozer, H. G.; Carramusa, L.; Avigdor, A.; Volinia, S.; Buchberg, A.; Mazo, A.; Kollet, O.; Largman, C.; Croce, C. M.; Nakamura, T.; Lapidot, T.; Canaani, E. *Proc Natl Acad Sci U S A* **2011**, *108*, 7956.

- (48) Ferrando, A. A.; Armstrong, S. A.; Neuberg, D. S.; Sallan, S. E.; Silverman, L. B.; Korsmeyer, S. J.; Look, A. T. *Blood* **2003**, *102*, 262.
- (49) Zeisig, B. B.; Milne, T.; Garcia-Cuellar, M. P.; Schreiner, S.; Martin, M. E.; Fuchs, U.; Borkhardt, A.; Chanda, S. K.; Walker, J.; Soden, R.; Hess, J. L.; Slany, R. K. *Mol Cell Biol* **2004**, *24*, 617.
- (50) Ayton, P. M.; Cleary, M. L. *Genes Dev* **2003**, *17*, 2298.
- (51) Thorsteinsdottir, U.; Kroon, E.; Jerome, L.; Blasi, F.; Sauvageau, G. *Mol Cell Biol* **2001**, *21*, 224.
- (52) Milne, T. A.; Kim, J.; Wang, G. G.; Stadler, S. C.; Basrur, V.; Whitcomb, S. J.; Wang, Z.; Ruthenburg, A. J.; Elenitoba-Johnson, K. S.; Roeder, R. G.; Allis, C. D. *Mol Cell* **2010**, *38*, 853.
- (53) Thiel, A. T.; Blessington, P.; Zou, T.; Feather, D.; Wu, X.; Yan, J.; Zhang, H.; Liu, Z.; Ernst, P.; Koretzky, G. A.; Hua, X. *Cancer Cell* **2010**, *17*, 148.
- (54) Patel, A.; Vought, V. E.; Dharmarajan, V.; Cosgrove, M. S. *J Biol Chem* **2008**, *283*, 32162.
- (55) Wysocka, J.; Swigut, T.; Milne, T. A.; Dou, Y.; Zhang, X.; Burlingame, A. L.; Roeder, R. G.; Brivanlou, A. H.; Allis, C. D. *Cell* **2005**, *121*, 859.
- (56) Schuetz, A.; Allali-Hassani, A.; Martin, F.; Loppnau, P.; Vedadi, M.; Bochkarev, A.; Plotnikov, A. N.; Arrowsmith, C. H.; Min, J. *EMBO J* **2006**, *25*, 4245.
- (57) Han, Z.; Guo, L.; Wang, H.; Shen, Y.; Deng, X. W.; Chai, J. *Mol Cell* **2006**, *22*, 137.
- (58) Odho, Z.; Southall, S. M.; Wilson, J. R. *J Biol Chem* **2010**, *285*, 32967.
- (59) Couture, J. F.; Collazo, E.; Trievel, R. C. *Nat Struct Mol Biol* **2006**, *13*, 698.
- (60) Song, J. J.; Kingston, R. E. *J Biol Chem* **2008**, *283*, 35258.
- (61) Patel, A.; Dharmarajan, V.; Cosgrove, M. S. *J Biol Chem* **2008**, *283*, 32158.
- (62) Nikolovska-Coleska, Z.; Wang, R.; Fang, X.; Pan, H.; Tomita, Y.; Li, P.; Roller, P. P.; Krajewski, K.; Saito, N. G.; Stuckey, J. A.; Wang, S. *Anal Biochem* **2004**, *332*, 261.
- (63) Trievel, R. C.; Shilatifard, A. *Nat Struct Mol Biol* **2009**, *16*, 678.
- (64) Karatas, H.; Townsend, E. C.; Bernard, D.; Dou, Y.; Wang, S. *J Med Chem* **2010**, *53*, 5179.
- (65) Ruthenburg, A. J.; Wang, W.; Graybosch, D. M.; Li, H.; Allis, C. D.; Patel, D. J.; Verdine, G. L. *Nat Struct Mol Biol* **2006**, *13*, 704.
- (66) Faber, J.; Krivtsov, A. V.; Stubbs, M. C.; Wright, R.; Davis, T. N.; van den Heuvel-Eibrink, M.; Zwaan, C. M.; Kung, A. L.; Armstrong, S. A. *Blood* **2009**, *113*, 2375.
- (67) Southall, S. M.; Wong, P. S.; Odho, Z.; Roe, S. M.; Wilson, J. R. *Mol Cell* **2009**, *33*, 181.
- (68) Khan, J. A.; Dunn, B. M.; Tong, L. *Structure* **2005**, *13*, 1443.
- (69) Daigle, S. R.; Olhava, E. J.; Therkelsen, C. A.; Majer, C. R.; Sneeringer, C. J.; Song, J.; Johnston, L. D.; Scott, M. P.; Smith, J. J.; Xiao, Y.; Jin, L.; Kuntz, K. W.; Chesworth, R.; Moyer, M. P.; Bernt, K. M.; Tseng, J. C.; Kung, A. L.; Armstrong, S. A.; Copeland, R. A.; Richon, V. M.; Pollock, R. M. *Cancer Cell* **2011**, *20*, 53.
- (70) Wu, X.; Hua, X. *Curr Mol Med* **2008**, *8*, 805.

- (71) Grembecka, J.; Belcher, A. M.; Hartley, T.; Cierpicki, T. *J Biol Chem* **2010**, *285*, 40690.
- (72) LaRonde-LeBlanc, N. A.; Wolberger, C. *Genes Dev* **2003**, *17*, 2060.
- (73) *Methods in Enzymology* Otwinowski, Z., Minor, W., Ed.; Academic Press: New York, 1997.
- (74) McCoy, A. J.; Grosse-Kunstleve, R. W.; Adams, P. D.; Winn, M. D.; Storoni, L. C.; Read, R. J. *J Appl Crystallogr* **2007**, *40*, 658.
- (75) Adams, P. D.; Afonine, P. V.; Bunkoczi, G.; Chen, V. B.; Davis, I. W.; Echols, N.; Headd, J. J.; Hung, L. W.; Kapral, G. J.; Grosse-Kunstleve, R. W.; McCoy, A. J.; Moriarty, N. W.; Oeffner, R.; Read, R. J.; Richardson, D. C.; Richardson, J. S.; Terwilliger, T. C.; Zwart, P. H. *Acta Crystallogr D Biol Crystallogr* **2010**, *66*, 213.
- (76) Emsley, P.; Cowtan, K. *Acta Crystallogr D Biol Crystallogr* **2004**, *60*, 2126.
- (77) Dou, Y.; Milne, T. A.; Tackett, A. J.; Smith, E. R.; Fukuda, A.; Wysocka, J.; Allis, C. D.; Chait, B. T.; Hess, J. L.; Roeder, R. G. *Cell* **2005**, *121*, 873.